Chem Soc Rev

REVIEW ARTICLE

Published on 14 October 2026
Licence and permissions

Check for updates

Cite this: *Chem. Soc. Rev.*, 2026, **55**, 11564

Metal–organic frameworks based on macrocycles: from design to function

Junyu Ren, *[ab] Joshua Phipps, [b] Shengqian Ma *[b] and Jian Tian *[a]

Metal–organic frameworks (MOFs) built from macrocyclic building blocks stand at the intersection of two Nobel-Prize-recognized traditions. Within such lattices, the framework amplifies individual molecular events into bulk material properties through periodic replication and geometric control allowing for recognition, gating, or catalytic specificity that conventional linkers struggle to bestow. The solid-state host–guest behaviour of these hybrid materials diverges from their homogeneous counterparts in solution. The lattice locks cavity conformations to sharpen selectivity, fixes orientations to enable cooperative multisite binding, and combines discrete recognition events with collective responses in conductivity, luminescence, or mass transport. This interplay has already led to macrocyclic MOFs whose performance surpasses that of both parent components. Despite rapid progress, the field still lacks a systematic way of relating macrocyclic properties to material function. Conceptualizing and realizing the full potential of these materials therefore demands a coherent understanding of how macrocycle characteristics dictate reticular compatibility, how synthetic mechanisms govern cavity accessibility, and how these aspects jointly determine function. This review develops that integrated understanding in stages: the physicochemical attributes that matter for the material's reticular nature, the synthetic logic that weaves macrocycles into periodic frameworks, and the emergent performance these architectures deliver. It concludes by outlining the frontiers where macrocyclic MOFs may transition from laboratory proof-of-concept to engineered technology.

Received 7th May 2026

DOI: 10.1039/d6cs00546b

rsc.li/chem-soc-rev

1. Introduction

Metal–organic frameworks are crystalline, permanently porous networks assembled from metal ions/clusters and polytopic organic linkers. They have matured from a structural concept into a foundational materials platform, recognized by the 2025 Nobel Prize in Chemistry.[1–5] A separate tradition, honoured

[a] *Department of Cardiovascular Surgery, Zhongnan Hospital of Wuhan University, School of Pharmaceutical Sciences, Wuhan University, Wuhan 430071, China. E-mail: Jian.Tian@whu.edu.cn*

[b] *Department of Chemistry, University of North Texas, Denton, Texas 76201, USA. E-mail: Shengqian.Ma@unt.edu, JunyuRen@my.unt.edu*



Junyu Ren

Junyu Ren received his PhD in Chemistry from the University of North Texas in 2022 under the supervision of Prof. Shengqian Ma. He is currently a research fellow at the National University of Singapore. His research focuses on the design and synthesis of macrocycle-based framework materials for the recognition, selective separation, and trace capture of molecular/ionic species under ultradilute conditions.



Joshua Phipps

Joshua Phipps obtained his BS in Biology from Southwest Baptist University in 2016 and began his PhD program at the University of Arkansas in 2017 where he studied the interactions between biological molecules and porous materials. He graduated in 2022 and began performing research under the supervision of Professor Ma at the University of North Texas as a postdoctoral researcher where he focuses on biological applications of porous materials.

This journal is © The Royal Society of Chemistry 2026

with the 1987 Nobel Prize, is that of macrocycles. These cyclic arrays of donor atoms can recognize molecular guests with a precision that acyclic hosts cannot match.[6–8] In this work, we detail the convergence of these two programs and describe how macrocyclic recognition embedded within reticular lattices can be leveraged for new functional outcomes.

The strength of reticular chemistry lies in its ordered composition. This characteristic endows it with the ability to position molecular components at crystallographically defined locations, to replicate that arrangement across macroscopic length scales, and to maintain permanent porosity through which matter can flow.[5] Two decades of sustained development have produced frameworks with surface areas exceeding 7000 $m^2\ g^{-1}$ and tuneable pore apertures spanning the micro- to mesopore range. These materials have demonstrated great success in applications across gas storage and carbon capture, molecular separation, heterogeneous catalysis, chemical sensing, atmospheric water harvesting, and biomedical delivery.[9,10] Yet, the pore surfaces of most conventional frameworks remain chemically limited in their mode of guest interaction. They are typically decorated with simple pendant groups (–NH_2, –OH, or –SO_3H for example) or open metal sites that engage guests through cumulative but geometrically underdefined contacts across a large surface area.[11–13] This mode of host–guest engagement is effective for tasks governed by aggregate affinity, total gas uptake, overall hydrophilicity, or bulk catalytic activity. But it leaves a performance gap in tasks that demand precise molecular discrimination, such as distinguishing one enantiomer from another, one alkali metal from the next, or one positional isomer from its near-twin. Reticular chemistry has mastered the architecture of porosity, while the specificity of the chemistry within that architecture, namely the capacity to programme a defined binding preference at each pore, remains comparatively underdeveloped. It is this gap that macrocyclic hosts are well positioned to fill.

The strength of macrocyclic chemistry lies in precisely this specificity. A macrocyclic cavity is not a functional group appended to a surface, instead, it is a volume of chemical space, a three-dimensional enclosure whose geometry, donor-atom arrangement, electronic character, and conformational dynamics are prescribed at the point of synthesis. Crown ethers and their nitrogen-substituted aza-macrocyclic derivatives for example encode cation selectivity through cavity-size complementarity, with tuneable exchange kinetics spanning the microsecond-to-day range depending on whether the donor atoms are oxygen or nitrogen.[14,15] Another group, cyclodextrins, encode chiral, amphiphilic encapsulation from aqueous media while pillar[*n*]arenes and calix[*n*]arenes encode electronic discrimination through π-electron-rich aromatic walls.[16] Finally, cucurbiturils encode near-irreversible guest sequestration at association constants approaching $10^{12}\ M^{-1}$, among the strongest non-covalent associations known.[17] Each of these families encodes a distinct recognition programme into a single, preassembled molecule. Yet, in solution, every program operates under the same constraint where the cavity acts alone, encountering guests one at a time through diffusion, competing with solvent for the binding site, and sampling all orientations isotropically. In the neat solid state, a different constraint applies in which the macrocycles pack into dense crystals that bury the cavity and block mass transport, rendering the recognition ability structurally intact but functionally silent.[18] Many years of research have allowed macrocyclic chemistry to master the programming of molecular recognition, however translating these designs into a bulk material property requires a structural context beyond what solution or dense-crystal environments can easily offer (Fig. 1).

The integration of macrocycles into MOF lattices addresses both deficiencies, but the result is not a simple sum. When a macrocyclic cavity occupies a site within a periodic, porous lattice, three things happen that neither solution-phase chemistry nor dense-crystal packing can produce. First, the recognition event is replicated, with every crystallographically equivalent site hosting an identical cavity, and countless simultaneous binding



Shengqian Ma

Shengqian Ma obtained his BS from Jilin University in 2003 and graduated with a PhD from Miami University (Ohio) in 2008. After a Director's Postdoctoral Fellowship at Argonne National Laboratory, he joined the University of South Florida (USF) as an Assistant Professor in 2010 and was promoted to Associate Professor with early tenure in 2015 and Full Professor in 2018. In 2020, he accepted an endowed position as the Welch Chair in Chemistry at the University of North Texas. His current research interest focuses on functional porous materials including MOFs, COFs, and POPs for energy, biology, and environment-related applications.



Jian Tian

Jian Tian obtained his Bachelor's degree in 2003 from Nankai University and his PhD in Chemistry from the University of Missouri-Columbia in 2009. From 2010 to 2015, he conducted his postdoctoral research at Pacific Northwest National Laboratory and Texas A&M University in the United States. In late 2015, he joined Wuhan University as a full professor at the School of Pharmaceutical Sciences. His research focuses on the structural design and synthesis of MOFs, with applications in host–guest chemistry, nanomedicine, and drug delivery.

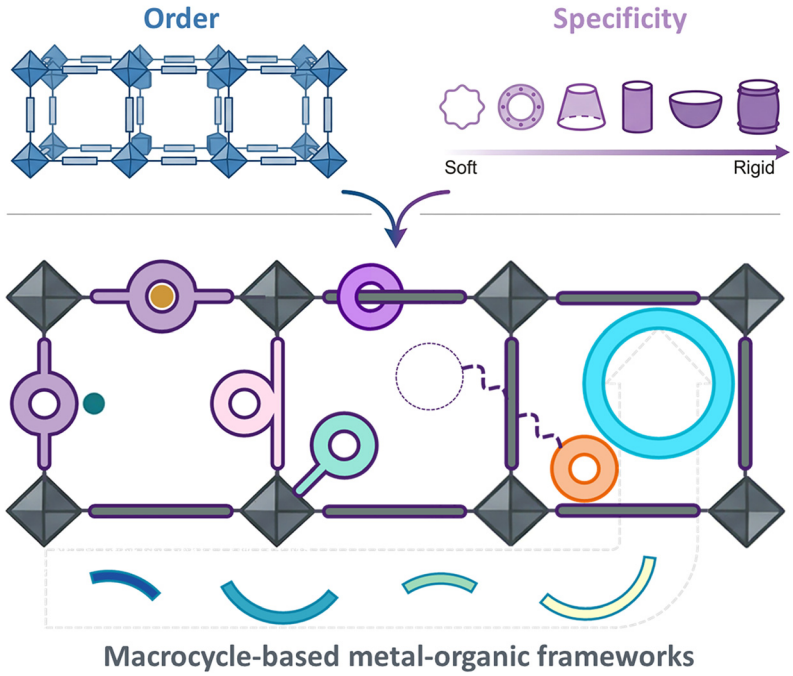


Fig. 1 Schematic illustration of macrocycle-based MOFs. The reticular lattice provides long-range periodic order (upper left), while macrocyclic linkers of varying conformational flexibility impart molecular-level host–guest specificity. The lower panel depicts a representative lattice in which various macrocycles are integrated into the scaffold *via* different strategies.

events convert a single-molecule preference into a cooperative material response. Examples include the periodic array of chiral cyclodextrin (CD) cavities that enable enantioseparation rivalling commercial HPLC columns, and the aligned CD hydroxyl network that sustains proton conductivities 300-fold higher in oriented thin films than in disordered powders.[19,20] Second, the conformational landscape is edited. The lattice permits only those cavity motions compatible with the local symmetry of the pore wall, channelling the macrocycle's induced-fit response along a lattice-defined coordinate rather than allowing it to dissipate isotropically. Crown ethers locked within sub-nanochannels achieve Li^+/Mg^{2+} selectivities of 125 through directed conformational switching, and crown ether wheels in metal–organic rotaxane frameworks display tuneable pirouetting dynamics.[21,22] Third, the functional outcome is contextualized. The framework topology, pore connectivity, and adjacent-site arrangement collectively determine whether a bound guest is captured, relayed to the next site, gated by a conformational switch, or transformed by a catalytic metal centre. In aza-macrocyclic frameworks, the Zr_6 node provides structural integrity while the cyclam metal centre independently catalyses CO_2 fixation; in calixarene MOF nanosheets, the 2D morphology maximizes the accessibility of chiral catalytic sites that the bulk 3D crystal partially occludes.[23,24]

This synergy, however, is not without internal tension, and it is the nature of these tensions, more than the catalogue of successes, that reveals the deeper design logic of the field. The first tension is synthetic. Macrocycles are conformationally rich, sterically demanding, and often chemically sensitive, while reticular assembly demands rigid, thermally robust, geometrically predictable building blocks. This challenge of reconciling macrocyclic complexity with lattice order, through covalent pre-engineering, non-covalent templating, sequential installation, or the elimination of hostile solvothermal environments, is of great importance and something we discuss in detail, particularly in Section 3. The second tension is thermodynamic. The same preorganization that maximizes a macrocycle's binding affinity also minimizes its conformational adaptability. This creates a diagonal constraint in the design space, where soft cavities trade affinity for responsiveness and rigid cavities trade responsiveness for affinity, a trade-off rooted in the conformational entropy cost of complexation.[25] This adaptability–affinity relationship shapes many of the application we discuss in this review, because different functions place different demands on the same two variables. While separation rewards equilibrium selectivity, gating rewards conformational switching, catalysis rewards turnover kinetics, and transport rewards the narrow residence-time window between trapping and indifference. The third tension is architectural since a macrocycle must be integrated into the lattice to benefit from periodic replication. However, this act of integration, covalent arm-grafting, conformational locking, coordinative tethering, risks distorting the very cavity geometry and dynamics that justify the macrocycle's presence. Structural integration and functional integrity often pull in opposite directions. In most systems, the lattice constrains the cavity and narrows its chemistry while in a few examples, the constraint itself becomes a functional advantage, a restrained conformation that sharpens selectivity, a restricted approach trajectory that imposes regiocontrol. Whether integration is a cost or benefit

 This journal is © The Royal Society of Chemistry 2026

depends on which degree of freedom the lattice removes and whether that degree of freedom was serving the function or hindering it.

Several comprehensive reviews have charted the structural and functional territory of this field from complementary perspectives. Early contributions established the conceptual connections between metal–organic macrocycles, polyhedra, and extended frameworks and between metallo-supramolecular macrocyclic chemistry and higher-order architectures.[26,27] Zhang and co-workers provided the first systematic taxonomy organized by macrocycle family.[28] The specific role of aza-macrocyclic ligands in framework assembly was examined independently by Stackhouse and Ma and by Lee and Moon.[29,30] Zhou, Huang, and co-workers introduced paradigms such as "adaptive crystals" and "porosity without pores" for supramolecular-macrocycle-based crystalline materials, while Tashiro and Shionoya highlighted porous crystals with macrocycle-based well-defined molecular recognition sites.[31,32] Cyclodextrin-based frameworks have received dedicated attention from Stoddart and from Dummert, Fischer, and co-workers with emphasis on their biomedical applications.[33,34] Liang, Zhou, Huang, and Fang surveyed hierarchical assembly strategies for macrocycle-containing MOFs and porous coordination cages.[35] Most recently, the scope has expanded to encompass both MOF and COF platforms, adsorption-driven applications, and macrocycle-based framework membranes.[36–38] These contributions have mapped the landscape of related materials. What remains uncharted is the landscape of why, the qualitative mechanistic link between where a macrocycle sits on the interaction-mode/rigidity map and how it performs during separation, sensing, catalysis, or transport. The answers are not idiosyncratic, and they trace back in every case to the same small set of physical variables including cavity geometry, donor-atom identity, conformational entropy cost, and exchange kinetics. This review bridges the gap by providing that link, not by cataloguing what each macrocycle–MOF system has achieved, but by identifying the physicochemical principles that connect a macrocycle's molecular coordinates to its material-level outcome. Doing so means reading the binding constants, conformational freedom, and exchange kinetics of the macrocycle against the symmetry, periodicity, and confinement of the lattice. These principles are qualitative but testable; translating them into quantitative structure–function models, a path outlined in Section 5.2, is where the field must go next.

We begin by mapping the intrinsic physicochemical attributes of each macrocycle family onto the design variables that govern their behaviour inside a periodic lattice (Section 2). Next, we examine how molecular recognition survives the thermodynamic demands of framework crystallization (Section 3). The core of the review (Section 4) examines whether material-level outcomes, selectivity, responsiveness, reactivity, and flux, can be traced back to the same small set of molecular-level coordinates. It further asks whether those coordinates account for not only which macrocycle–function pairings succeed, but why the others fail. We then evaluate the distance between molecular elegance and engineering reality (Section 5) and distil the conceptual architecture that unites the field (Section 6). The ambition throughout this work is to demonstrate that a macrocycle inside a lattice is neither a better macrocycle nor a better linker, but a fundamentally different object. Its function is not inherited from either parent but emerges from their combination.

2. Physicochemical profiles of macrocycles and their reticular compatibility

A meaningful classification of macrocycle-based MOFs benefits from a perspective that complements chemical nomenclature with physical reasoning. Organizing materials by macrocycle identity has provided the field with an essential structural foundation, and successive reviews have mapped this landscape with increasing completeness.[28,35,36,39,40] Building on this foundation, the present chapter asks a question that taxonomy alone is not designed to address: what molecular-level variables determine how a macrocyclic cavity behaves once embedded in a periodic lattice? The answer, we argue, traces to a compact set of physicochemical coordinates: cavity geometry, donor-atom character, conformational freedom, and exchange kinetics. These are variables whose governing role in host–guest complementarity has been recognized since Cram's formulation of the preorganization principle, but whose implications for reticular design remain largely unexamined.[41] To make these coordinates navigable, here we attempt to organize them along two axes, host–guest interaction mode and structural rigidity, whose intersection opens a continuous landscape rather than a discrete catalogue. The mapping indicates that these axes are not independent but physically coupled, so that the choice of where to operate along one constrains what is achievable along the other. The coupling is presented here as a qualitative trend rather than a quantified relationship. It is this coupling, and not macrocycle identity *per se*, that connects molecular design to material function.

2.1. Conformational adaptability: crown ethers as dynamic dampeners

Crown ethers, cyclic polyethers whose host–guest chemistry originates from Pedersen's discovery of dibenzo-18-crown-6, are distinguished among macrocyclic hosts by the conformational freedom of their flexible polyether backbone.[6,42–44] Low barriers to C–O–C torsional rotation permit the ring to contract around a cation, expand upon release, and return to its resting geometry with minimal hysteresis. This induced-fit cycle derives its selectivity from the match between cavity diameter and ionic radius (Fig. 2a).[14] This conformational softness is the source of both the crown ether's power and its peculiarity. Unlike rigid macrocycles that discriminate guests by exclusion, crown ethers discriminate by adaptation, reshaping themselves to amplify small differences in cation size into large differences in binding free energy.

What changes when this adaptive cavity is embedded in a crystalline lattice is not the recognition chemistry but its context. In solution, a crown ether's conformational response

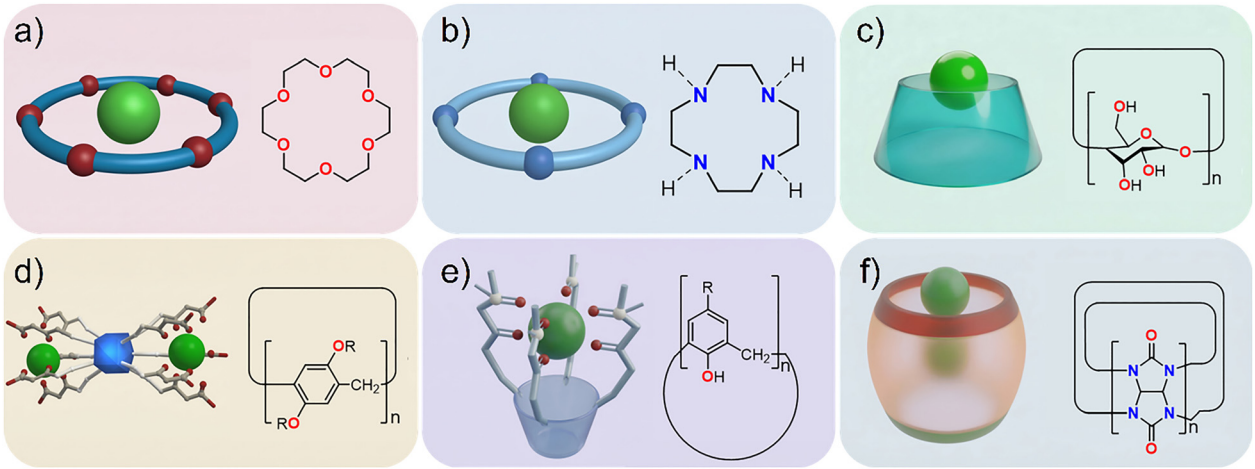


Fig. 2 Physicochemical profiles of six macrocyclic families and their design coordinates. (a) Crown ethers: soft polyether rings with O-donor cavities. (b) Aza-macrocycles: N-donor cyclic polyamines with programmable pendant arms. (c) Cyclodextrins: chiral truncated-cone oligosaccharides with hydroxyl-rich rims. (d) Pillararenes: rigid π-electron-rich tubes. (e) Calixarenes: mobile bowls with tuneable cone/partial-cone geometries. (f) Cucurbiturils: glycoluril barrels with carbonyl-fringed portals. In each panel, the 3D representation (left) shows the cavity geometry and host–guest interaction mode (green sphere = guest); the chemical structure (right) shows the repeating monomer unit.

is isotropic, it reorganizes equally in all directions, diluted by solvation and thermal averaging. In a framework, the lattice constrains which conformational pathways remain accessible and only the motions compatible with the local symmetry of the pore wall are permitted, while all others are prohibited.[45] The result is a directed conformational response, an induced fit that operates along a single coordinate defined by the lattice geometry. This directional constraint converts what is a modest thermodynamic preference in solution, into a sharp, switchable gate. For example, crown ethers in sub-nanochannels achieve Li^+/Mg^{2+} selectivity of 125 through charge-regulated conformational switching while crown ethers confined in octahedral MOF cavities accomplish complete ion dehydration during transport.[21,46] The lattice does not suppress the crown ether's softness; it directs it.

2.2. Aza-macrocycles: kinetic inertness and programmable metal-site chemistry

Replacing ethereal oxygens with nitrogen donors shifts the coordination profile of the macrocyclic cavity. Here, N-donors provide stronger σ-donation to transition metals, forming complexes of markedly higher kinetic inertness compared to the rapid, reversible ion exchange that characterizes crown ether–alkali metal pairs (Fig. 2b).[14] The two regimes are not a hierarchy but a complementarity with crown ethers excelling where fast turnover is needed and aza-macrocycles where sustained metal retention is required. Moreover, each ring nitrogen can bear a pendant substituent, carboxylate, pyridyl, or phosphonate, a chemical handle unavailable at ether oxygen positions.

This opens a design dimension specific to the aza-macrocycle platform allowing the ring to provide metal retention with the pendant arms providing framework connectivity while the axial coordination sites on the metal remain available for substrate binding or guest exchange.[47–49] A note on nomenclature: "aza-crown ether" strictly describes rings in which nitrogen replaces only some ethereal oxygens; when all are replaced, the resulting cyclic polyamines, cyclam (14-membered), cyclen (12-membered), TACN (9-membered), are properly termed aza-macrocycles. We use *aza-macrocycle* throughout as the inclusive term covering both mixed N/O and fully N-substituted rings, united by their derivation from the crown ether scaffold through progressive O → N replacement.

What makes this family distinctive in the MOF context is that nitrogen, unlike oxygen, is a junction simultaneously bonding to the ring, to the metal inside the cavity, and to a pendant substituent projecting outward. This triple connectivity gives each nitrogen atom a dual allegiance, inward to the guest, outward to the lattice and to whatever chemical information the pendant arm carries. Change the arm, and you change the electron density at the nitrogen, which changes the ligand field at the metal and the catalytic behaviour of the cavity, all without touching the ring geometry. The consequence is dimensional. A crown ether cavity is defined by one variable, ring size. An aza-macrocyclic cavity is defined by two orthogonal variables, ring size and pendant-arm identity, which can be varied independently.[23,50–52] This second axis is what allows a single aza-macrocyclic scaffold, without changing a single atom in the ring, to address fundamentally different chemical problems, simply by manipulating the pendant arm. While crown ethers select by adapting their shape to the guest, aza-macrocycles allow the chemist to adapt the cavity to the problem before the guest ever arrives.

2.3. Cyclodextrins: chirality and amphiphilicity from nature's toolkit

Cyclodextrins are cyclic oligosaccharides of six, seven, or eight α-1,4-linked D-glucopyranose units (α-, β-, γ-CD), produced industrially from starch at commodity scale. Two features inherited from the chiral glucose building blocks define the platform. First, intrinsic homochirality, with every stereogenic

 This journal is © The Royal Society of Chemistry 2026

centre set by an enzyme, requiring no resolution or asymmetric synthesis. Second, an amphiphilic truncated-cone architecture, in which a hydrophobic interior (4.7–8.3 Å depending on ring size) is ringed by a dense belt of hydroxyl groups on both rims (Fig. 2c).[16,53]

No other macrocycle in this review simultaneously offers chirality, water solubility, biocompatibility, and commodity availability. What the MOF lattice adds to this combination is periodicity, and this periodicity transforms each of these attributes. The homochirality that in solution produces a modest enantiomeric preference becomes, in a crystalline framework, a space-group constraint. As a result, any lattice built from CD nodes is forced into a non-centrosymmetric structure, converting achiral alkali-metal salts into homochiral frameworks in a single assembly step.[33,54–58] The hydrophobic cavity that in solution encapsulates one guest at a time becomes, in a periodic array, a volumetrically dense field of chiral recognition sites operating in concert, enabling enantioseparation performance that approaches commercial chiral HPLC columns.[19] The hydroxyl-rich exterior that in solution merely provides water solubility becomes, in the framework context, a continuous hydrogen-bonding network that sustains proton relay at conductivities 300-fold higher in oriented thin films than in randomly packed powders.[20] Finally, the biocompatibility that in solution enables pharmaceutical formulation becomes, in a porous crystalline scaffold, the basis for the only MOF family reported to date that is assembled entirely from food-grade, FDA-recognized components. The pattern is consistent. What cyclodextrins offer to reticular chemistry is not a new property but the crystallographic amplification of properties that the discrete macrocycle already possesses. The lattice does not change the CD; rather, it multiplies it.

2.4. Pillararenes and calixarenes: π-electron-rich cavities with tuneable geometry

Pillar[*n*]arenes (*n* = 5, 6), first reported by Ogoshi, and calix[*n*]arenes (typically *n* = 4–8) are aromatic macrocycles whose recognition logic differs fundamentally from the lone-pair-mediated chemistry of Sections 2.1 and 2.2.[59] Their cavities are lined not with lone pairs but with π-electron density. The aromatic panels create a region of high polarizability that binds guests through charge-transfer, CH–π, and π–π interactions rather than through direct coordination.[25] The two families share this electronic basis but differ in geometry. While pillararenes are rigid, symmetric tubes, calixarenes are conformationally mobile bowls that can lock into cone, partial-cone, or alternate conformations, each presenting a different cavity shape to the guest (Fig. 2d and e).[59,60]

What these macrocycles bring to the MOF lattice is a recognition mode rooted in electronic complementarity, operating orthogonally to the size-based and affinity-based discrimination available in conventional pore environments. An electron-deficient guest—a nitroaromatic, a quaternary ammonium, or a halogenated pollutant—interacts preferentially with the π-basic macrocyclic walls through donor–acceptor stacking, and is kinetically retarded or thermodynamically trapped while electronically neutral species pass through. This ''chemical-affinity brake'' shifts the separation paradigm from physical sieving to electronic selectivity, a capability particularly valuable for isomer separations where size and boiling point are nearly identical.[61]

The geometric difference between the two families maps onto a functional division. Pillararene tubes are rigid and symmetric. Their electron-rich channels provide uniform, directional host–guest contacts suited to continuous molecular transport and stimuli-responsive gating, the pillar[5]arene nanovalves of Section 4.2 exploit precisely this tubular geometry.[62] In contrast, calixarene bowls are conformationally adaptive. Their ability to switch between cone and alternate geometries provides an additional stereochemical variable that pillararenes lack. When this bowl is locked into a single conformation by the framework lattice, the result is a chiral pocket capable of asymmetric induction. The calixarene-capped Zn_4 MOF nanosheets that achieve up to 94% ee explore the lattice freezing of a calixarene conformation that free rotation in solution would average away.[24]

While there are stark contrasts, such as tube *versus* bowl, rigidity *versus* conformational switching, and directional transport *versus* stereochemical control, the two families are complementary precisely because they exploit the same electronic basis through different geometries.

2.5. Cucurbiturils: rigid barrels with ultra-high binding affinity

Cucurbit[*n*]urils (CB[*n*], *n* = 5–8, 10) are barrel-shaped macrocycles assembled from glycoluril units linked by methylene bridges.[17] Two properties distinguish them from every other macrocyclic host in this review.[63] The first is binding strength. CB[7] routinely achieves association constants of 10^9–10^{12} M^{-1} in water for diammonium guests, among the highest non-covalent affinities ever recorded.[64] The second is structural rigidity. The methylene bridges and glycoluril backbone create a cavity that neither contracts upon guest departure nor expands upon guest entry, a container that does not adapt to its contents but demands that its contents adapt to it (Fig. 2f).

This rigidity reverses the design logic of the flexible macrocycles in Sections 2.1–2.3. While crown ethers succeed through induced fit, cucurbiturils succeed through preformed geometric complementarity, accepting only guests whose size and charge distribution are already matched to the cavity before binding occurs. The carbonyl-fringed portals provide ion–dipole attraction that steers cationic guests into the barrel and the hydrophobic interior provides the thermodynamic driving force for staying. Release from this interior requires overcoming an energy barrier so steep that, in practical terms, what enters a cucurbituril often does not leave on any experimentally relevant timescale.

In the MOF context, this kinetic trapping transforms cucurbiturils from hosts into anchors.[65] In contrast to crown ethers which relay guests and cyclodextrins that exchange them, cucurbiturils immobilize them, stabilizing reactive intermediates, sequestering radical cation species, or locking charge-transport pathways into permanent configurations. CB[7]-polypyrrole assemblies delivered the highest areal capacitance (1533 mF cm^{-2})

among five macrocyclic hosts tested precisely because the cucurbituril's binding affinity prevents the radical cation intermediate from diffusing away from the electrode surface.[66] CB[6] carbonyl portals sustain proton relay and, upon iodine uptake, organize polyiodide chains into continuous charge-transport pathways, functions that depend on the portal geometry remaining invariant under operational conditions.[67] The same chemical inertness that makes cucurbiturils resistant to rim functionalization, and therefore incompatible with the linker strategies of Section 3.1, is what makes them exceptionally robust once confined within a framework lattice.

2.6. Beyond the classical: emerging macrocyclic platforms

The preceding sections cover the macrocycle families that dominate the current macrocycle–MOF literature. However, they do not exhaust the macrocyclic design space. A growing number of less-explored macrocyclic hosts have begun to appear in crystalline framework contexts, and a recent comprehensive survey catalogues their structural diversity and early functional demonstrations.[36]

Calix[4]pyrroles are pyrrole-based macrocycles whose NH groups point inward to provide a recognition mode absent from the families above. This allows for selective anion binding through convergent N–H···anion hydrogen bonds. The anion-specific affinity complements the cation selectivity of crown ethers and the neutral–guest binding of cyclodextrins, filling a gap in the host–guest charge landscape. Resorcin[4]arenes and pyrogallol[4]-arenes, deeper-cavity analogues of calixarenes, self-assemble with metal ions into metal–organic nanocapsules (MONCs) whose enclosed volumes exceed those of any macrocycle previously mentioned, enabling the confinement of multiple guest molecules or even nanoparticles within a single discrete cage. When these nanocapsules are further organized into extended lattices, the result is a hierarchical architecture with two nested levels of molecular recognition. One level is the cage within the framework and the next, the cavity present within the cage. Metal–macrocycle frameworks (MMFs) built from synthetic polyaza-macrocyclic ligands, such as the hexamine-based Pd framework reported by Shionoya, demonstrate that entirely new macrocycle topologies can direct framework assembly while simultaneously providing photochemically activatable metal sites along the channel walls.[68] Calix[4]resorcinarene-based MOFs have revealed unexpected electronic behaviour demonstrated by an eight-order-of-magnitude conductivity enhancement upon NO_2 adsorption driven by cooperative binding across the macrocyclic hydroxyl network. This creates a gas-responsive electronic switch with no precedent among the classical six families.[69]

What these emerging platforms share is not a common chemistry but a common message. The above families of Sections 2.1–2.5 represent well-explored peaks in a much larger landscape, and the valleys between them contain functional territory that reticular chemistry has barely begun to map.

2.7. Summary: design logic and cross-comparison

Each of the preceding profiles examined one family from both sides of the supramolecular–reticular boundary. The six established families were treated in turn, but the patterns that matter only appear when they are studied across families. This study proceeds first from what each family offers as a host, then to where a reticular lattice can take hold of it, and finally to what the resulting material makes of its chemistry once it is inside.

The supramolecular palette is broad, and Section 2.6 shows it is not closed. Read as a set of hosts, the families answer three questions, namely what fits the cavity, what holds it there, and how long it stays. On size, tabulated cavity and portal dimensions run from about 1.2 to 11.7 Å. Fit alone does not bind, however, and the second question is electronic. Cations and neutral guests dominate the palette, while directional anion recognition appears only with the calix[4]pyrroles of Section 2.6. The imbalance carries into applications, since cation capture fills Section 4.1 whereas high-affinity anion capture from water remains the unfilled regime that Section 5.2 assigns to future bambusuril frameworks. The third question, residence time, separates the families most sharply. An alkali ion leaves a flexible crown in microseconds, whereas a cucurbituril guest need not leave on any experimentally relevant timescale, and the clock is set jointly by donor identity, ring topology, and metal-ion inertness. Residence time, more than affinity, later decides which family suits cycling capture, catalysis, or permanent sequestration (Section 4.5). Affinity, the number attached to the second question, is also the least portable one. Reported values run from 10^1 to above 10^{12} M^{-1}, yet guest and solvent shift them as much as family does. 18-Crown-6 binds K^+ above 10^6 M^{-1} in methanol and near 10^2 M^{-1} in water, and crown or pillararene synthons register only 10^1 to 10^3 M^{-1} in acetone. Solution numbers therefore travel poorly. γ-CD binds 1-anthracenecarboxylate near 10^2 M^{-1}, too weak to preorganize a reactive pair, yet the $(\gamma\text{-CD})_6$ cages of CD-MOF-1 deliver 91% regioselectivity and 79% ee (Section 4.3.1). Immobilization supplies the organization that affinity cannot, and the comparisons of this review are correspondingly qualitative rather than quantitative.[7]

From the reticular side, the profiles sort the families by where a rigid lattice-bonding handle can be installed, and handle position sets which roles are available rather than one fixed role. Cyclodextrins combine high symmetry, a large footprint, and metal-binding rims, so they serve as nodes and become the load-bearing fabric of their lattices. Aza-macrocycles, pillararenes, and calixarenes accept rigid arms at nitrogen or at the rim, appearing as linkers in VPI-100 and MMCF-2 or as cluster caps in the calixarene Zn_4 nanosheets. Crown ethers carry no handle at their ether oxygens, yet benzo-fusion supplies one, and the same family therefore appears as carboxylate linkers in ZJU-X100 and NKU-300, as an annulated passenger in MOF-1001, and as threaded wheels in MORFs. Cucurbiturils resist rim functionalization and enter as templated guests, coordination-polymer components, or threaded wheels. Role and synthetic route are therefore correlated rather than dictated, as Section 3 develops.

Across the six families, the lattice does not erase the property that resists integration. It relocates it. Crown ether flexibility is bypassed by rigid arms in MOF-1001, yet preserved when the same ring enters as a threaded wheel or an

 This journal is © The Royal Society of Chemistry 2026

Table 1 Macrocyclic building blocks for reticular architectures[a]

Macrocycle	Interaction mode	Rigidity	Cavity	Lattice-bonding handle	Functional signature
Crown ethers	Labile cation–dipole; induced fit	Low	O-donor, 1.2–5.0 Å (12-crown-4 to 24-crown-8)	None at ether O; rigid carboxylate arms installed by benzo-fusion	Adaptive gating, reversible ion transport
Aza-macrocycles	σ-Coordination (kinetically inert M–N)	Low–moderate; arm-tuneable	N-donor, ∼2.0–4.0 Å (TACN, cyclen, cyclam)	N-pendant arms	Site-isolated catalysis, redox mediation
Cyclodextrins	Hydrophobic encapsulation + H-bonding	Moderate	Amphiphilic cone, 4.7–8.3 Å	Rim hydroxyls coordinate alkali cations directly	Chiral recognition, biocompatible delivery
Pillararenes/ calixarenes	π-Cavity: charge-transfer, CH–π/π–π	High (pillararenes)/ moderate (calixarenes)	π-Rich tube or bowl, 3.0–11.7 Å	Bis-carboxylate/dipyridyl arms; upper-rim carboxylate/sulfonate; lower-rim O as cluster caps	Electronic discrimination, gating, asymmetric induction
Cucurbiturils	Ultra-high-affinity ion–dipole + hydrophobic	Very high	Carbonyl portal barrel; cavity 4.4–8.8 Å (CB[5]–CB[8]), portals ≈ 2.4–6.9 Å	Rim functionalization resisted; portal carbonyls coordinate metals	Kinetic trapping, guest immobilization

[a] Internal diameters are based on reported cavity sizes for crown ethers,[6,14] cyclodextrins,[16] calix[4]–[8]arenes and pillar[5]/[6]arenes,[25,59,60] and cucurbituril cavities/portals.[17,64] For aza-macrocycles, ring size is given because the cavity size is metal-dependent.

encapsulated guest. Cyclodextrin symmetry blocks the linker route and becomes the basis of the node route. Cucurbituril inertness excludes rim grafting and qualifies the barrel for templating. Aza-macrocycle, pillararene, and calixarene handles sit clear of the cavity, so their recognition chemistry survives integration intact. The recurring pattern is therefore not the conversion of a liability into a function. It is selection. Each lattice allows one facet of a macrocycle's chemistry to be expressed and leaves the rest dormant.

Table 1 gathers both sides of this summary. It locates the six established families within a single design space, with interaction mode and cavity rigidity as its coordinates, and lists for each family the cavity dimensions, lattice-bonding handles, and functional signatures developed above. The table also makes the central constraint visible at a glance. Soft macrocycles cluster in the weak and reversible corner, while rigid macrocycles cluster in the strong and quasi-irreversible corner, for the entropic reasons given above. Macrocycle selection is therefore never a free choice along two independent coordinates. It is a constrained walk along a diagonal that trades adaptability for affinity, with crown ethers at one end, cucurbiturils at the other, and aza-macrocycles standing partly aside through their metal-set exchange kinetics. The art of macrocycle–MOF design lies in choosing where on this diagonal to operate. The opportunity, as the platforms of Section 2.6 suggest, lies in macrocycles that leave it entirely. Quantifying the diagonal, so that a target function could be translated into a position on it, remains an open problem for the field.

3. Synthetic strategies: reconciling macrocyclic complexity with reticular order

Reticular chemistry assembles crystalline frameworks from geometrically predictable building blocks with minimal residual entropy.[4] Macrocyclic chemistry does the opposite and designs cavities whose function depends on conformational richness, rotational freedom, and the ability to reorganize around a guest.[7] Forcing these two traditions into the same crystal is the central synthetic challenge of this field and the challenge is not singular. Depending on the macrocycle, the challenge may manifest as a conformational entropy problem (flexible crown ethers resisting lattice periodicity) or a symmetry mismatch (high-symmetry cyclodextrins incompatible with ditopic linker paradigms). It may also appear as a chemical fragility (thermally sensitive hosts degrading under solvothermal conditions) or a dynamics-versus-order dilemma (mechanically mobile wheels demanding crystallographic rigidity). Each manifestation requires its own resolution.

We survey and organize these strategies not by the macrocycle's eventual function, but by the temporal relationship between macrocycle introduction and the lattice-forming event. These include direct assembly, indirect assembly, sequential functionalization, and other emerging modalities (Fig. 3). Each of these strategies has its own set of strengths and challenges and will be discussed in more detail below.

3.1. Direct assembly: covalent integration of macrocycles as framework building blocks

Reticular chemistry derives its predictive power from the geometric regularity of its building blocks. Here, a rigid, shape-persistent linker connected to a well-defined inorganic node produces a periodic lattice whose topology can be designed before a crystal is grown.[4,70] Macrocycles, by default, violate this premise. Their conformational flexibility, multidirectional donor-atom arrays, and high internal symmetry make them geometrically ambiguous, capable of coordinating metals in multiple orientations, none of which may correspond to the single, well-defined connectivity that reticular design demands.[18] Direct assembly solves this problem before it arises by chemically converting the macrocycle into a geometrically predictable building block prior to solvothermal crystallization so that the framework inherits molecular recognition without sacrificing crystallographic order.

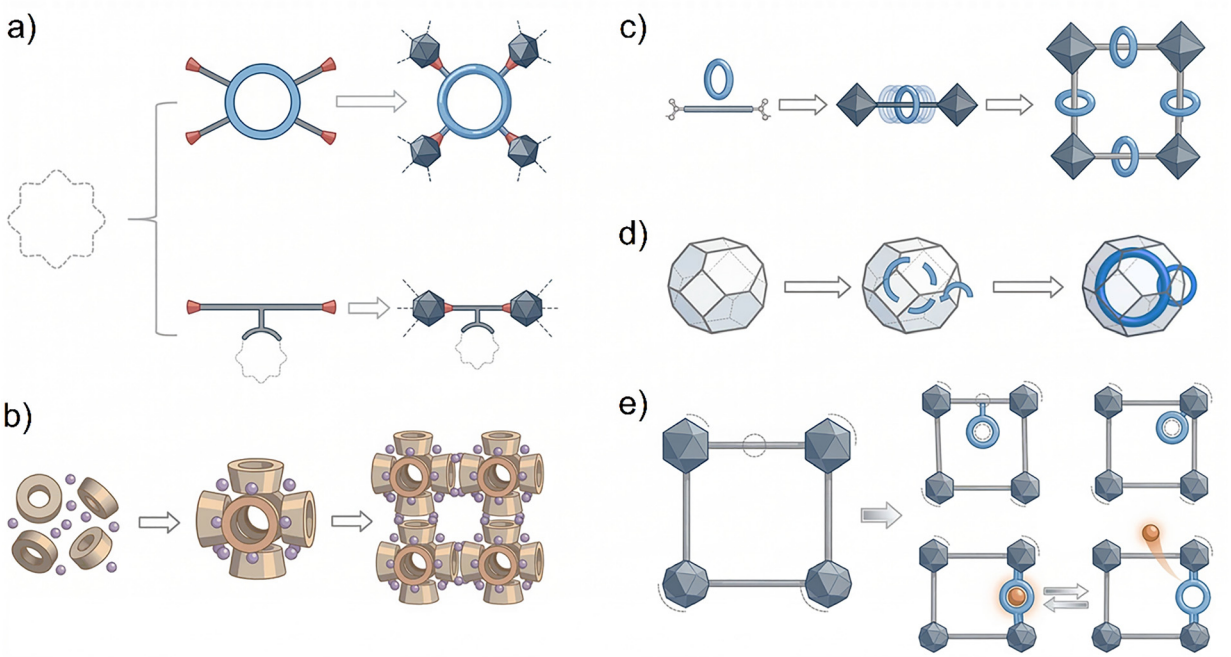


Fig. 3 Schematic overview of the five representative strategies for integrating macrocycles with reticular lattices. (a) Direct assembly, ligand approach: the macrocycle acts as a multitopic linker bearing rigid coordination arms (top) or as a topologically passive pendant on a linear strut (bottom). (b) Direct assembly, node approach: high-symmetry macrocycles coordinate metal cations through their rims, forming polyhedral SBUs. (c) Mechanical interlocking: a macrocyclic wheel is threaded onto an axle ligand to give a [2]rotaxane strut before assembly. (d) Ship-in-a-bottle encapsulation: the framework crystallizes around a macrocyclic template too large to escape the cage windows. (e) Sequential functionalization: macrocycles are installed into a pre-formed scaffold under mild conditions.

From this group, two sub-strategies emerge that are distinguished by the reticular role assigned to the macrocycle. First, in the ligand approach, rigid coordination arms are grafted onto the macrocyclic scaffold, transforming it into a multitopic linker that bridges inorganic nodes. The macrocycle's conformational freedom is suppressed by the appended arms, and the framework topology is governed by linker geometry as in any conventional MOF (Fig. 3a). The second, node approach, leverages the macrocycle's native symmetry and dense donor-atom array. Here, the macrocycle coordinates metal cations through its own rim, forming high-connectivity secondary building units (SBU) without requiring external rigidification. The first strategy domesticates the macrocycle by imposing an external geometry while the second embraces the geometry the macrocycle already possesses. The approach chosen depends on whether the macrocycle is more naturally a linker or a node, a distinction dictated by its symmetry, steric footprint, and donor-atom density.

3.1.1. The ligand approach: rigidity engineering through covalent appendage. The central chemical challenge is conformational entropy.[71] In solution, conformationally flexible macrocycles, crown ethers, aza-macrocycles, and their derivatives, undergo rapid interconversion among multiple low-energy states. If introduced directly into a solvothermal synthesis without geometric pre-organization, this conformational heterogeneity frustrates the establishment of periodic lattice order, often yielding amorphous or non-porous products.[18] Two complementary rigidification tactics have emerged to circumvent this problem.

The first appends the intact macrocycle as a pendant decoration on an otherwise rigid linker backbone, so that the macrocyclic cavity is carried into the framework as a functional passenger without bearing any topological load. In MOF-1001, a bis-*p*-phenylene-34-crown-10 macrocycle is annulated onto a linear dicarboxylate strut, so that the rigid phenylethynyl arms define the framework connectivity while the crown ether core is locked into a symmetric conformation within the pore wall (Section 4.1.1); the same annulation strategy was subsequently used to carry a Cram-type bisbinaphthyl[22]crown-6 into a Zn_4O-based framework, installing enantiopure chiral recognition sites along the struts.[72] Because the topological burden falls entirely on the aromatic backbone, the macrocycle's conformational flexibility becomes irrelevant to lattice formation, an elegant circumvention of the entropy problem rather than a head-on confrontation with it. The second tactic inverts this hierarchy. This tactic uses rigid aromatic arms, benzoate, isophthalate, or pyridyl groups, that are covalently grafted onto the macrocyclic rim, transforming the macrocycle itself into a directional linker. The arms serve a dual function by providing coordination termini for metal-node binding and simultaneously restricting the conformational phase space of the macrocyclic backbone. The geometric prerequisite is that the bite angle imposed by the grafted arms must match the linker geometry required by the target topology. For example, in the VPI-100 family dicarboxylate-functionalized cyclam linkers bridge Zr_6 clusters in a UiO-type topology, with the metallocyclam sites positioned at crystallographically defined locations along the framework strut.[23] MMCF-2

 This journal is © The Royal Society of Chemistry 2026

applies the same strategy to cyclen, grafting four methylbenzoate arms onto the tetraaza ring to generate a tetratopic linker directing an nbo-topology Cu framework.[50] The approach generalizes beyond aza-macrocycles. Pillararenes bearing bis-carboxylate arms function as linear linkers that orient their electron-rich tubular cavities directly into the channel space. Calixarenes capped with carboxylate or sulfonate groups on the upper rim serve as multitopic linkers, directing three-dimensional assembly with bowl-shaped cavities lining the pore walls.[24,61] In both tactics an overarching principle emerges: channelling the macrocycle into a crystallographically compliant role, whether as a topologically passive passenger or an active load-bearing linker. In this way, reticular order is achieved without sacrificing the chemical availability of the macrocyclic cavity.

3.1.2. The node approach: exploiting intrinsic macrocyclic symmetry. Certain macrocycles, most notably cyclodextrins, resist the ligand approach because their large steric footprint, multidirectional hydroxyl arrays, and high rotational symmetry (C_6, C_7, or C_8 for α-, β-, γ-CD) are fundamentally incompatible with simple ditopic or tetratopic linker paradigms. Rather than fighting this geometric mismatch, the node approach embraces it. In this approach, the macrocycle's intrinsic symmetry and dense donor-atom array are exploited to coordinate metal cations directly, forming high-symmetry SBUs in which multiple macrocycles self-organize into polytopal clusters (Fig. 3b).

In CD-MOF-1, for example, six γ-CD units coordinate K^+ cations through their hydroxyl-rich toroidal rims to form cuboidal $(\gamma\text{-CD})_6$ clusters. These hollow cubic SBUs propagate in a body-centred cubic array, generating a framework in which the cyclodextrins are not guests filling pre-existing pores but the structural fabric of the lattice itself.[73,74] This distinction is chemically consequential. Because each CD unit is a load-bearing element of the framework, the density of chiral, hydrophobic recognition sites per unit volume far exceeds what post-synthetic loading of CDs into a conventional MOF void could achieve. Replacing the alkali metal cation with Rb^+ or Cs^+ produces CD-MOF-2 and CD-MOF-3, respectively, confirming that the $(\gamma\text{-CD})_6$ cubic SBU is a robust structural motif tolerant of systematic metal-node variation.[33,75] More recently, the extension to β-cyclodextrin, whose lower C_7 symmetry and smaller cavity had long been considered incompatible with the cubic assembly, has yielded new framework topologies with both Na^+ and K^+. This expands the accessible structural landscape beyond the classical γ-CD series.[76]

The node approach succeeds where the ligand approach cannot. This is a result of aligning the synthetic strategy with the macrocycle's native geometry rather than imposing an external one. The macrocycle need not be stiffened, arm-extended, or conformationally locked; it need only be matched with a metal cation whose coordination preferences are compatible with the donor-atom arrangement already present on the macrocyclic rim.

3.2. Indirect integration: ship-in-a-bottle encapsulation and mechanical interlocking

While strategies in the prior section ask the macrocycle to become a building block, to subordinate its identity to the geometric demands of a lattice, the strategy of indirect integration refuses this subordination. When a macrocycle cannot be engineered into a linker or a node because it lacks derivatizable sites, directional coordination groups, or topologically compatible geometry, the alternative is not to abandon it but to change the terms of integration. By forming the lattice around the macrocycle, or having a strut thread through it, confinement can be achieved by topology or geometry rather than by covalent obligation.[18] The macrocycle enters the framework intact, unmodified, owing nothing to the lattice, and yet is inseparable from it. What emerges is a composite held together not by shared bonds but by shared space; a relationship closer to symbiosis than to construction.

3.2.1. Thermodynamic templating: ship-in-a-bottle encapsulation. The chemical basis of this approach lies in the sequence of bond-forming events during crystallization. In a conventional solvothermal synthesis, metal ions and organic linkers condense into a lattice whose topology is governed by the coordination geometry of the SBU and the directionality of the linker. When a macrocycle is introduced into the precursor mixture, its steric bulk and host–guest affinity can redirect this self-assembly, with the framework crystallizing around the macrocyclic template. The result is a composite in which the macrocycle occupies a cage whose window apertures are smaller than its own cross-section, permanently trapping it in a ship-in-a-bottle configuration (Fig. 3d). The macrocycle thus shifts from being a passive guest filling pre-existing voids to an active structure-directing agent whose size and shape encode the local topology of the cage that encloses it.

This principle is particularly consequential for cucurbiturils, whose extreme chemical inertness and poor covalent derivatizability preclude the aforementioned ligand approach, but make them ideal encapsulation candidates. The ''bottle-around-ship'' synthesis of MC5@MIL-100(Fe) demonstrates this logic. When decamethylcucurbit[5]uril is present during the mechanochemical assembly of the MIL-100 framework from $Fe(NO_3)_3$ and trimesic acid, the cucurbituril becomes permanently confined within the mesoporous cages. The MIL-100 window apertures ($\sim$8.6 Å) are smaller than the MC5 outer diameter, preventing leaching under operational conditions.[77] The resulting hybrid exhibits enhanced methane uptake and selective Pb^{2+} capture at low concentrations, functions attributable to the cucurbituril's carbonyl-portal binding sites that the empty MIL-100 framework does not possess. The framework literally provides the container and the macrocycle provides the chemistry, creating a division of labour that preserves the strengths of both components without demanding that either be chemically modified.

The generality of this approach depends on a single geometric criterion. The macrocycle must be larger than the framework window but smaller than the framework cage. When this criterion is met, any macrocycle–MOF pair becomes, in principle, accessible to thermodynamic templating, a far less demanding synthetic requirement than the covalent arm-grafting and symmetry-matching of the direct assembly strategies we discussed in Section 3.1.

3.2.2. Mechanical interlocking: rotaxane and catenane frameworks. The second sub-strategy of mechanical interlocking

addresses a distinct challenge of how to introduce molecular-scale dynamics, translational shuttling, rotational pirouetting, into a crystalline lattice without sacrificing long-range structural order. The chemical solution is topological confinement through this mechanical bonding (Fig. 3c). In the metal–organic rotaxane framework (MORF) platform, a large crown ether wheel (typically 24-crown-8) is threaded onto a linear axle ligand, a bis-pyridinium or bis-benzimidazolium strut, before coordination to metal nodes.[78–84] The threading event converts the macrocycle into a mechanically interlocked captive. Its steric bulk is localized along the linker shaft and segregated from the node-binding termini, allowing the metal SBUs to assemble into predictable high-symmetry topologies, including interpenetrated and non-interpenetrated variants, as though connected by simple linear struts.[85] The chemical consequence of mechanical rather than covalent confinement is the preservation of internal degrees of freedom within the rigid lattice. Because the wheel is not covalently fixed to the axle, it retains both rotational (pirouetting) and translational (shuttling) mobility in the solid state. Variable-temperature solid-state ^{2}H NMR has quantified these dynamics and demonstrated that pirouetting barriers are systematically tuneable by varying the crown ether ring size, from the tighter 22-crown-6 to the looser 26-crown-6. This produces a family of frameworks (the UWDM series) in which lattice rigidity and molecular motion are independently controlled.[22,82]

This decoupling of lattice order from molecular dynamics has enabled progressively sophisticated mechanical behaviour. Solid-state molecular shuttles, in which the wheel translates between two inequivalent recognition sites on an asymmetric axle, have been achieved within crystalline MORFs. The positional switching underlying molecular machines can thus operate in the constrained environment of a coordination network.[86–88] In a complementary approach, catenane-based frameworks, in which interlocked rings form the lattice backbone itself, exhibit unusual elastic mechanical properties arising from inter-ring sliding under applied stress.[89] Together, these developments establish mechanical bonding as a general resolution to the order-versus-dynamics conflict; the framework provides crystallographic periodicity, while the interlocked macrocycle provides the molecular-level adaptive behaviour that rigid covalent bonding cannot deliver.

3.3. Sequential functionalization: temporal decoupling of lattice construction and macrocyclic activation

The previous strategies discussed introduce the macrocycle at the moment of framework crystallization, either as a building block or as a template present in the reaction mixture. Sequential functionalization removes this simultaneity.[90] When the thermal or chemical conditions required for lattice crystallization are incompatible with the macrocycle's integrity, the resolution is temporal decoupling: construct the scaffold first, introduce the macrocycle second, with each step optimized under its own conditions (Fig. 3e). Zr-based MOFs, for example, demand temperatures exceeding 120 °C and strongly acidic modulators that would degrade many macrocyclic hosts.[11] However, incompatibility is not the only motivation. Even when one-pot assembly succeeds, sequential approaches can offer advantages that direct co-crystallization cannot. This decoupling offers distinctive advantages: the ability to install macrocycles into lattice positions inaccessible from the outside, or to exchange one macrocyclic linker for another without rebuilding the framework. It further allows the choice of intra-cavity metal to be decoupled from the identity of the SBU cation. Together, these achieve a modularity that one-pot synthesis excludes.

3.3.1. Post-synthetic exchange and modification. The chemical logic of post-synthetic methods is straightforward. First, construct a robust, highly crystalline scaffold using simple, thermally stable linkers under harsh solvothermal conditions to guarantee structural integrity. Next, introduce macrocyclic functionality under mild conditions that preserve the macrocycle's chemical identity. This two-step decoupling resolves the fundamental tension between the high thermal budget required for framework crystallization and the chemical fragility of most macrocyclic hosts.

Two mechanistically distinct routes to accomplish these goals are available. The first is post-synthetic modification (PSM), which grafts new functionality onto the pre-formed scaffold through covalent bond formation at pendant reactive handles, azide, amine, or hydroxyl groups, pre-installed on the framework struts. The broader PSM toolkit, established through click chemistry, amide coupling, and related transformations on frameworks such as IRMOF-3 and UiO-66-NH_2, provides a versatile platform for introducing functional groups of arbitrary complexity.[11] Alternatively, post-synthetic exchange (PSE) instead replaces labile linkers with functional linkers through diffusion-driven substitution in solution, exploiting the thermodynamic preference for the incoming ligand at the metal node.[91] Both approaches have been extended to macrocyclic components. The installation of a bistable [2]catenane, a mechanically interlocked macrocyclic switch, into the mesoporous channels of NU-1000 *via* solvent-assisted ligand incorporation (SALI) shows that even sterically demanding, topologically complex macrocyclic architectures can be accommodated within a pre-formed Zr_6-based scaffold.[92] Solvent-assisted ligand incorporation (SALI), which anchors carboxylate or phosphonate functionalities to coordinatively unsaturated Zr_6 nodes, offers a complementary handle for tethering macrocycle-bearing ligands to the SBU rather than exchanging framework struts.[93]

The principal limitation shared by all post-synthetic routes is the potential for incomplete exchange or inhomogeneous spatial distribution of the macrocyclic component. This introduces defect heterogeneity and can compromise the periodicity of functional sites. Achieving high loading with uniform distribution requires careful optimization of solvent polarity, exchange temperature, macrocycle concentration, and diffusion kinetics, parameters for which systematic studies remain scarce in the macrocycle–MOF context.

3.3.2. Pre-metalation, demetalation, and temporal decoupling of cavity activation. For many aza-macrocyclic MOFs, the macrocyclic cavity must contain a specific metal ion to deliver catalytic, redox, or sensing function. In favourable cases, where

 This journal is © The Royal Society of Chemistry 2026

the intra-cavity metal and the SBU-forming cation occupy distinct coordination environments and do not compete, pre-metalated macrocyclic complexes can be co-assembled directly with framework nodes in a one-pot solvothermal synthesis.[94] This is the dominant route and is illustrated in both the VPI-100 family (Cu(II)– or Ni(II)–cyclam with Zr_6 clusters) and MMCF-2 (Cu(II)–cyclen with Cu paddlewheel nodes). Both frameworks incorporate pre-formed metallomacrocyclic complexes that crystallize into ordered lattices; in the VPI-100 family, where the intra-cavity metal (Cu(II) or Ni(II)) differs from the Zr_6 node, this proceeds without cross-contamination between the macrocyclic and nodal metal sites.[23,50]

The deeper synthetic opportunity, however, lies in the modularity that pre-metalation enables. The VPI-100 synthesis reveals that the Cu(II)–cyclam complex can be demetalated by refluxing in concentrated HCl, yielding a free-base cyclam dicarboxylate linker. This free-base is then re-metalated with $NiCl_2$ and assembled into VPI-100(Ni) under otherwise identical solvothermal conditions. The demetalation–re-metalation sequence establishes a single macrocyclic scaffold as a universal platform for installing different catalytic metals, producing isostructural frameworks whose function is switched simply by changing which metal occupies the cavity. Given that VPI-100 retains crystallinity across a wide pH range, performing such metal exchange directly on the assembled framework, stripping and re-loading the cavity metal without dismantling the lattice, is a plausible next step. Explicit demonstration, however, remains lacking. The result is a multi-tier temporal separation where metalation defines the catalytic identity, crystallization establishes the lattice, and post-synthetic guest binding at the labile axial sites activates the catalytic cycle. Three independently tuneable stages are decoupled within a single synthetic workflow.

3.4. Emerging synthetic modalities

Sections 3.1 through 3.3 offer increasingly sophisticated answers to the same question: how to reconcile macrocyclic host–guest chemistry with the demands of framework crystallization.[95] However, most implementations of these strategies share a premise: that the macrocycle must, at some stage, coexist with a solvothermal environment. There, solvent molecules compete for the cavity, modulators may degrade the host, and prolonged heating may erase the conformational definition that makes the macrocycle worth incorporating. The emerging strategies below challenge this premise directly. Rather than engineering the macrocycle or the sequence to survive solvothermal conditions, they change the conditions themselves.

Mechanochemical synthesis (ball milling, liquid-assisted grinding) assembles the framework in the near-absence of solvent, eliminating cavity poisoning at its source. "Wash-free" mechanochemical CD-MOF synthesis produces crystalline product in five minutes with a BET surface area of 906 $m^2 g^{-1}$ in quantitative solid yield, comparable to conventional vapour-diffusion material but with zero solvent waste.[96] The same solvent-free principle underpins the cucurbituril encapsulation discussed in Section 3.2.1, where the absence of coordinating solvent protects the carbonyl portals during lattice assembly. Microwave-assisted synthesis offers a complementary solution. By compressing the heating profile into minutes, it incorporates thermally sensitive macrocyclic linkers before decomposition becomes competitive, producing CD-MOF nanocrystals with controlled size distributions inaccessible *via* slow conventional heating.[97] What unites these approaches is a design logic absent from Sections 3.1–3.3, that is, protecting the macrocyclic cavity not by chemical modification or temporal sequencing, but by removing the hostile environment altogether.

3.5. Summary

Every synthesis reviewed in this chapter is a negotiation between two forms of order: the translational symmetry the lattice demands and the rotational freedom the macrocycle requires. Direct assembly settles it for the lattice, stiffening and arming the macrocycle; indirect integration settles it for the macrocycle, the lattice forming around its bulk or through its ring. Sequential methods let each party establish itself in solitude before introducing them under controlled conditions, and the emerging solvent-free approaches remove the arena of conflict altogether.

No strategy is universally superior because no macrocycle is universally compliant. The cyclam chemistry that accepts carboxylate arms without complaint would shatter a cucurbituril. The cyclodextrin that self-assembles into cubic SBUs from aqueous KOH would never survive the acidic modulator bath that a Zr_6 node requires. Each macrocycle arrives at the framework with its own terms, and the art of macrocycle–MOF synthesis is not the mastery of one method but the judgement to know which terms can be met and which must be refused.

4. From molecular recognition to material function: applications of macrocycle-MOF systems

A macrocyclic cavity is, at its foundation, a pre-organized decision. Its donor atoms are arranged to accept one guest and reject all others before the guest even arrives.[7] This principle, Cram's preorganization, has powered half a century of solution-phase supramolecular chemistry. Yet a single macrocycle in solution makes a single decision, once. When the same cavity is incorporated into a metal–organic framework, the reticular lattice replicates that decision at every crystallographically equivalent site, converting a molecular recognition event into a material property.[18] Critically, the lattice introduces phenomena that the discrete macrocycle cannot access, including cooperative binding across adjacent cavities, long-range charge relay through continuous donor-atom networks, and periodic chiral environments that enforce enantioselectivity without conformational averaging. Here, the macrocycle provides the selectivity while the framework provides the amplification.

The four functional domains examined below are not independent applications but successive stages of a single host–guest narrative. Affinity-driven capture (Section 4.1) asks: which guest does the cavity prefer? Exploiting equilibrium selectivity for separation. Adaptive gating and sensing (Section 4.2) asks: what

happens to the cavity when the guest binds? Harnessing conformational and electronic responses. Catalysis (Section 4.3) asks: can binding accelerate a chemical transformation? Coupling recognition to reactivity. Transport (Section 4.4) asks: can the cavity hand its guest to the next site? Sustaining directional flux across the lattice. In sequence, these four questions trace the complete lifecycle of a guest molecule within a macrocyclic framework, from initial capture, through responsive gating, to chemical transformation, and finally onward transport.

4.1. Affinity-driven capture: macrocyclic frameworks for precise separation

Separation is essentially a thermodynamic sorting problem: a mixture is resolved into its components by exploiting differences in the free energy of interaction between each component and a selective medium.[98–102] Porous materials (zeolites, activated carbons, and conventional MOFs alike) achieve selectivity through a spectrum of mechanisms ranging from size exclusion and shape sorting to open-metal-site coordination and linker-based hydrogen bonding.[103] These strategies are powerful for many separations, yet they share a common limitation in that the binding site is typically a single functional group or coordinatively unsaturated metal whose interaction with the guest is monovalent and geometrically underdefined. Macrocyclic hosts overcome this limitation through preorganization: a three-dimensional, multivalent donor-atom array locked into a defined cavity geometry prior to guest encounter. The pre-organized array drastically reduces the entropic penalty of binding and enables simultaneous, cooperative interactions with a single target in a stereochemically precise manner.[18,104] This distinction is not merely quantitative but mechanistic. A pendant amine or open metal site binds any species that satisfies a single energetic criterion. By contrast, a crown ether cavity rejects Na^+ in favour of K^+ through optimal ion–dipole complementarity, a cyclodextrin pocket discriminates one enantiomer from its mirror image *via* multipoint chiral recognition, and a pillar[5]arene portal selects a guest by both shape and electronic character simultaneously.[19,100,105] Embedding these molecular-level sorting engines within a MOF lattice marries the chemical precision of the macrocycle with the high surface area, permanent porosity, and long-range periodicity of a crystalline framework. The macrocycle dictates what is recognized, and the framework determines how many binding events occur per unit volume and how fast. The functional niche of each macrocycle class follows directly from the two axes established in Section 2. Interaction mode sets which guests a cavity recognizes, while structural rigidity modulates the exchange kinetics that govern capture-versus-release behaviour.[106–108]

4.1.1. Ion capture and radioactive waste remediation. Affinity-driven capture is not confined to ions: a cucurbit[6]uril simply encapsulated within a MOF, for example, already enhances CO_2 separation.[109] It was with ions, however, that macrocycles first demonstrated selective capture within a MOF lattice: bis-*p*-phenylene-34-crown-10 was integrated into the struts of a cubic Zn_4O-based framework (MOF-1001), giving an ordered array of crown ether recognition sites in permanent channels.[110,111] This work established a key design principle: embedding crown ethers within rigid, porous architectures enhances cation-capture selectivity beyond that of the free macrocycle. The enhancement arises because the framework channel restricts the cation approach geometry to the optimal face of the macrocyclic ring, eliminating the diffusion-averaged binding that dilutes selectivity in homogeneous solution. Since then, crown ether and related macrocyclic MOFs have been shown to selectively bind a variety of cations, including K^+, Li^+, and Na^+/K^+ in competitive monovalent-ion separations. Meanwhile, calixarene-based 2D MOF nanosheets have extended the approach to heavy-metal pollutants such as Pb^{2+} and trace UO_2^{2+}.[39,42,100,112–115]

The most compelling application lies in radioactive waste remediation. Nuclear waste streams contain ^{90}Sr ($t_{1/2}$ = 28.8 years), ^{137}Cs ($t_{1/2}$ = 30.17 years), and ^{226}Ra ($t_{1/2}$ = 1600 years), each requiring separation from competing cations at 10^3–10^6-fold excess. Conventional sorbents struggle with slow kinetics and poor selectivity. Crown ethers possess intrinsic cavity-size selectivity (18-crown-6 for Sr^{2+}, 24-crown-8 for Cs^+), but deployed in solution they are difficult to recover and reuse. Embedding them as struts within zirconium MOFs addresses both limitations as the framework pre-organizes macrocycles along permanent channels while strong Zr–carboxylate bonding ensures chemical robustness.[116–119]

Li, Xiao, and co-workers realized this design by incorporating 18-crown-6 and 24-crown-8 into two zirconium MOFs, ZJU-X100 and ZJU-X102.[106] Both frameworks retain crystallinity in boiling water, across a pH range from 0–11, and in concentrated HCl. Sorption equilibrium is reached within 1 minute, with capacities of 149 mg g^{-1} (1.70 mmol g^{-1}) for Sr^{2+} and 121 mg g^{-1} (0.91 mmol g^{-1}) for Cs^+, advancing significantly beyond the benchmark established by the zinc-based SNU-200 (44 mg g^{-1}, 0.50 mmol g^{-1}).[112] Single-crystal diffraction provided the first atomic-level proof that cations reside inside the crown ether cavity within a MOF: Sr^{2+} coordinates six ether oxygens in a twisted hexagonal-pyramidal geometry, while Cs^+ occupies the 24-crown-8 centre in an eight-coordinate complex (Fig. 4a and d).

ZJU-X100 maintains high Sr^{2+} selectivity even with 100-fold excess competing ions, confirming that channel-confined cavity recognition suppresses the competitive binding inherent in solution-phase crown ethers (Fig. 4). Pushing further, the same group constructed an anionic crown ether framework whose negatively charged backbone electrostatically pre-concentrates cations, achieving a high Sr^{2+} capacity ($>$200 mg g^{-1}, $>$2.3 mmol g^{-1}) with Sr/Na selectivity exceeding 10^3 under simulated nuclear waste conditions (Fig. 5a–c).[120] The labile binding enables rapid capture–release cycling essential for high-throughput decontamination (Fig. 5).

The most ambitious target, $^{226}Ra^{2+}$, demands ultra-high affinity rather than recyclability owing to its extreme half-life and radiotoxicity. Wang, Yin, Xiao, and co-workers addressed this by engineering ZJU-X102-SO_4 through post-synthetic sulfate installation (Fig. 6a).[121] Each 24-crown-8 strut is flanked by a proximal sulfate on the Zr_6 cluster, integrating size-selective crown ether encapsulation with strong sulfate chelation inspired by the low K_{sp} of $RaSO_4$. DFT and EXAFS confirm cooperative binding, indicating simultaneous engagement of ether oxygens, sulfate oxygens, and sulfur in a multi-shell geometry, with binding energies double

 This journal is © The Royal Society of Chemistry 2026

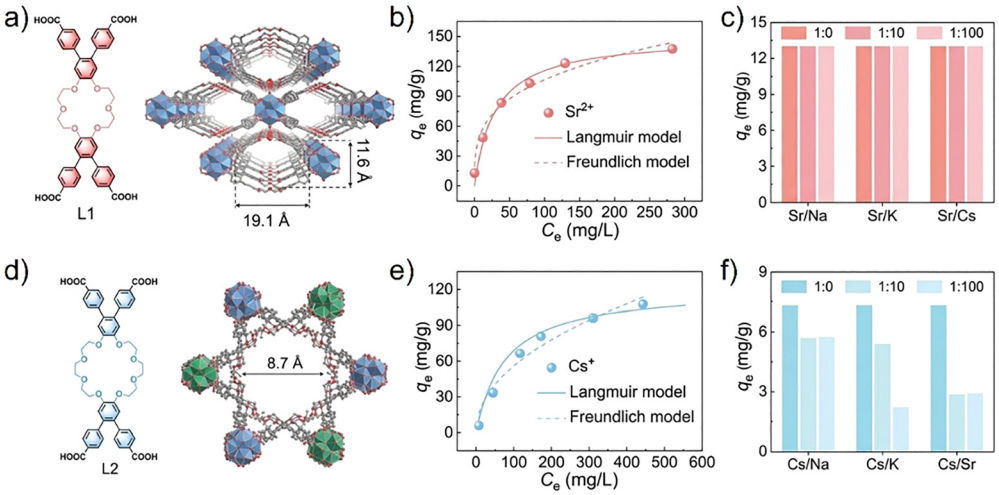


Fig. 4 Crown ether-functionalized Zr-MOFs for selective radioactive ion capture. (a) Chemical structure of the 18-crown-6 linker (L1) and crystal structure of ZJU-X100. (b) Sr^{2+} adsorption isotherm of ZJU-X100 fitted with Langmuir and Freundlich models. (c) Competitive adsorption of Sr^{2+} in the presence of Na^+, K^+, and Cs^+ at molar ratios of 1 : 0, 1 : 10, and 1 : 100. (d) Chemical structure of the 24-crown-8 linker (L2) and crystal structure of ZJU-X102. (e) Cs^+ adsorption isotherm of ZJU-X102. (f) Competitive adsorption of Cs^+ against Na^+, K^+, and Sr^{2+}. Reproduced with permission from ref. 106. Copyright 2024 Wiley-VCH.

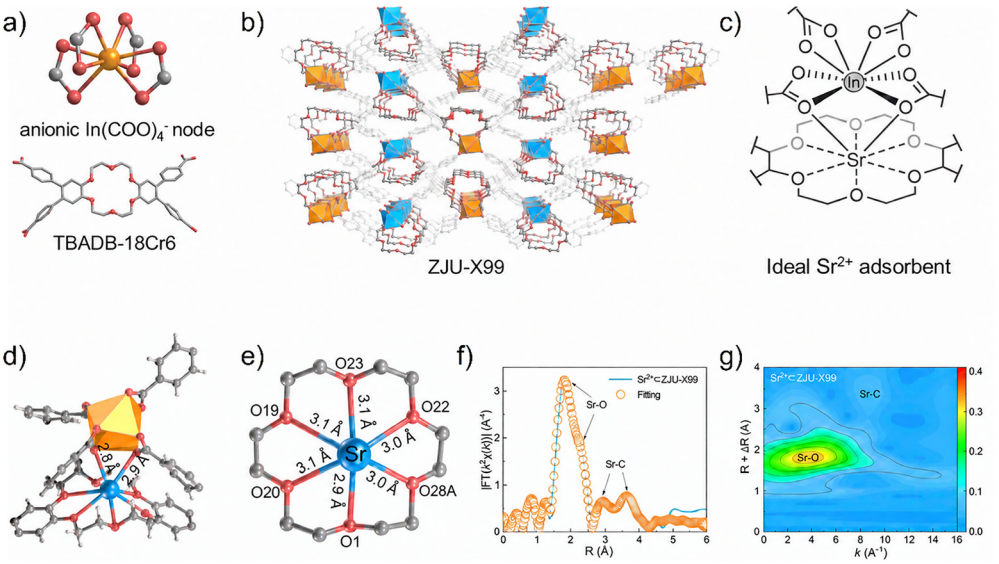


Fig. 5 Negatively charged crown ether MOF for precise strontium capture. (a) Building units of ZJU-X99: anionic $In(COO)_4^-$ node and the TBADB-18Cr6 linker. (b) Framework structure of ZJU-X99 showing crown ether-lined channels. (c) Schematic illustration of the ideal Sr^{2+} adsorbent design. (d) Structure illustration of Sr^{2+}⊂ZJU-X99 showing the SrO_8 coordination polyhedron. (e) Detailed coordination geometry of Sr^{2+} within the 18-crown-6 cavity with bond distances. (f) Sr K-edge EXAFS fitting of Sr^{2+}⊂ZJU-X99. (g) Wavelet transform analysis of the EXAFS data. Reproduced with permission from ref. 120. Copyright 2025 Springer Nature.

those of the parent framework (Fig. 6b and c). ZJU-X102-SO_4 was shown to remove >70% of $^{226}Ra^{2+}$ within 10 minutes, achieved K_d = 5.3 × 10^4 mL g^{-1}, retained 93% efficiency in artificial groundwater, and tolerated 3 M HNO_3 (Fig. 6d). The spent sorbent is designed for permanent immobilization, as single-use sequestration is considered safer than cyclic regeneration for long-lived α-emitters.

The progression from the seminal MOF-1001 (2009) through size-matched Zr-MOFs (2024) and anionic traps (2025) to cooperative radium sequestration (2026) charts a clear trajectory. Each of these generations adds a recognition layer, cavity size-matching, electrostatic pre-concentration, sulfate co-chelation, that narrows selectivity toward increasingly challenging radionuclides. This arc also exposes a recurring kinetic–thermodynamic design choice: labile crown ether capture suits high-throughput $^{90}Sr/^{137}Cs$ decontamination, while cooperative irreversible trapping addresses permanent ^{226}Ra immobilization. The same trade-off will reappear in modified form across the catalytic and transport domains discussed below.

4.1.2. Gas separation and carbon capture. Cyclodextrin-based MOFs occupy a distinct niche in gas separation, where the hydroxyl-rich CD rims profiled in Section 2.3 supply

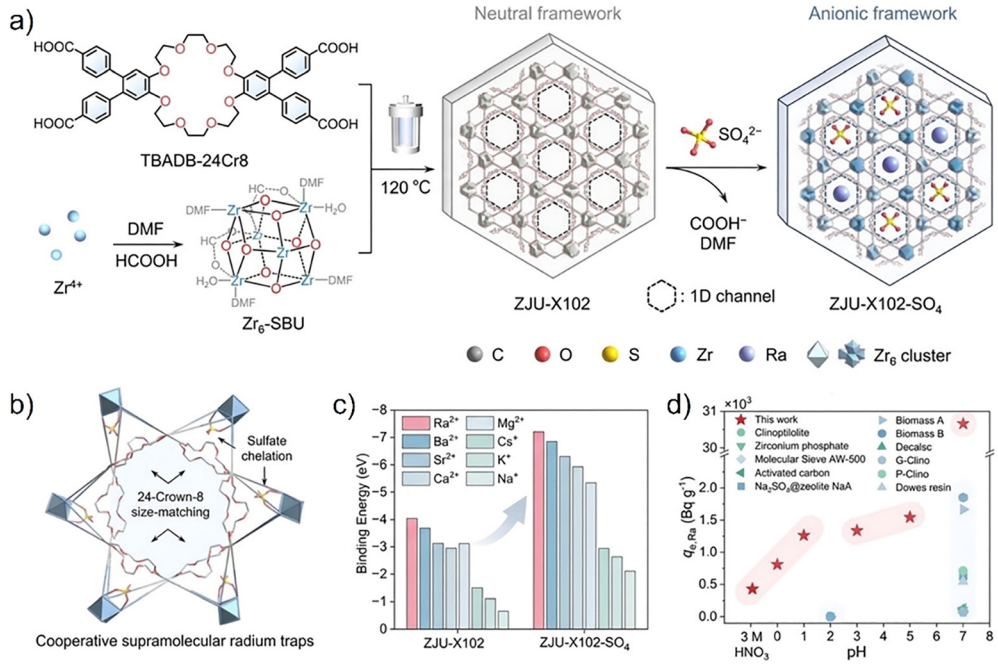


Fig. 6 Cooperative supramolecular trapping of $^{226}Ra^{2+}$ by a sulfate-functionalized crown ether MOF. (a) Synthetic route: TBADB-24Cr$_8$ and Zr$_6$-SBU assemble into neutral ZJU-X102, followed by postsynthetic SO_4^{2-}/$HCOO^-$ exchange to give anionic ZJU-X102-SO$_4$. (b) Cooperative recognition mechanism: size-matched encapsulation by 24-crown-8 combined with chelation by proximal Zr$_6$-cluster sulfates. (c) DFT-calculated binding energies of alkali and alkaline-earth ions in ZJU-X102 *versus* ZJU-X102-SO$_4$. (d) $^{226}Ra^{2+}$ adsorption capacity of ZJU-X102-SO$_4$ compared with benchmark sorbents across pH. Reproduced with permission from ref. 121. Copyright 2026 American Chemical Society.

chemisorptive as well as physisorptive sites for polar guests.[122,123] CD-MOF-2 (γ-CD/Rb^+) was the first to show strong, reversible CO_2 capture by carbonate formation at the primary hydroxyls, a chemisorptive pathway distinct from the physisorption of conventional MOFs (Fig. 7a–c).[107] Zick, Milner, and co-workers subsequently elucidated the mechanism as bicarbonate (HCO_3^-) formation at nucleophilic OH^- sites within the framework pores, and developed an oxidation-resistant $KHCO_3$ CD-MOF that retains high CO_2 capacity under simulated flue gas containing O_2, addressing a critical limitation of amine-based sorbents (Fig. 7).[124] Most recently, the same group showed that a solvothermally prepared Rb_2CO_3 CD-MOF captures CO_2 from

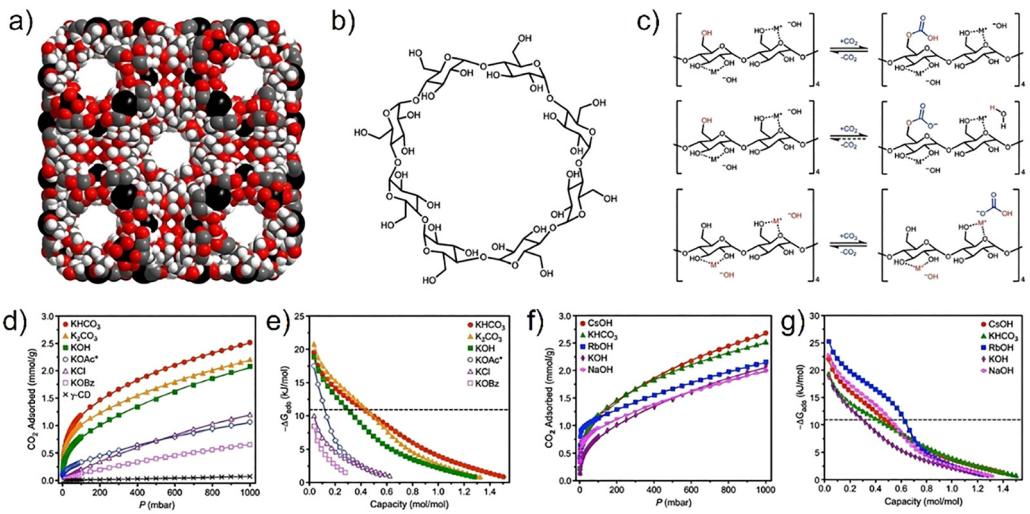


Fig. 7 CO_2 chemisorption at nucleophilic hydroxide sites in cyclodextrin-based MOFs. (a) Space-filling model of KOH CD-MOF. (b) Molecular structure of γ-cyclodextrin. (c) Proposed CO_2 chemisorption pathways. (d) CO_2 adsorption isotherms (40 °C) of CD-MOFs prepared with different counteranions and free γ-CD. (e) Free energies of adsorption ($-\Delta G_{ads}$) *versus* CO_2 loading. (f) CO_2 adsorption isotherms (40 °C) of OH^--containing CD-MOFs with varying alkali cations (Cs^+, Rb^+, K^+, Na^+). (g) Corresponding $-\Delta G_{ads}$ profiles for the different alkali cations. Reproduced with permission from ref. 124. Copyright 2022 Wiley-VCH.

 This journal is © The Royal Society of Chemistry 2026

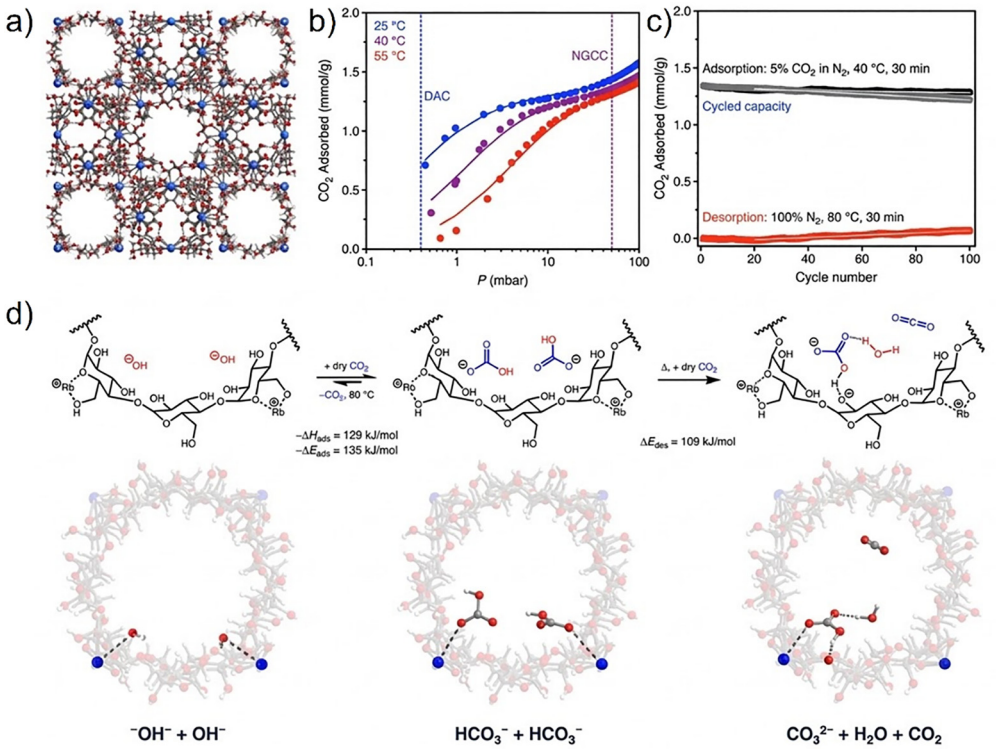


Fig. 8 Carbon capture in a cyclodextrin-based MOF. (a) Crystal structure of Rb_2CO_3 CD-MOF showing the porous cubic framework assembled from γ-cyclodextrin and Rb^+ ions. (b) Low-pressure CO_2 adsorption isotherms at 25, 40, and 55 °C; dashed lines mark the partial pressures relevant to direct air capture and NGCC flue gas. (c) Cycling stability over 100 adsorption–desorption cycles. (d) Proposed mechanistic pathway with DFT-optimized binding configurations. Reproduced with permission from ref. 125. Copyright 2025 American Chemical Society.

both natural gas flue emissions (~4% CO_2) and ambient air (~0.04% CO_2) with good thermal, oxidative, and cycling stabilities, and revealed a mechanistic switch from reversible bicarbonate to irreversible carbonate under dry, hot conditions (Fig. 8b and c).[125] In parallel, Xu, Li, Zhang, and co-workers constructed NH_2-β-CD-MOF, the first amino-functionalized cyclodextrin framework, achieving a CO_2/N_2 selectivity of 947 with improved water stability compared to parent β- and γ-CD-MOFs.[126]

Beyond CO_2, CD-MOFs also show versatile molecular discrimination. CD-MOF-1 and CD-MOF-2 preferentially adsorb CO_2 over C_2H_2, an inverse selectivity rarely achieved in porous materials, enabling single-step purification of high-purity acetylene.[127] The shape-selective transverse channels of CD-MOFs resolve all BTEX components in the liquid phase, with *ortho-* > *meta-* > *para*-xylene retention.[128] γ-CD-MOF-K captures formaldehyde with capacities and kinetics roughly nine times those of activated carbon, exploiting hydrogen bonding between the polar aldehyde and the hydroxyl-rich CD cavity.[129]

Crown ether and aza-macrocyclic MOFs extend the separation toolbox through distinct recognition mechanisms.[130–133] Chen, Yang, Shi, and co-workers reported NKU-300, a robust MOF with triangular channels decorated by crown ether moieties, that discriminates trace benzene from cyclohexane with a selectivity of 8615. The selectivity arises from cooperative supramolecular interactions that immobilize benzene within the crown ether-lined channel (Fig. 9a–c).[131] In the domain of noble gas separation, Gong, Cui, Farha, and co-workers designed NU-1107, a cubic Zr-MOF built from tetratopic linkers bearing cyclen (1,4,7,10-tetraazacyclododecane) cores that chelate transition-metal ions post-synthetically. The Ag(I)-docked variant achieved an IAST Xe/Kr selectivity of 13.4 at 298 K, among the highest for MOF materials, by programmatically tuning framework polarizability through metal–macrocycle coordination (Fig. 10).[134] Systematic comparison across Cu^{2+}, $Co^{2+/3+}$, Ag^+, and Pd^{2+}-metalated variants reveals that Ag(I) docking maximizes both Xe uptake and IAST selectivity, with isosteric heats of adsorption exceeding those of benchmark frameworks Ag@MOF-303 and Ag@MOF-74-Ni (Fig. 10b and c). Successful extension of this metalation strategy to the MOF-525 platform confirms its generality across different Zr-MOF topologies (Fig. 10d and e).

4.1.3. Molecular recognition and crystalline sponge analysis. The shape-selective cavities of macrocyclic MOFs enable not only bulk separation but also precise molecular recognition at the single-molecule level, culminating in absolute structure determination of unknown compounds by single-crystal X-ray diffraction (SCXRD).[135,136] Pillar[5]arene MOFs have emerged as a particularly powerful platform for selective molecular capture (Fig. 12a). Wang, Wu, Huang, and co-workers incorporated perethylated pillar[5]arene into a stable Zr-MOF (EtP5-Zr-scu) and demonstrated rapid, highly selective adsorption of the mustard gas simulant CEES, with breakthrough performance (566 min g^{-1})

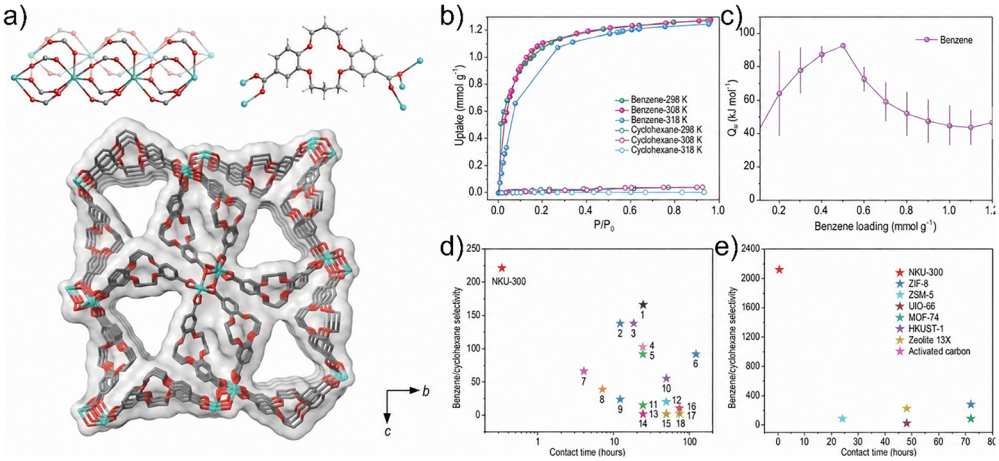


Fig. 9 Crown ether-lined triangular channels for benzene/cyclohexane separation. (a) Crystal structure of NKU-300 built from Eu^{3+} and a dibenzo-14-crown-4 dicarboxylate linker. (b) Single-component vapour adsorption isotherms of benzene and cyclohexane in desolvated NKU-300 at 298, 308, and 318 K. (c) Isosteric heat of adsorption (Q_{st}) for benzene *versus* loading. (d) Liquid-phase benzene/cyclohexane selectivity of NKU-300 compared with 17 state-of-the-art materials as a function of contact time. (e) Comparison with benchmark porous materials. Reproduced with permission from ref. 131. Copyright 2024 Oxford University Press.

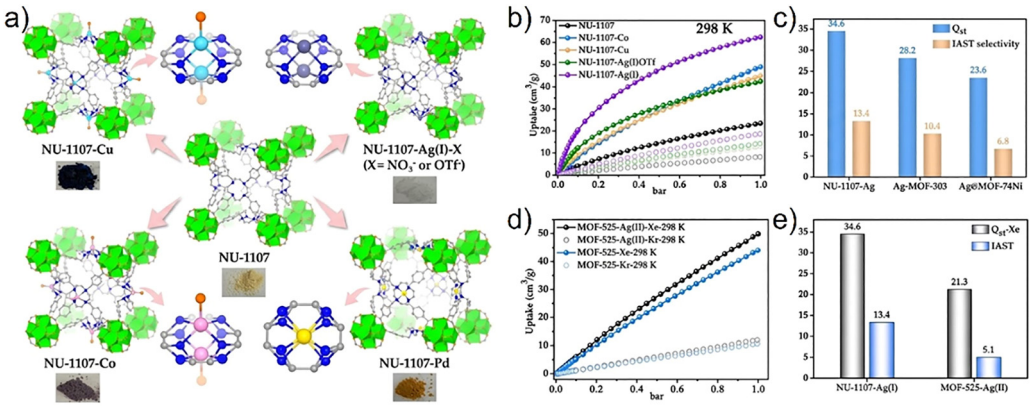


Fig. 10 Programmed polarizability engineering in a cyclen-based Zr-MOF for Xe/Kr separation. (a) Schematic of the NU-1107 platform. (b) Single-component Xe and Kr adsorption isotherms at 298 K for NU-1107 and its metalated variants. (c) Isosteric heat of Xe adsorption (Q_{st}) and IAST Xe/Kr selectivity for NU-1107-Ag, Ag@MOF-303, and Ag@MOF-74-Ni. (d) Xe and Kr isotherms at 298 K for MOF-525 and MOF-525-Ag(II). (e) Comparison of Q_{st} and IAST selectivity between NU-1107-Ag(I) and MOF-525-Ag(II). Reproduced with permission from ref. 134. Copyright 2023 American Chemical Society.

far surpassing the non-macrocyclic control (Fig. 11).[108] SCXRD and solid-state NMR confirmed specific host–guest complexation between CEES and the pillar[5]arene cavity, thus providing the first direct structural evidence of selective molecular capture within a pillararene-based MOF (Fig. 11b). Calixarene frameworks extend this recognition chemistry: three lattices built from carboxyl-modified inverted azocalix[4]arenes generate hierarchical nanocavities from metal-bridged pairs of bowl-shaped macrocycles. These MOFs achieve fast iodine adsorption with SCXRD directly mapping the host–guest binding geometry (Fig. 13).[137] Notably, the La-CAC4A framework outperforms eleven benchmark MOFs–including HKUST-1, UiO-66, and ZIF-8–in iodine uptake kinetics (Fig. 13b), while SCXRD analysis resolves the I_2 binding geometry within the azocalix[4]arene cavity at host–guest contact distances of 2.5–4.1 Å (Fig. 13c).

A qualitatively new application is supramolecular docking for crystallographic structure determination, a macrocycle-specific evolution of the crystalline sponge method.[138] Wu, Shi, Sessler, Huang, and co-workers showed that pillar[5]arene units within EtP5-MOF-2 can capture alkyl-chain-containing molecules from solution and order them sufficiently for SCXRD analysis.[105] Leveraging the intrinsic affinity of pillar[5]arenes for alkyl guests, this supramolecular docking approach resolved the structures of 48 compounds, including 6 natural products, 2 FDA-approved drugs, and an unstable alkene sulfide. All were solved within minutes of soaking, without independent crystallization (Fig. 14a and b). Fourteen unknowns were unambiguously identified through blind experiments combining SCXRD with NMR spectral data. Critically, crude reaction mixtures could be analyzed directly, bypassing purification altogether.[105,139] This work elevates macrocyclic MOFs from passive separation media to active

 This journal is © The Royal Society of Chemistry 2026

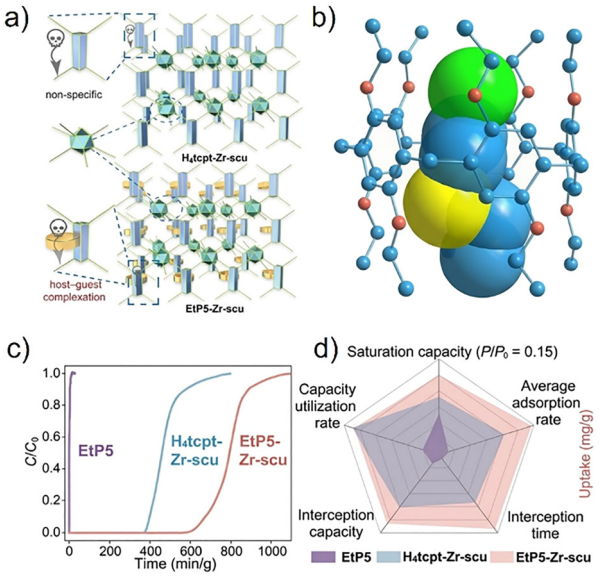


Fig. 11 Pillar[5]arene-based Zr-MOF for selective capture of a mustard gas simulant. (a) Comparison of the non-macrocyclic control framework (H_4tcpt-Zr-scu, top) and the pillar[5]arene-containing analogue (EtP5-Zr-scu, bottom). (b) Single-crystal X-ray structure showing CEES (yellow/green) encapsulated within the electron-rich pillar[5]arene cavity (blue). (c) Breakthrough curves for CEES adsorption. (d) Radar chart comparing saturation capacity. Reproduced with permission from ref. 108. Copyright 2024 American Chemical Society.

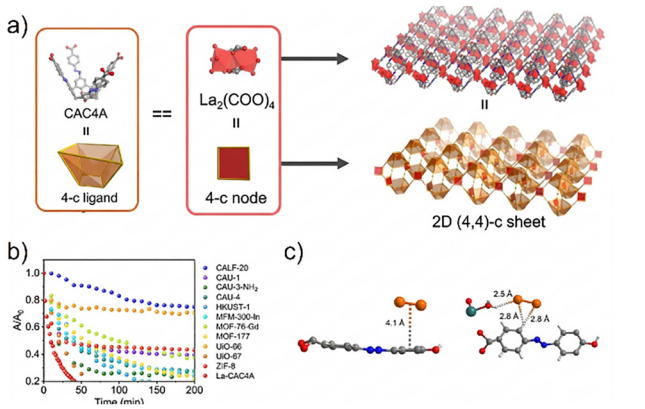


Fig. 13 Inverted azocalix[4]arene-based MOFs for iodine capture with crystallographically resolved binding sites. (a) Reticular assembly of La-CAC4A. (b) Comparison of iodine adsorption kinetics (A/A_0) of La-CAC4A (red) *versus* benchmark MOFs. (c) Binding geometry of I_2 within the calixarene cavity. Reproduced with permission from ref. 137. Copyright 2025 American Chemical Society.

analytical instruments. Here, the molecular recognition encoded in the macrocyclic cavity is harnessed not for capture or release but for atomic-resolution structural elucidation of previously intractable molecules.

4.1.4. Chiral separation. The inherent chirality of certain macrocycles, such as the multiple stereogenic centres of cyclodextrins and the planar chirality of pillar[5]arenes, provides a

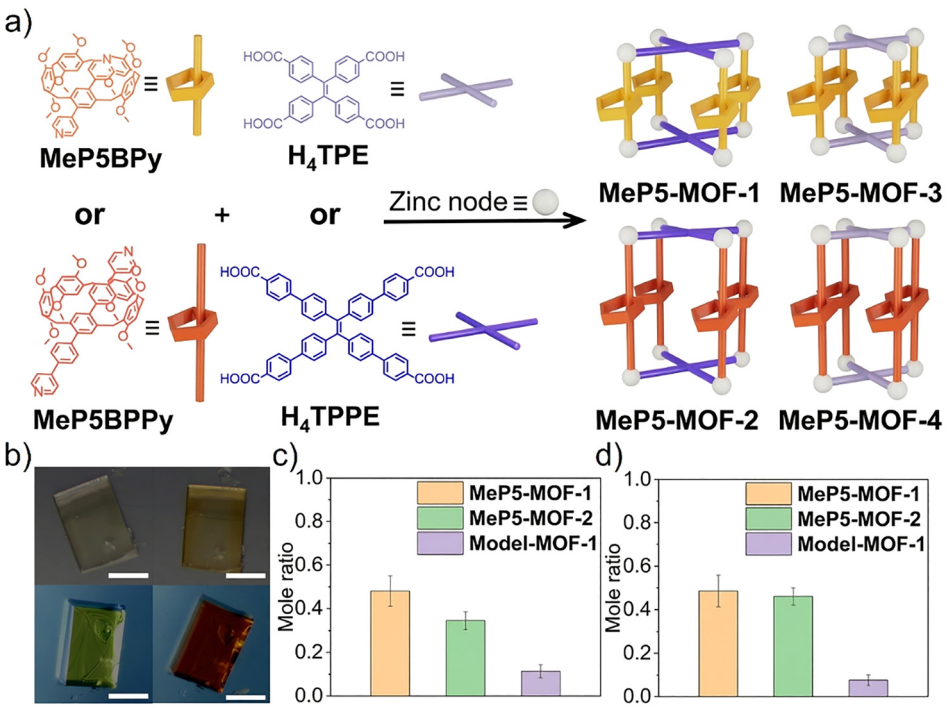


Fig. 12 Pillar[5]arene-incorporated MOFs for supramolecular recognition and selective separation. (a) Design strategy: two methyl-substituted pillar[5]arene-based dipyridyl struts (MeP5BPy and MeP5BPPy) serve as pillars, while H_4TPE and H_4TPPE act as tetratopic carboxylate layers. (b) Optical photographs of as-synthesized MeP5-MOF crystals. (c) Mole ratios of paraquat (PQT^{2+}) to struts after host–guest uptake: MeP5-MOF-1 and MeP5-MOF-2 capture significantly more PQT^{2+} than Model-MOF-1 (a non-macrocyclic control). (d) Mole ratios of 1,2,4,5-tetracyanobenzene (TCNB) to struts. Reproduced with permission from ref. 58. Copyright 2023 Springer Nature.

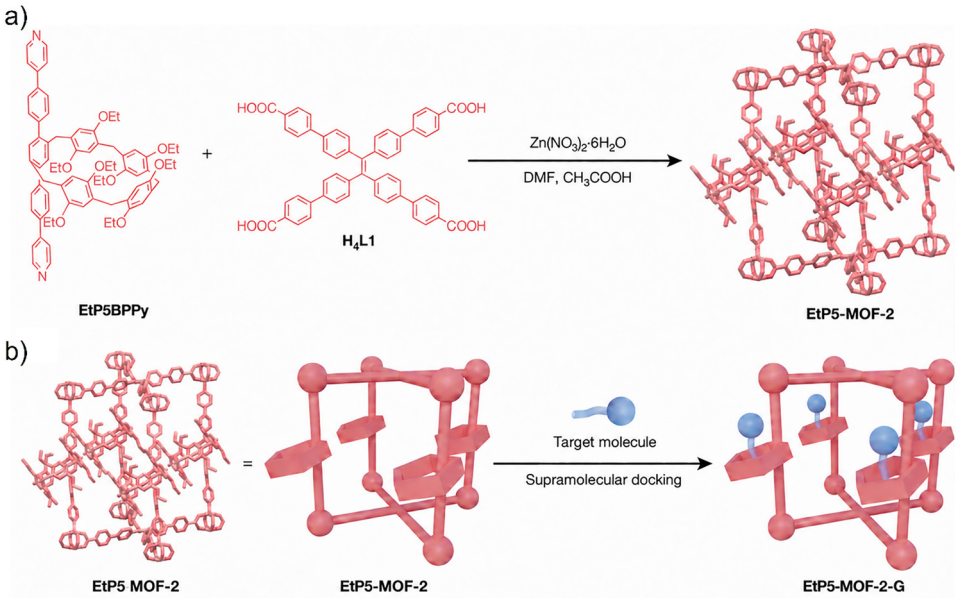


Fig. 14 Supramolecular docking for crystallographic structure determination. (a) Synthesis of EtP5-MOF-2. (b) Supramolecular docking principle. Reproduced with permission from ref. 105. Copyright 2025 Springer Nature.

natural foundation for constructing homochiral MOFs capable of enantioselective separation. Crown ethers, cyclodextrins, and pillararenes have all been exploited as chiral building blocks in this context, enabling applications spanning chromatographic separation and membrane-based resolution.[140]

Jiang, Cui, and co-workers demonstrated the first use of Zr(IV)-based MOFs as chiral stationary phases (CSPs) for reversed-phase high-performance liquid chromatography (RP-HPLC).[141] By designing three enantiopure 1,1′-biphenyl-20-crown-6 tetracarboxylate linkers with varying peripheral arm lengths, they constructed isostructural Zr-MOFs (CE-1, CE-2, and CE-3) adopting the flu topology. Chiral crown ether moieties were periodically aligned within the framework channels, serving as enantioselective recognition sites through supramolecular host–guest interactions.[142] Under acidic aqueous eluent conditions, the CE-MOF-packed HPLC columns achieved baseline separation of 16 racemates, including unprotected and protected amino acids and N-containing drugs, with performance either comparable to or exceeding several commercial chiral columns (Fig. 15a, b and d). DFT calculations revealed that the confined microenvironment around the chiral crown ethers dictates the separation selectivity (Fig. 15c). The exceptional chemical stability of these Zr-MOFs, which retained crystallinity and porosity after treatment in boiling water, concentrated HCl, and pH 12 NaOH for seven days, is particularly advantageous for RP-HPLC applications.

Cyclodextrin-based MOFs have also demonstrated remarkable promise in chiral chromatography.[143] Hartlieb, Stoddart, and co-workers showed that γ-CD-MOF functions as a versatile chiral separation medium in HPLC, resolving a broad scope of chiral compounds including pinene and limonene enantiomers.[19] The 40 stereogenic centres per γ-CD ring and the accessible hydroxyl groups within the pores provide abundant chiral recognition sites. In a complementary approach, Liu and Yuan reported that

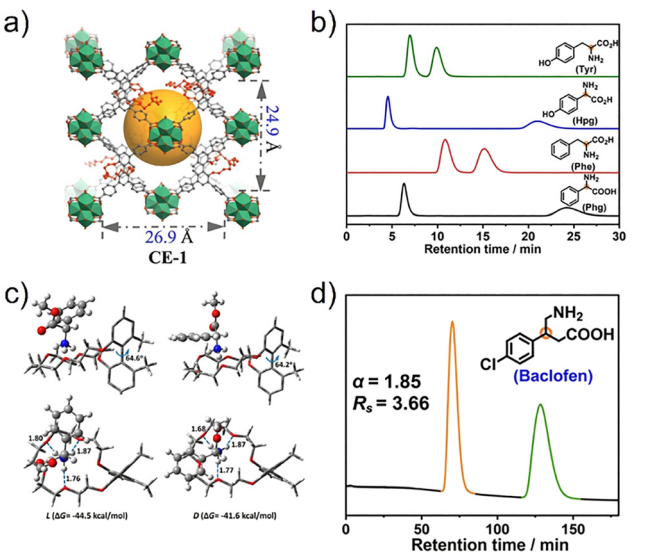


Fig. 15 Chiral crown ether Zr-MOF as a stationary phase for reversed-phase HPLC enantioseparation. (a) Crystal structure of CE-1 adopting the flu topology. (b) Representative RP-HPLC chromatograms demonstrating baseline separation of unprotected amino acid enantiomers. (c) DFT-optimized binding geometries of L- and D-enantiomers within the chiral crown ether cavity. (d) Chiral separation of the drug baclofen. Reproduced with permission from ref. 141. Copyright 2021 American Chemical Society.

combining a chiral MOF with peramylated β-cyclodextrin as a composite GC stationary phase enhanced enantioseparation of terpenoids and amino acid derivatives compared with the CD phase alone.[144] Beyond column chromatography, Lu, Wang, and co-workers fabricated CD-MOF/polyethersulfone mixed-matrix membranes for continuous chiral resolution, achieving near-perfect enantioselectivity (ee approaching 100%) for the separation of R-(+)-1-phenylethanol from its racemic mixture in non-polar solvents.[145]

 This journal is © The Royal Society of Chemistry 2026

Beyond separation, the inherent chirality of cyclodextrins can be translated into programmable architectural helicity at the framework level.[146] Jiang and co-workers assembled one-dimensional Ag_6L_2 nanochannels from α-cyclodextrin-derived pyridinyl ligands and Ag^+ ions. The nanochannel helicity, either P or M form, can be switched by varying the steric bulk of *ortho*-methyl substituents on the ligand (Fig. 16a). The resulting two-dimensional coordinative network displays periodically arranged helical channels with internal diameters of 19.1 Å and heights of ~20.0 Å, whose chirality is governed by the distorted tetrahedral coordination geometry around Ag^+ (Fig. 16b–e).

Pillar[5]arenes introduce a distinct form of chirality, that is planar chirality, into MOF platforms. An A1/A2-difunctionalized pillar[5]arene with resolvable planar chirality was first incorporated into P5A-MOF-1, an IRMOF-16-type framework that selectively binds electron-poor aromatic guests.[61] Building upon this foundation, the same group resolved the racemic pillar[5]arene strut into its (Sp) and (Rp) enantiomers and constructed homochiral (Sp)-P5A-MOF-1 and (Rp)-P5A-MOF-1. Both frameworks rank among the early examples of porous materials with enantiopure active domains possessing planar chirality, holding promise for enantioselective chromatographic applications.[147] The examples surveyed above converge on a single operational principle: macrocyclic affinity, once confined within a crystalline lattice, becomes both amplified and tuneable. Several examples demonstrate the principle. Crown ethers discriminate Ra^{2+} from a ten-thousand-fold excess of competing cations through cooperative sulfate-bridged relay; cyclodextrin hydroxyl arrays convert CO_2 chemisorption into a regenerable (bi)carbonate cycle viable for direct air capture; and pillar[5]arene pockets permit single-crystal diffraction mapping of host–guest docking geometries previously accessible only by computation.[105,121,125] In each case, the framework does not merely house the macrocycle, it enforces a spatial and electronic microenvironment that sharpens selectivity far beyond what the free host achieves in solution. The progression from single-ion recognition to multicomponent mixture separation and ultimately to real-world sorbent operation charts a clear trajectory for affinity-driven porous materials.

4.2. Adaptive gating and chemical sensing

In Section 4.1, macrocyclic recognition serves as an endpoint where the host captures or discriminates a guest, and the task is complete. This section treats recognition as a beginning with the binding event triggering a downstream consequence that extends beyond the cavity itself. In adaptive gating, guest binding or an external stimulus reshapes the macrocyclic pore environment, switching transport on or off. In chemical sensing, the same recognition event is transduced into a readable optical or electrical output. What unites both functions is that the macrocycle must do more than bind, it must respond. For instance, crown ethers undergo cation-induced conformational reorganization of their polyether backbone, and cyclodextrins alter their truncated-cone geometry and hydrogen-bonding network upon guest encapsulation. Calixarenes switch between cone, partial-cone, and 1,3-alternate conformations, and mechanically interlocked macrocycles shuttle between recognition sites along a molecular axle.[14,16,60,148–151] When these molecular-level responses are arrayed across a crystalline MOF lattice, they are collectively amplified into macroscopic material behaviour, gated diffusion, adaptive porosity, luminescence modulation, and conductivity switching.[18] The rigidity of the macrocyclic component governs the character of this response and is therefore reflected differently depending on the group. For example, flexible crown ethers provide low-barrier, fast-switching gates while moderately rigid cyclodextrins and calixarenes enable stimulus-selective activation with sharper thresholds, and pillararenes combine a rigid

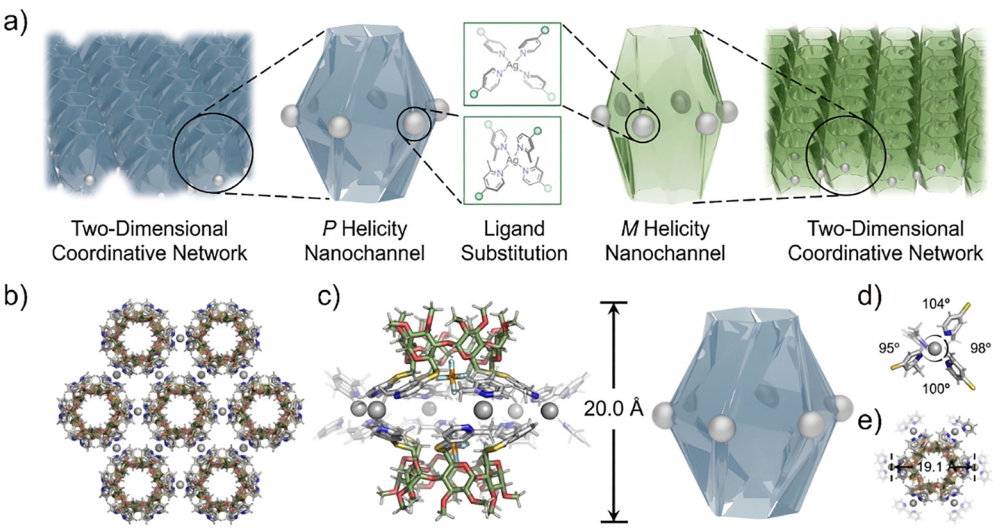


Fig. 16 Engineering helical chirality in metal-coordinated α-cyclodextrin nanochannels. (a) Schematic illustration of helicity control. (b) Top-down view of the 2D coordinative network showing the periodic arrangement of α-CD-based helical channels. (c) Side view of a single nanochannel (height ≈20.0 Å) with the crystal structure. (d) Coordination geometry around Ag^+ showing bond angles (95°–104°) characteristic of a distorted tetrahedral environment that enforces helical twist. (e) Cross-sectional view of the nanochannel. Reproduced with permission from ref. 146. Copyright 2025 American Chemical Society.

aromatic cavity with tuneable portal chemistry, bridging gating and sensing in a single platform.

4.2.1. Molecular machines and mechanical gating in frameworks. The incorporation of mechanically interlocked molecules (MIMs)—rotaxanes and catenanes—into MOF lattices represents a frontier that exploits the conformational dynamics of macrocycles, particularly crown ethers, within a crystalline environment.[152] Loeb and co-workers pioneered the field with UWDM-1, whose 24-crown-6 wheel rotates about its rotaxane axle in the crystalline solid.[78] Successive generations brought this motion under design control: ring-size variation from 22- to 26-crown-6 tuned the rotational barrier through macrocycle–axle fit and solvent occupancy, a reversible phase change in UWDM-3 switched rotation on and off, UWDM-4 achieved station-to-station shuttling, and later designs added directional bias and two independently addressed moving parts within one lattice.[22,84,86,153,154] Stoddart and co-workers approached the problem from the switching perspective. Their bistable[2]catenane strut, incorporating a redox-active tetrathiafulvalene recognition site, can be mounted inside the Zr-based NU-1000 and toggled between two co-conformational states by chemical oxidation/reduction while crystallinity is fully retained.[92] Their mechanisorption concept further showed that a molecular pump appended to a MOF surface directionally transports $CBPQT^{4+}$ rings under ratchet-like kinetic conditions, achieving energy-driven accumulation at far-from-equilibrium stoichiometries (Fig. 17).[155] In a structurally distinct strategy, Aida, Sato, and co-workers constructed a porous crystal whose backbone comprises densely interlocked [2]catenane units. Here, the mechanical bonds endow the crystal with rubber-like elasticity, creating a reversible bending deformation of up to 7.2% while maintaining permanent porosity, directly linking mechanical interlocking to macroscopic mechanical properties (Fig. 18b and c).[89] Saura-Sanmartin, Berna, and co-workers further incorporated copper-linked rotaxane struts into UMUMOF frameworks that undergo photo-triggered co-conformational change, enabling light-controlled cargo delivery from the MOF pores.[156]

4.2.2. Chemical sensing. The well-defined host–guest chemistry of macrocycles provides an intrinsic transduction mechanism for chemical sensing. This can be described as a recognition event within the macrocyclic cavity perturbing a measurable physical property such as ionic conductivity, optical absorption, or luminescence that enables selective, label-free detection without the need for extrinsic receptor grafting.[157,158] Gassensmith, Stoddart, Farha, and co-workers exploited the dynamic covalent reaction between CO_2 and the free hydroxyl groups of CD-MOF-2 (γ-CD-Rb^+) to build an electrochemical carbon dioxide sensor. CO_2 chemisorption forms alkyl carbonate that plugs the β-windows of the framework, reducing proton conductivity by approximately 550-fold, a signal sufficient for quantitative atmospheric CO_2 detection at room temperature.[159] Cyclodextrin sensing extends to the biomedical domain in RT@CDMOF, a dual-responsive chiral sensor co-assembling rhodamine 6G hydrazide and tetracyanovinylindane within a γ-CD-MOF matrix (Fig. 19).[160] The embedded chromophores inherit the homochirality of the CD-MOF host, enabling fluorescence and reflectance dual-channel discrimination of L- and D-lactate enantiomers.[161] A flexible membrane sensor fabricated from this material can achieve wearable point-of-care health monitoring by indexing exercise intensity through lactate chirality (Fig. 19a–c). Schulz, Schaate, and co-workers introduced calixarene cavities as colorimetric gas sensors by constructing the first Zr-based calixarene MOF adopting the rare gar topology.[162] The electron-rich calixarene bowls are directly accessible through the pore channels. Exposure to NO_2 induces charge-transfer complexation with NO^+, producing a vivid color change detectable by the naked eye with high selectivity over H_2O, NH_3, and SO_2 (Fig. 22b and c). Liu, Zang, Tang, and co-workers demonstrated a complementary luminescence-based strategy using oxacalix[2]arene[2]pyrazine (OAP) as an AIE-active MOF linker. The restriction of intramolecular vibration upon the assembly of this framework activates intense emission that is reversibly switched by guest adsorption and desorption (Fig. 20).[163] Four structural variants of OAP ligands–OBP, ONP, OPsP, and OBpP–yield MOFs with tuneable solid-state emission spanning 540 to 600 nm (Fig. 20a and b). The vapochromic switching of these materials arises from methanol coordination to Cu^{2+} centres, which increases OAP backbone conformational freedom and activates non-radiative decay (Fig. 20c and d). Aza-macrocyclic frameworks bring a distinct sensing paradigm through second-sphere interactions at lanthanide nodes. Ren, Ma, and co-workers designed MMCF-4, a Tb(III)-based metal–macrocyclic framework in which the lanthanide centre adopts a nine-coordinate geometry with a saturated first coordination sphere, rendering it inaccessible to direct analyte binding (Fig. 21).[52] Instead, sensing proceeds *via* the secondary coordination sphere. As methylamine molecules form hydrogen bonds with the dangling carboxylate oxygen atoms of the macrocyclic TACN-derived ligand, the soft framework becomes rigid and suppresses non-radiative relaxation pathways. This binding-induced rigidification boosts Tb^{3+} green emission in a turn-on mode, with an ultra-low detection limit of 86 nM in aqueous solution. The sensor marks the first turn-on organic amine sensing in Ln-MOFs, confirmed by single-crystal X-ray diffraction and molecular dynamics simulations (Fig. 21b and c). Crown ether–MOF selectivity has also been translated in vivo:

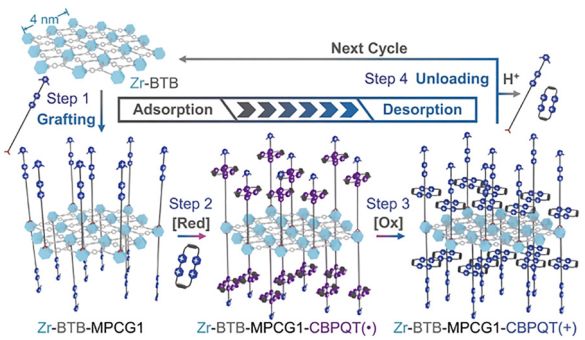


Fig. 17 Schematic illustration of the mechanisorption cycle on a Zr-BTB MOF surface. Reproduced with permission from ref. 155. Copyright 2021 American Association for the Advancement of Science.

 This journal is © The Royal Society of Chemistry 2026

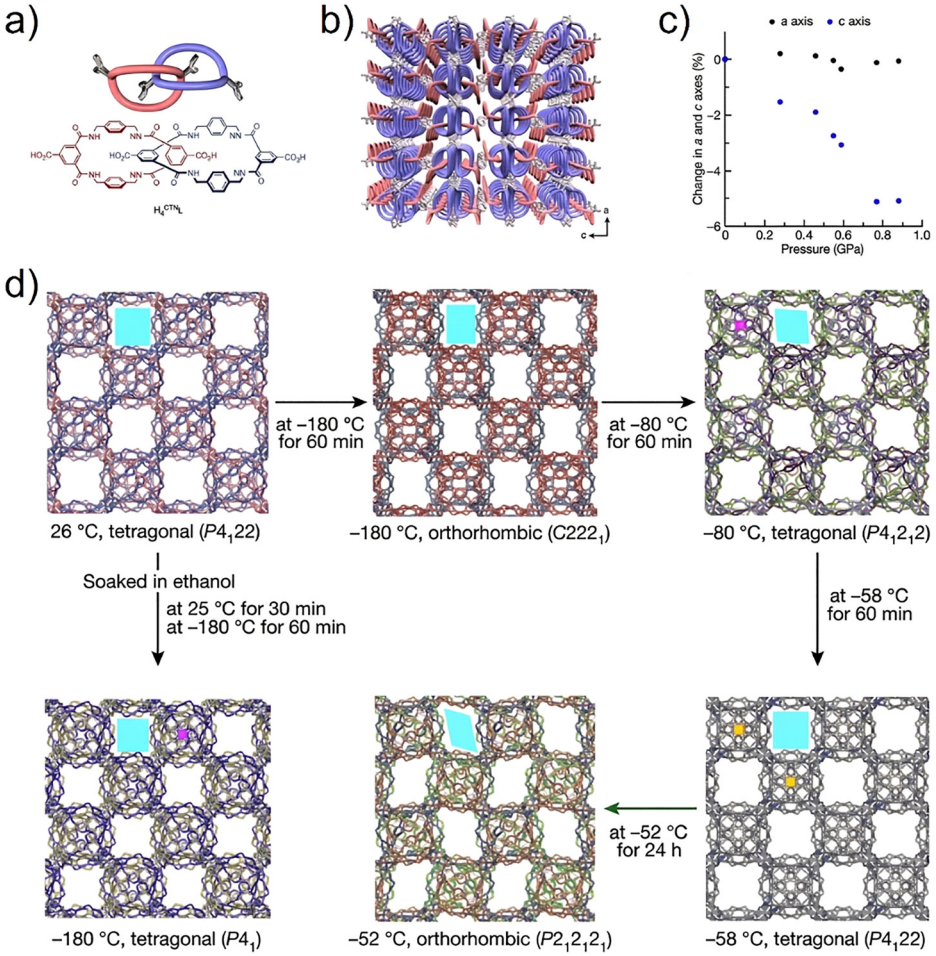


Fig. 18 Elastic metal–organic framework with a densely catenated backbone. (a) Chemical structure of the [2]catenane-based tetracarboxylate ligand H_4CTN-L and schematic representation of its mechanically interlocked topology. (b) Crystal structure of CTN[4]MOF viewed along the b axis. (c) Anisotropic lattice response under hydrostatic pressure. (d) Variable-temperature single-crystal X-ray diffraction revealing a rich polymorphic landscape. Reproduced with permission from ref. 89. Copyright 2021 Springer Nature.

18-crown-6@ZIF-8 nanoparticles synthesized at a micropipette tip give an ion-selective sensor that monitors Na^+ dynamics in rat brains during cortical spreading depression.[164]

4.2.3. Stimuli-responsive nanovalves and adaptive cavities. Macrocycles can function as supramolecular gatekeepers when threaded onto or capping the pore apertures of MOFs, converting molecular recognition events into material-level on/off switches of mass transport. Yang, Wang, and co-workers provided the first demonstration, capping the mesoporous channels of UMCM-1-NH_2 with carboxylato-pillar[5]arene (CP5A) *via* host–guest complexation with surface pyridinium stalks; the cap is displaced under acidic pH or by competitive binders, releasing encapsulated doxorubicin with negligible leakage at physiological pH.[62] Wu, Yang, and co-workers advanced the valve from switch to logic: Fe_3O_4@UiO-66 nanoparticles bearing pillar[6]arene nanovalves respond independently to pH, competitive binding, and Zn^{2+} coordination, three orthogonal inputs on a single carrier, the larger pillar[6]arene cavity admitting the bulkier stalks this expanded input set requires.[165] Generality followed: a universal silane anchor grafts benzimidazole stalks onto virtually any MOF surface for capping with β-cyclodextrin polymer valves, demonstrated across UiO-66, MIL-101, and ZIF-8.[166] The trajectory, one stimulus, orthogonal stimuli, universal anchoring, follows from the valve's modularity: its chemistry belongs to the macrocycle–stalk pair, not to the framework it caps.

Beyond gating, macrocyclic cavities can themselves serve as adaptive recognition elements whose geometry reconfigures in response to a target analyte. Ren, Ma, and co-workers constructed a metal–macrocyclic framework (MMCF) whose cyclam-derived tetracarboxylate linker retains a flexible 14-membered aza-macrocyclic pocket; Pd^{2+} triggers a rectangular-to-square contraction of the cavity, achieving near-perfect complementarity with the square-planar d^8 cation, a distribution coefficient $K_d > 10^6$ mL g^{-1}, and palladium recovery from spent automotive catalysts and electronic-waste leachates (Fig. 23d and e).[51] The stimulus-responsive element here is the linker itself, the response is woven into the lattice rather than bolted on. In the vocabulary of Section 2, the nanovalve works purely on the interaction-mode axis, binding and unbinding at the rim, whereas the adaptive cavity recruits the rigidity axis, spending conformational freedom

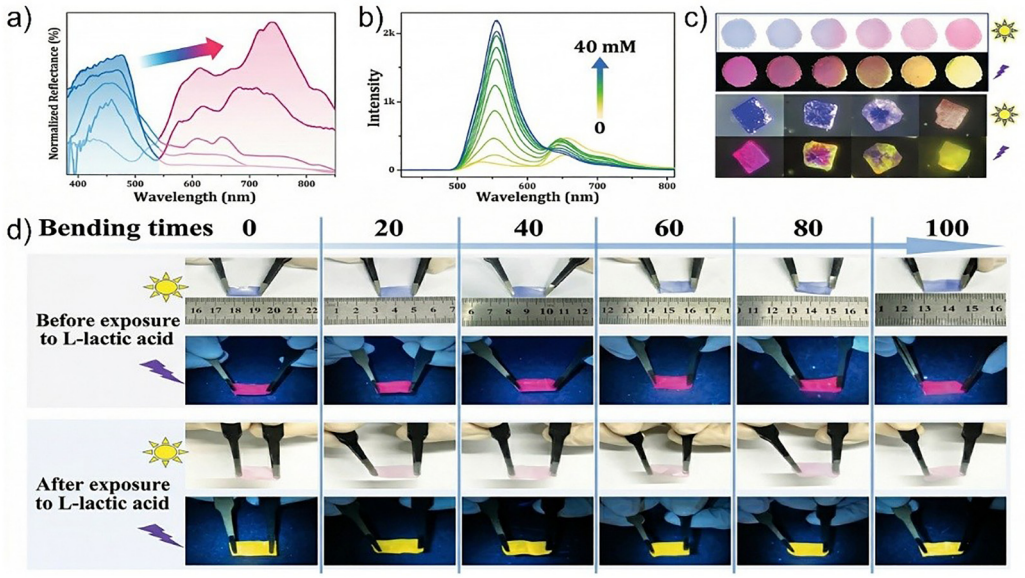


Fig. 19 Dual-responsive chiral sensing in a γ-CD-MOF-based wearable platform. (a) Reflectance spectra of RT@CDMOF upon exposure to increasing concentrations of L-lactic acid. (b) Fluorescence emission spectra with 0–40 mM L-lactic acid. (c) Photographs of RT@CDMOF bulk samples (upper) and single crystals (lower) under daylight and UV after treatment with L-lactic acid. (d) Mechanical durability of the RT@CDMOF mixed-matrix membrane (MMM) sensor. Reproduced with permission from ref. 160. Copyright 2023 Wiley-VCH GmbH.

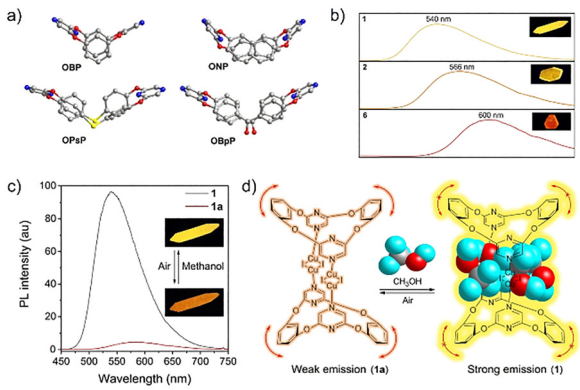


Fig. 20 Oxacalix[2]arene[2]pyrazine (OAP)-based MOFs with aggregation-induced emission (AIE) activity and vapochromic sensing. (a) Crystal structures of four OAP AIEgen linkers. (b) Solid-state luminescence spectra and corresponding crystal photographs (under UV irradiation) of MOFs 1, 2, and 6. (c) PL intensity of compound 1 (air-exposed) *versus* 1a (methanol-treated). (d) Proposed vapochromic switching mechanism: methanol coordination at the Cu centres in 1a increases OAP backbone conformational freedom (red arrows). Reproduced with permission from ref. 163. Copyright 2021 Wiley-VCH GmbH.

to purchase selectivity at the moment the target arrives. Neither strategy yet in this field reports quantitative gating metrics, on/off flux ratios, switching kinetics, fatigue over repeated cycles, without which macrocyclic gates cannot be benchmarked against the biological channels they emulate.

A recurring motif across molecular machines, sensors, and nanovalves is the tension between order and motion. Crystallinity demands periodicity while responsiveness demands conformational freedom. Macrocycle–MOF systems resolve this paradox not by compromise but by partitioning. The rigid framework supplies long-range order while the macrocycle supplies local dynamics, rotation, shuttling, gating, adaptive fit, within a spatially defined pocket. This partitioning mirrors the architecture of biological proteins where a folded scaffold positions a flexible active site. Yet, macrocycle–MOFs possess what proteins do not, translational symmetry. Every pore contains an identical machine, every channel an identical gate. The collective consequence is that a single-molecule event, one ring shuttling, one cavity contracting, is repeated identically in every unit cell of the crystal. Whether this crystallographic amplification can ultimately approach the coherence of biological signal transduction remains an open and defining question for the field.

4.3. Synergistic catalysis: macrocyclic confinement meets framework periodicity

Catalysis is molecular recognition with a chemical consequence; the catalyst selectively binds the substrate, stabilizes the transition state, and releases the product. Macrocyclic cavities are intrinsically suited to the recognition step, their pre-organized donor-atom arrays provide the same shape-selective, electronically matched binding that underlies the separation and sensing functions discussed in Sections 4.1 and 4.2.[64] The catalytic question is whether that recognition can be productively coupled to chemical activation. Three mechanistically distinct regimes emerge. In confinement catalysis, the macrocyclic cavity pre-organizes substrates through non-covalent interactions but does not participate in bond-making or -breaking. Cyclodextrins and calixarenes exemplify the mode: their "artificial enzyme" chemistry, long developed in homogeneous solution, gains new power once the cavity is immobilized within a periodic framework.[167] In coordination catalysis, the macrocyclic metal centre is itself the active site, the regime of nitrogen-donor aza-macrocycles, whose

 This journal is © The Royal Society of Chemistry 2026

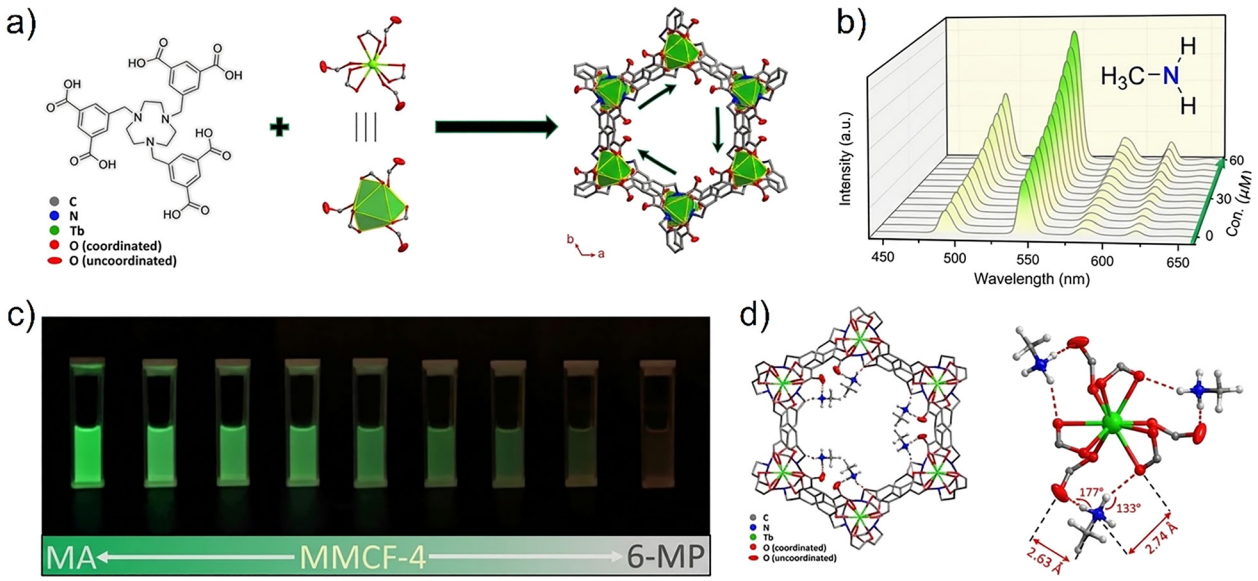


Fig. 21 Turn-on fluorescence sensing of organic amines. (a) Assembly of MMCF-4 from a TACN-derived hexacarboxylate ligand and Tb^{3+} ions. (b) Fluorescence spectra of MMCF-4 aqueous suspensions upon incremental addition of methylamine, showing progressive enhancement of characteristic Tb^{3+} green emission. (c) Photographs under 260 nm UV irradiation of MMCF-4 suspensions in the presence of varying MA/6-mercaptopurine (6-MP) concentration ratios. (d) Crystal structure of MA@MMCF-4 viewed along the channel axis. Reproduced with permission from ref. 52. Copyright 2021 Wiley-VCH GmbH.

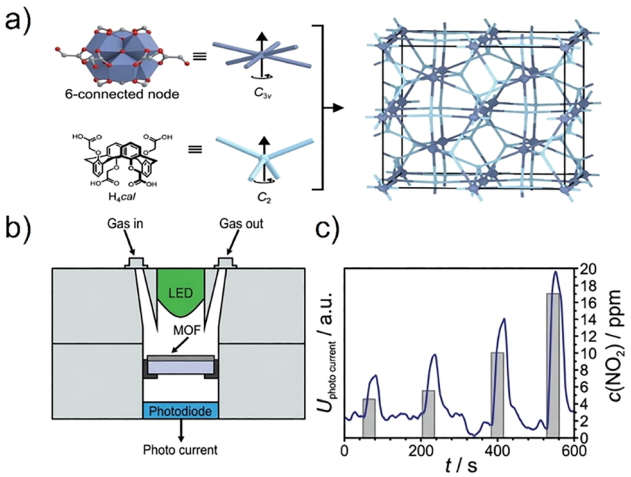


Fig. 22 Calixarene-based Zr-MOF for colorimetric NO_2 detection. (a) Assembly of the Zr-cal framework. (b) Schematic of the home-made colorimetric sensor cell. (c) Time-resolved photocurrent response upon cyclic exposure to NO_2 at increasing concentrations (2–18 ppm, grey bars). Reproduced with permission from ref. 162. Copyright 2018 Wiley-VCH.

kinetic inertness ensures catalytic durability under conditions that would strip open-chain ligands from the metal. In photochemical catalysis, the macrocycle or its coordinated metal serves as a photoactive component, absorbing light, generating reactive intermediates, or redirecting excited-state pathways through confinement. The three regimes are complementary rather than ranked: confinement supplies substrate selectivity, coordination supplies electronic activation, and photoexcitation supplies energy input. The most potent of these systems, as we shall see, combine more than one.

4.3.1. Confinement-directed selectivity: cyclodextrin and calixarene nanoreactors. The chiral, hydrophobic interior of cyclodextrin tori has long been exploited in supramolecular catalysis, the "artificial enzyme" paradigm pioneered by Breslow.[167] However, homogeneous CD catalysis suffers from host aggregation, conformational averaging that dilutes chiral discrimination, and impractical catalyst recovery. Incorporation into a MOF lattice addresses all three limitations and adds framework-specific advantages including a periodic array of identical nanoreactors, crystallographically enforced cavity geometry, and permanent porosity for substrate access.

The most striking illustration is the regio- and enantioselective [4+4] photodimerization of 1-anthracenecarboxylate within CD-MOF-1.[168] Inside the (γ-CD)$_2$ tunnels, substrate pairs are pre-organized into a single co-facial arrangement (Fig. 24b–e) through cooperative hydrogen bonding to CD hydroxyl groups, hydrophobic encapsulation, and electrostatic stabilization by K^+ cations. Photoirradiation produces the anti-HH/2 regioisomer with 91% regioselectivity and 79% ee (Fig. 24f), whereas solution-phase dimerization, even with stoichiometric γ-CD, shows no selectivity. What the extended framework enforces, discrete cyclodextrin in solution cannot sustain (Fig. 24). Confinement can also redirect entire reaction pathways. For example, pyrrole monomers loaded into Rb-CD-MOF (*i.e.*, CD-MOF-2) undergo oxidative coupling restricted to terpyrrole cation $[TPy]^+$ formation, rather than the uncontrolled polypyrrole produced in solution or conventional porous hosts.[169] Single-crystal X-ray diffraction directly visualizes the trapped reactive intermediate, a rare crystallographic snapshot of confinement-controlled reactivity (Fig. 25b–d).

Calixarene-based MOFs extend confinement catalysis to asymmetric organic transformations.[170] Layered MOFs constructed

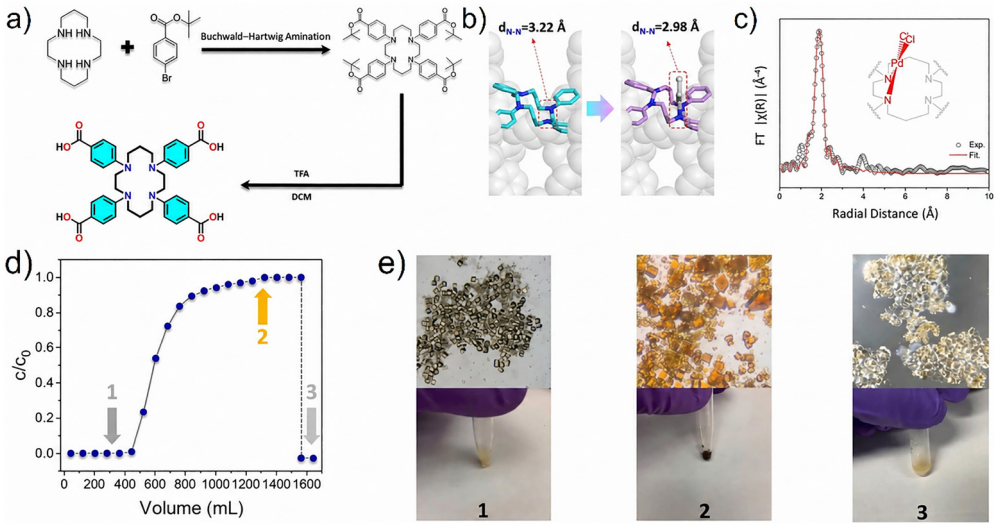


Fig. 23 Adaptive-cavity metal–macrocyclic framework for precise palladium recognition and recovery. (a) Synthetic route to the cyclam-derived tetracarboxylate linker. (b) Conformational rearrangement of the cyclam cavity upon Pd^{2+} coordination. (c) Fourier-transformed extended X-ray absorption fine structure (EXAFS) spectrum of Pd@MMCF-6 with corresponding fit. (d) Dynamic breakthrough curve of a MMCF-6-packed column for Pd^{2+} separation. (e) Optical micrographs of MMCF-6 crystals corresponding to stages 1–3. Reproduced with permission from ref. 51. Copyright 2024 Elsevier Inc.

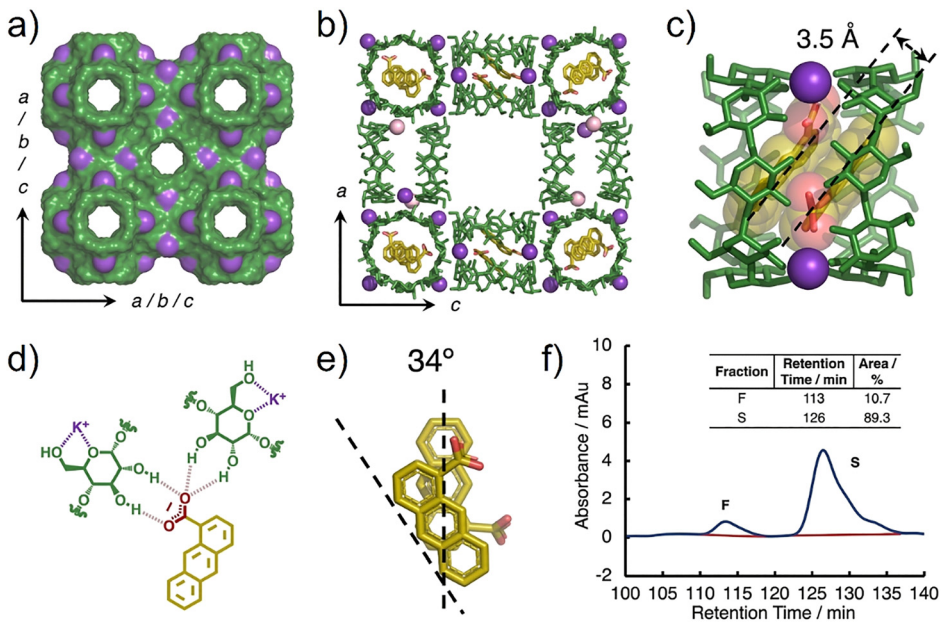


Fig. 24 Regio- and enantioselective [4+4] photodimerization of 1-anthracenecarboxylate (1-AC^-) confined within CD-MOF-1. (a) Space-filling representation of the body-centred cubic packing of CD-MOF-1, with γ-CD tori in green and K^+ cations in purple. (b) Tubular representation of a slice through the solid-state superstructure of 1-AC^-⊂CD-MOF-1 viewed from the b-axis. (c) Two 1-AC^- anions co-facially pre-organized within the $(\gamma\text{-CD})_2$ tunnel (π···π distance 3.5 Å). (d) Hydrogen-bonding network anchoring 1-AC^-: four hydrogen bonds from its carboxylate to the C-2 and C-3 hydroxyls on the secondary γ-CD face. (e) Dihedral angle of 34° between the two anthracene planes. (f) Tandem chiral HPLC chromatogram of the anti-HH/2 photodimer obtained from 1-AC^-⊂CD-MOF-1. Reproduced with permission from ref. 168. Copyright 2021 American Chemical Society.

from *p-tert*-butylsulfonylcalix[4]arene-capped Zn_4 clusters and chiral BINOL-derived linkers catalyse the condensation–cyclization of 2-aminobenzamide with aldehydes to give 2,3-dihydroquinazolinones.[24] The free chiral diol in solution produces 0% ee, however, the bulk 3D MOF boosts enantioselectivity to 56–90% ee and ultrasonic exfoliation into ultrathin 2D nanosheets raises it further to 72–94% ee. This progressive enhancement reveals two cooperating effects. First, the framework confinement restricts substrate approach trajectories and amplifies the chiral environment of the BINOL backbone while, second, the nanosheet morphology maximizes catalytic-site accessibility.

4.3.2. Coordination catalysis: aza-macrocyclic active sites. In contrast to these catalytically passive hosts, aza-macrocycles participate directly in catalytic cycles through their coordinated

 This journal is © The Royal Society of Chemistry 2026

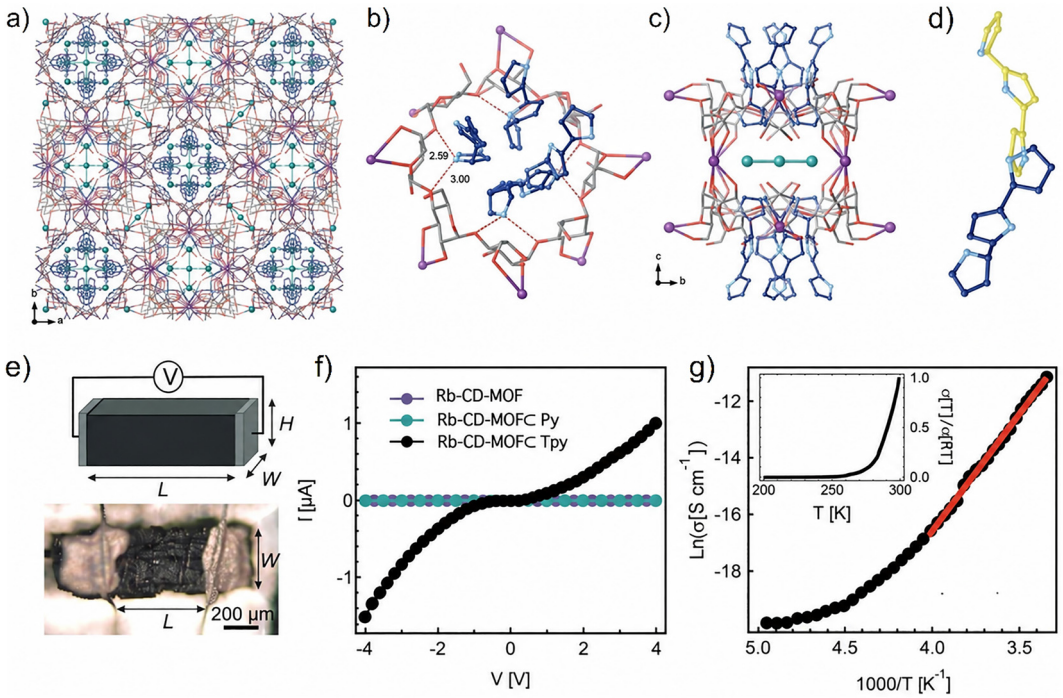


Fig. 25 Direct visualization of pyrrole reactivity and terpyrrole capture upon confinement within Rb-CD-MOF. (a) Crystal structure of Rb-CD-MOF viewed along the c axis. (b) Crystal structure of the terpyrrole cation confined within the γ-CD cavity. (c) View along the a axis showing terpyrrole molecules (blue) aligned within the CD channels; Rb^+ ions are shown as green spheres. (d) Molecular structure of the captured terpyrrole cationic intermediate. (e) Single-crystal two-probe conductivity setup (top) and optical micrograph of a contacted Rb-CD-MOF⊃Tpy crystal (bottom; scale bar 200 μm). (f) *I*–*V* curves of pristine Rb-CD-MOF, Rb-CD-MOF⊃Py, and Rb-CD-MOF⊃Tpy. (g) Arrhenius plot of ln(*σ*) *versus* 1000/*T* for Rb-CD-MOF⊃Tpy, confirming semiconducting transport behaviour; inset shows the temperature-dependent conductivity *σ*(*T*). Reproduced with permission from ref. 169. Copyright 2019 Wiley-VCH.

metal centres. The macrocyclic effect, enhanced thermodynamic stability and kinetic inertness relative to open-chain analogues, ensures that the metal centre remains coordinated throughout the catalytic cycle, even under elevated temperatures, corrosive media, and oxidizing conditions. Ring-size variation (9-membered TACN → 12-membered cyclen → 14-membered cyclam) and pendant-arm functionalization provide electronic fine-tuning without altering the framework topology. CO_2 chemical fixation provides the clearest demonstration. The cycloaddition of CO_2 to epoxides requires a Lewis-acidic metal centre that remains coordinatively active through a multi-step mechanism, epoxide ring-opening, CO_2 insertion, and ring closure. MMCF-2, a Cu-azamacrocycle framework constructed from a tetracarboxylate-functionalized cyclen ligand (tactmb), catalyses this reaction at room temperature under 1 bar CO_2, achieving 95.4% yield of propylene carbonate (Fig. 26c). The yield is roughly double the 47.5% of the homogeneous Cu(tactmb) analogue and well above benchmark MOFs such as HKUST-1 (49.2%) and MOF-505 (48.0%).[50] The enhancement arises from the high density of well-oriented Cu sites within cuboctahedral nbo-topology cages (Fig. 26a and b). VPI-100, a Zr_6-based framework incorporating cyclam linkers with accessible axial coordination sites on Cu(II) or Ni(II) centres, extends the CO_2 fixation platform to sterically demanding epoxides (Fig. 27a–f). Hafnium analogues combined with electronic

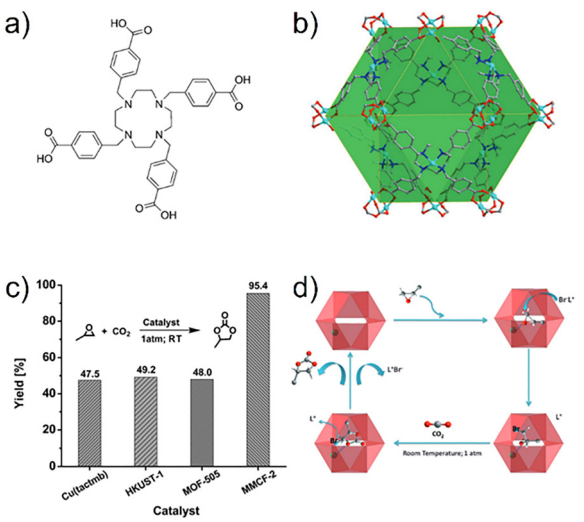


Fig. 26 Cu(II)-cyclen-based metal–macrocyclic framework for CO_2 chemical fixation. (a) Chemical structure of the tetracarboxylate-functionalized cyclen ligand (H_4tactmb). (b) Crystal structure of MMCF-2. (c) Catalytic performance of MMCF-2 for the cycloaddition of CO_2 to propylene oxide at room temperature and 1 bar CO_2, compared with the benchmark catalysts. (d) Proposed catalytic cycle. Reproduced with permission from ref. 50. Copyright 2014 Wiley-VCH Verlag GmbH & Co. KGaA.

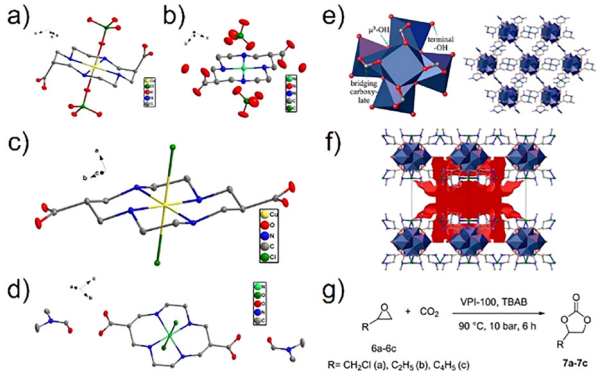


Fig. 27 Aza-macrocyclic Zr_6-based frameworks VPI-100 for CO_2 fixation. (a) Crystal structure of the $[CuL(ClO_4)_2]$ compound. (b) Crystal structure of the $[NiL(ClO_4)_2]\cdot H_2O$ compound. (c) Crystal structure of the $[CuLCl_2]$ compound. (d) Crystal structure of the $[NiLCl_2]\cdot 2DMF$ compound. (e) Structure of the $Zr_6(\mu_3\text{-}OH)_8(OH)_8$ cluster node. (f) Framework topology of VPI-100 with the solvent-accessible pore volume shown in red. (g) Catalytic CO_2 cycloaddition to sterically demanding epoxides (VPI-100 with TBAB co-catalyst, 90 °C, 10 bar CO_2, 6 h). Reproduced with permission from ref. 23. Copyright 2018 American Chemical Society.

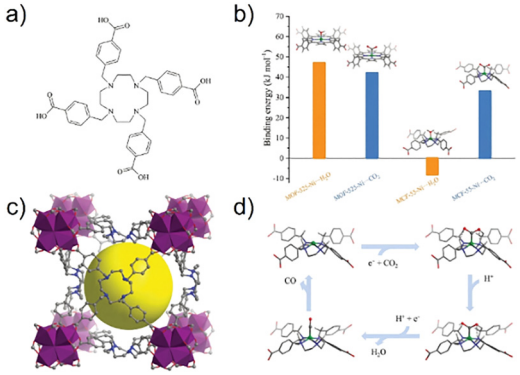


Fig. 29 Ni(II)-cyclen-based framework for photocatalytic CO_2-to-CO conversion. (a) Chemical structure of the tetracarboxylate-functionalized cyclen ligand. (b) DFT-calculated binding energies for H_2O and CO_2 at the Ni(II) centres in MOF-525-Ni (porphyrin-based) and MCF-55-Ni (cyclen-based). (c) Crystal structure of the nbo-topology cuboctahedral cage in MCF-55. (d) Proposed photocatalytic cycle for CO_2 reduction at the Ni(II)–cyclen active site. Reproduced with permission from ref. 172. Copyright 2019 Royal Society of Chemistry.

structure calculations confirm that the open metal centres within the cyclam ring, rather than the Hf_6 cluster nodes, serve as the dominant Lewis acid sites for epoxide activation (Fig. 28c and d).[171] The cyclen platform extends naturally to photocatalysis. MCF-55-Ni, isostructural to MMCF-2 but bearing Ni(II)-cyclen active sites, achieves photocatalytic CO_2-to-CO conversion with a turnover frequency of 73.8 h^{-1} and 96% CO selectivity in the presence of water. MCF-55-Ni outperforms both the porphyrin-based MOF-525-Ni and the cyclam-based VPI-100(Ni) under identical conditions (Fig. 29).[172] The decisive design insight is that the methylene groups flanking the cyclen nitrogen donors create a local hydrophobic microenvironment around the metal centre, repelling water molecules and suppressing the competing hydrogen-evolution pathway. The hydrophobic shielding thus resolves a selectivity problem that has long plagued heterogeneous CO_2 photoreduction (Fig. 29b).

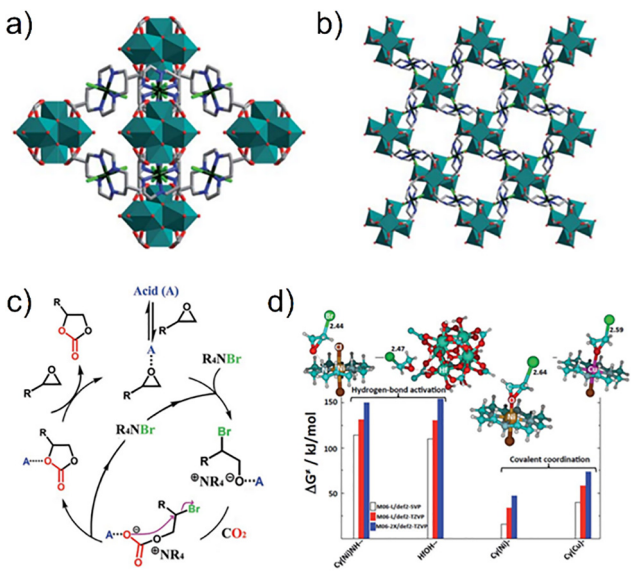


Fig. 28 Hafnium-based aza-macrocyclic framework VPI-100(Hf) for CO_2 cycloaddition. (a) Crystal structure of the Hf_6 cluster node coordinated by cyclam dicarboxylate linkers. (b) Extended three-dimensional framework topology of VPI-100(Hf). (c) Proposed catalytic mechanism for the cycloaddition of CO_2 to epoxides. (d) DFT-calculated activation free energies (ΔG) for epoxide ring-opening at different candidate active sites. Reproduced with permission from ref. 171. Copyright 2018 Royal Society of Chemistry.

More demanding redox catalysis becomes accessible through polyoxometalate–aza-macrocycle hybrids. A decavanadate/Cu(cyclam) open framework achieves 99% conversion in the H_2O_2-mediated oxidation of adamantane, a benchmark C–H activation substrate, within 6 hours, outperforming conventional Keggin-type heteropolyacid catalysts under identical conditions.[173] In the electrocatalytic domain, Co-TMBT-MOF, built from a TACN-derived tricarboxylate ligand, serves as an effective pre-catalyst for the oxygen evolution reaction. Here, nickel foam electrodes loaded with Co-TMBT-MOF sustain 20 mA cm^{-2} at an overpotential of only 294 mV with 20-hour stability in 1 M KOH.[174] The macrocyclic amine core prevents metal leaching during processing, enabling clean *in situ* transformation into catalytically active cobalt oxyhydroxide. Aza-macrocyclic frameworks can thus serve not only as direct catalysts but also as structurally defined precursors to high-performance electrocatalytic materials.

4.3.3. Photochemical transformations: macrocycles as photoactive components. In the preceding subsections, macrocyclic cavities serve either as passive confinement vessels (Section 4.3.1) or as scaffolds for catalytically active metal centres (Section 4.3.2). A third paradigm emerges when the macrocycle itself participates in the photochemical event, not merely hosting a substrate but actively generating reactive intermediates through light absorption.

The clearest demonstration of this is a Pd-mediated metal–macrocycle framework (MMF) constructed from trinuclear $PdCl_2$ complexes of a macrocyclic hexamine ligand.[68] A 1,6-diene that quantitatively undergoes intramolecular [2+2] photocycloaddition

 This journal is © The Royal Society of Chemistry 2026

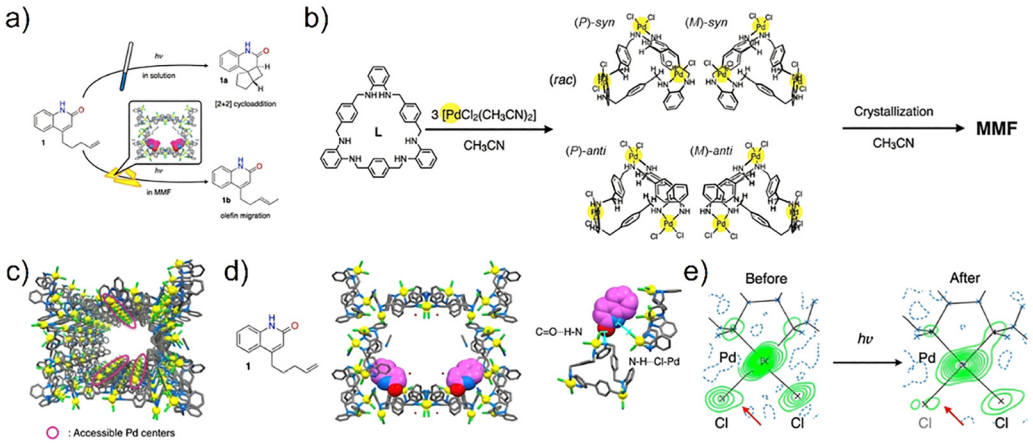


Fig. 30 Photoinduced olefin migration in a porous metal–macrocycle framework (MMF). (a) Divergent photoreaction pathways of 1,6-diene 1. (b) Self-assembly of hexamine ligand L with three equivalents of $PdCl_2(CH_3CN)_2$ into four stereoisomeric trinuclear complexes. (c) Crystal structure of the MMF channel viewed along the channel axis. (d) Site-selective uptake of substrate 1 within the MMF channel (39% occupancy, CPK model in magenta). (e) 2D electron density maps around a channel-ceiling $PdCl_2$ centre before (left) and after (right) photoirradiation. Reproduced with permission from ref. 68. Copyright 2018 American Chemical Society.

in solution is completely redirected toward olefin migration when encapsulated within the MMF channels (Fig. 30a). The pathway switch arises from a dual mechanism. Photoirradiation cleaves the Pd–Cl bonds lining the channel walls, generating coordinatively unsaturated Pd(0) centres that activate the terminal olefin *via* [1,3]-sigmatropic rearrangement, while the confined space simultaneously suppresses the conformational reorganization required for [2+2] ring closure. Single-crystal X-ray diffraction before and after irradiation directly visualizes the reduction in Cl electron density around the Pd centres, a rare crystallographic snapshot of photocatalytic activation within a porous framework. The substrate scope extends to substituted allylbenzene derivatives (41–82% conversion), confirming generality of this activation–inhibition strategy (Fig. 30d and e).

At the opposite end of the photocatalytic spectrum, the macrocyclic scaffold itself can serve as an electron-rich photosensitizing antenna. Co-C[3]PTZ-MOF, for example, assembled from a phenothiazine-functionalized calix[3]arene ligand and cobalt nodes, achieves CO_2 photoreduction at an initial rate of 17 800 μmol g^{-1} h^{-1} with 81% CO selectivity (Fig. 31h and i).[175] The electron-donating phenothiazine units embedded within the calixarene scaffold broaden visible-light absorption and facilitate photogenerated charge separation, while the bowl-shaped macrocyclic topology pre-organizes the cobalt active sites for CO_2 binding. Phenothiazine electronics and bowl-shaped confinement thus combine the logic of Section 4.3.1 with the coordination catalysis of Section 4.3.2 in a single photoactive platform (Fig. 31).

Three catalytic logics coexist within macrocycle–MOF systems and their boundaries are not as firm as the preceding subsections suggest. Confinement pre-organizes, coordination activates, and photoexcitation redirects, yet the most powerful examples blur these distinctions. This can be demonstrated with a calixarene bowl that simultaneously confines a substrate

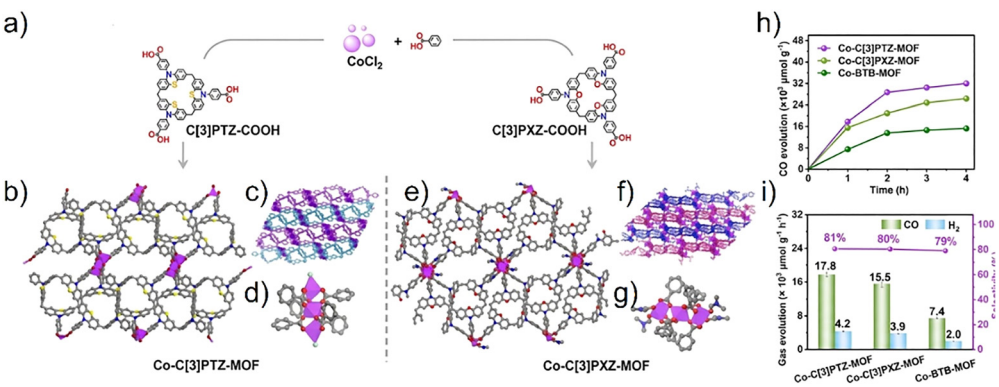


Fig. 31 Phenothiazine- and phenoxazine-functionalized calix[3]arene MOFs for photocatalytic CO_2 reduction. (a) Synthetic scheme. (b)–(d) Crystal structure of Co-C[3]PTZ-MOF viewed along the channel axis, with top and side views of the calixarene bowl (Co nodes, pink polyhedra). (e)–(g) Corresponding views for Co-C[3]PXZ-MOF (h) Time-dependent CO evolution under visible-light irradiation for Co-C[3]PTZ-MOF, Co-C[3]PXZ-MOF, and the non-macrocyclic control Co-BTB-MOF. (i) Total CO and H_2 production rates and CO selectivities. Reproduced with permission from ref. 175. Copyright 2025 American Chemical Society.

and harvests light or a cyclam that holds a metal centre in place while the framework channels funnel reagents toward it. The deeper lesson is that macrocycles are not catalysts in the classical sense, they are environments. What a macrocyclic MOF offers to catalysis is not a single active site but a complete reaction context: a defined cavity geometry, a tailored electronic field, and a controlled approach trajectory. The framework reproduces the same environment with crystallographic precision at every pore. The field has demonstrated proof of concept, however, what it has not yet achieved is design, the deliberate, predictive matching of a macrocyclic environment to a target transition state. When that capacity emerges, macrocycle–MOF catalysis will move from serendipitous discovery to rational synthesis, from chemistry to engineering.

4.4. Ordered transport and functional platforms

In Sections 4.1–4.3, the macrocyclic cavity captures, discriminates, or transforms a guest, and in each case, strong binding is an asset. Transport inverts this logic. Here, the macrocycle must bind a species just long enough to relay it to the next site, then release it, and the penalty for binding too strongly is not poor selectivity but zero flux. The design target shifts from maximizing affinity to optimizing residence time. A proton must linger on a CD hydroxyl long enough to establish directionality but briefly enough to sustain a Grotthuss-type current. A lithium ion, likewise, must nestle into a crown ether cavity long enough to shed its solvation shell but not so long that it becomes trapped.[176,177] This tension between capture and release, absent in separation, sensing, and catalysis, is the defining physical chemistry of macrocyclic transport. When these elementary binding–release events are organized by the translational symmetry of a MOF lattice, a molecular-scale kinetic process becomes a material-scale transport property, such as: proton conduction, electronic conductivity, ion shuttling, or cargo delivery. The efficiency of each depends not on the strength of a single host–guest interaction, but on the continuity of the relay chain, its periodicity, its defect tolerance, and, above all, its ability to sustain directional flux under a driving force.

4.4.1. Proton and ion conduction. The hydroxyl-rich surfaces of cyclodextrin tori, the carbonyl portals of cucurbiturils, and the crown ether oxygen arrays each provide hydrogen-bonding networks capable of sustaining proton relay through Grotthuss or vehicular mechanisms. Oriented CD-MOF thin films, grown epitaxially on (3-aminopropyl)trimethoxysilane (APTMS)-functionalized substrates, exhibit proton conductance up to 300-fold higher than randomly packed powders (Fig. 33a and b), attributed to the continuous, defect-free hydrogen-bonding network of aligned γ-CD tori.[20] The same films function as CO_2 sensors that can exhibit a 50-fold conductivity decrease within 3 seconds upon CO_2 exposure, with full recovery in 10 seconds. Proton conduction and chemical sensing thus coexist in a single macrocyclic MOF thin film (Fig. 33c).

Cucurbituril-based frameworks provide complementary proton-conducting platforms.[178–180] A porous CB[6]-based coordination polymer enhances its electrical conductivity upon iodine uptake. Here, polyiodide chains assembled within the channels from discrete iodide ions and adsorbed I_2 create continuous charge-transport pathways, highlighting the role of the cucurbituril carbonyl portal as a guest-binding site.[67] More recently, CB[6]-based metal–organic rotaxane frameworks (MORFs) incorporating proton donors (–COOH) and acceptors ($–NH_2$) simultaneously achieve a proton conductivity of 8.7×10^{-5} S cm^{-1} at 75 °C and 98% RH, a strategy that demonstrates how the unique threading topology of MORFs can be exploited to engineer dense hydrogen-bonding networks within the cucurbituril channels.[181]

Crown ether–MOF composites have been engineered into biomimetic ion-channel membranes operating on a fundamentally different principle: selective ion dehydration and transport rather than proton hopping.[182] Crown ethers (dibenzo-15-crown-5 and dibenzo-18-crown-6) confined within the octahedral cavities of UiO-66 membranes achieve essentially complete dehydration of monovalent ions during transport, which conventional size-exclusion membranes do not achieve (Fig. 32a and b).[46] The DB18C6@UiO-66 membrane delivers a K^+ permeation rate of 1.2 mol m^{-2} h^{-1} and a K^+/Mg^{2+} selectivity of 57, with first-principles calculations confirming that the crown ether cavity lowers the dehydration energy barrier below that of the bare UiO-66 pore. Encapsulation of benzo-12-crown-4-ether within ZIF-7 sub-nanochannels provides an orthogonal selectivity handle in which cation-induced surface charge inversion shifts Li^+/Mg^{2+} selectivity from ∼25 to 125, recapitulating the charge-regulation mechanism of biological ion channels (Fig. 34a).[21]

The most ambitious biomimetic design integrates carboxybenzo-15-crown-5 into UiO-66-COOH, creating a dual-pathway membrane that recapitulates the NaK channel architecture. Here, carboxyl groups conduct K^+ while the anchored crown ethers provide flexible Na^+ pathways; depending on the salt environment, the membrane switches between selectivity regimes, K^+/Mg^{2+} of $\sim 10^2$ and Na^+/K^+ of up to 10^3, alongside dynamic Mg^{2+}-triggered gating with on/off ratios around 30 (Fig. 35a–c).[183]

4.4.2. Electrically conductive macrocyclic frameworks. Electrical conductivity in MOFs has traditionally been limited by insulating organic linkers and poor metal–ligand orbital overlap. Macrocyclic linkers with extended π-conjugation offer a fundamentally different approach where the shape-persistent macrocyclic core provides a continuous conjugation pathway, while coordinated metal nodes serve as charge-hopping sites that bridge adjacent macrocyclic units into a continuous transport pathway.

Cu-HHTC, a 2D conductive MOF constructed from 2,3,8,9,14,15-hexahydroxytribenzocyclyne (HHTC) and Cu(II) nodes, achieves an electrical conductivity of up to 3.02×10^{-3} S cm^{-1} (Fig. 36a and c) with a surface area of up to 1196 m^2 g^{-1}, among the highest reported for 2D EC-MOFs (Fig. 36).[184] The enlarged macrocyclic pore and intrinsic alkyne-based pocket of HHTC provide both the extended conjugation needed for charge transport and the functionalizable void space absent in smaller triphenylene-based ligands. Replacing the six hydroxyl donors with amino groups yields a dramatic electronic transformation. For example, Ni-HATC, built from the hexaaminotribenzocyclyne (HATC) ligand, achieves 20 S cm^{-1} in thin films and 3 S cm^{-1} in bulk, a nanoporous synthetic metal with 1000 m^2 g^{-1} surface area (Fig. 37).[185] The

 This journal is © The Royal Society of Chemistry 2026

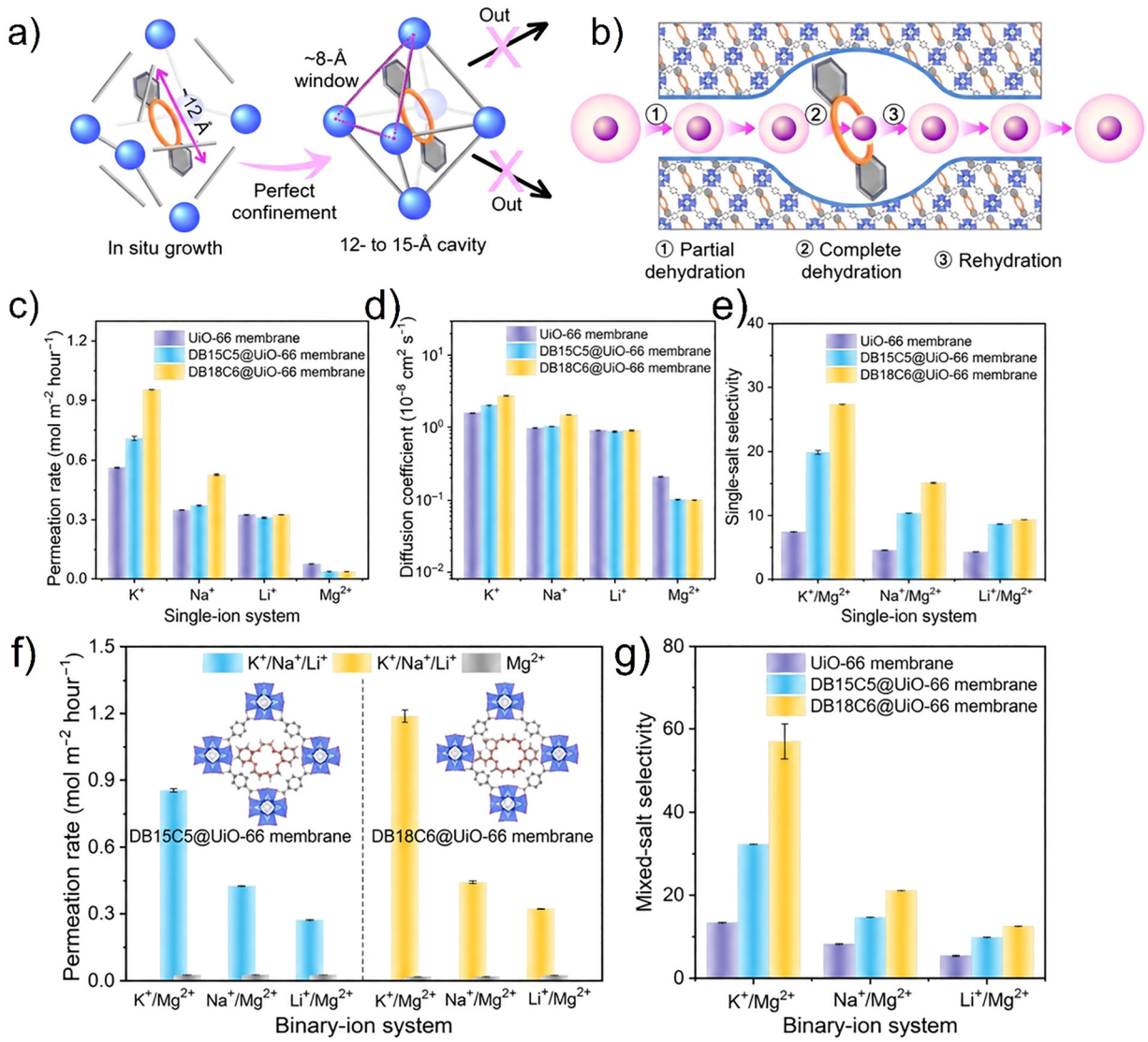


Fig. 32 Biomimetic ion-channel membranes based on crown ether@UiO-66 composites. (a) *In situ* confinement strategy. (b) Ion transport mechanism through the membrane. (c) Single-ion permeation rates for K^+, Na^+, Li^+, and Mg^{2+} across bare UiO-66, DB15C5@UiO-66, and DB18C6@UiO-66 membranes. (d) Corresponding ion diffusion coefficients. (e) Single-salt mono-/divalent ion selectivities. (f) Binary-ion permeation rates for DB15C5@UiO-66 and DB18C6@UiO-66 membranes in competitive monovalent/divalent ion mixtures. (g) Mixed-salt selectivities. Reproduced with permission from ref. 46. Copyright 2024 American Association for the Advancement of Science.

six electron-donating amino groups combined with three alkyne units raise the electron density sufficiently to cross the semiconductor–metal boundary. Substituent design thus renders the electronic ground state of a macrocyclic MOF continuously tuneable, a molecular-level handle with no analogue in conventional inorganic conductors (Fig. 37c and e).

The progression from HHTC to HATC (hydroxyl → amino substitution, $10^{-3} \rightarrow 10^{1}$ S cm^{-1}) points to substituent electron density as a decisive variable governing charge transport in macrocyclic EC-MOFs, although the metal node also changes between the two frameworks; the Cu-HATC analogue (Fig. 37b) provides the controlled comparison. Extending this logic to mixed-donor coordination environments, a Salphen macrocycle-based 2D c-MOF (SM-MOF-Cu) constructed from a multidentate hexaaza-macrocycle with N_2O_2 binding pockets achieves 96.6% faradaic efficiency (Fig. 38b and c) for electrocatalytic acetylene semi-hydrogenation to ethylene at −0.85 V *vs.* RHE.[186] The mixed N_2O_2 donor set supports a dual Cu(I)/Cu(II) oxidation state confirmed by XPS, enabling a redox-cycling mechanism for selective acetylene binding and reduction, a rationale consistent with the catalytic advantages of aza-macrocyclic frameworks discussed in Section 4.3 (Fig. 38). The convergence of electronic tunability, permanent porosity, and catalytic activity in these macrocyclic EC-MOFs positions them as versatile platforms where ion transport and electron transport coexist within a single crystalline material.

4.4.3. Energy storage. Energy storage demands rapid, reversible, and fatigue-resistant ion shuttling over thousands of charge–discharge cycles, a kinetic requirement that would seem to favour oxygen-donor macrocycles with fast exchange kinetics

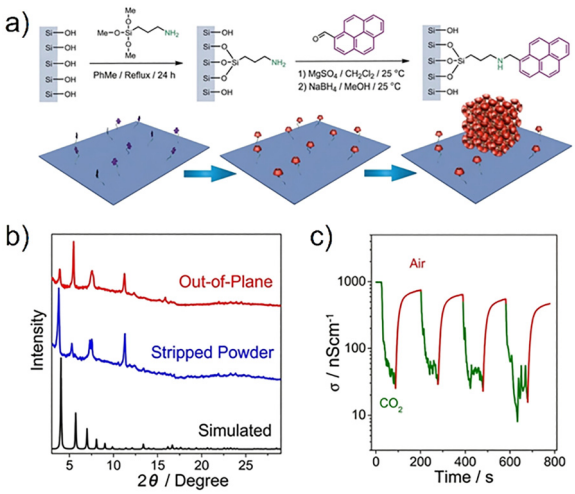


Fig. 33 Epitaxial growth of oriented γ-CD-MOF thin films and their CO_2-responsive proton conductivity. (a) Fabrication strategy. (b) X-ray diffraction patterns of the oriented thin film (out-of-plane), the stripped powder, and the simulated pattern. (c) Time-resolved ionic conductivity (σ) upon cyclic switching between air and CO_2 atmospheres. Reproduced with permission from ref. 20. Copyright 2018 American Chemical Society.

over kinetically inert nitrogen-donor complexes. The three systems below, however, deploy the macrocycle in three distinct roles, interface regulator, mechanical buffer, and intermediate stabilizer, and in none of them does the macrocycle store the charge: its job is to discipline the conditions under which storage happens elsewhere.

NKU-2000, a 2D crown ether coordination network applied as an interfacial layer for lithium metal anodes, sustains 8500 hours of cycling at 1 mA cm^{-2} (Fig. 39a and b), 1700 hours even at 10 mA cm^{-2} and 10 mAh cm^{-2}, and 2000 cycles with 81.8% retention in a $LiFePO_4$ full cell.[187] The ordered lithiophilic crown sites lower the Li^+ desolvation barrier, guiding uniform, dendrite-free deposition (Fig. 39c–e), the labile end of the interaction-mode axis put to work: the crown must bind Li^+ strongly enough to organize its delivery, yet weakly enough to release it several thousand times without fatigue.

POM–CD-MOF hybrids access a fundamentally different storage mechanism.[188] POT-CD, assembled from Keggin-type PW_{12} polyoxotungstate and γ-cyclodextrin, gains rather than loses capacity on cycling, from ∼130 to 695 mAh g^{-1} over 450 cycles (Fig. 40b–e), a 482.6% retention relative to the second cycle, unprecedented in MOF anodes.[189] Stepwise amorphization during lithiation progressively exposes fresh active sites, while the weak $K^+/Na^+\cdots O$ bonds between CD and POM layers absorb the structural reorganization without catastrophic failure (Fig. 40). Here the macrocycle's contribution is mechanical rather than chemical: the weak, distributed bonding that makes CD lattices fragile elsewhere becomes, under electrochemical stress, a designed failure mode, the electrode survives by breaking gracefully. In the supercapacitor domain, five macrocyclic hosts (α-CD, sulfo-β-CD, sulfonatocalix[4]arene, CB[6], and CB[7]) were co-assembled with polypyrrole on ZIF-8/carbon nanotube electrodes; CB[7] delivers the highest areal capacitance, 1533 mF cm^{-2} with 83% retention over 2000 cycles.[66] The margin traces to the carbonyl portals' affinity for the polypyrrole radical cation, which anchors the redox-active intermediate at the electrode. That the least labile host wins here completes the lesson of this section: transport-limited functions reward the weak-binding end of the diagonal, whereas intermediate stabilization rewards the strong end.

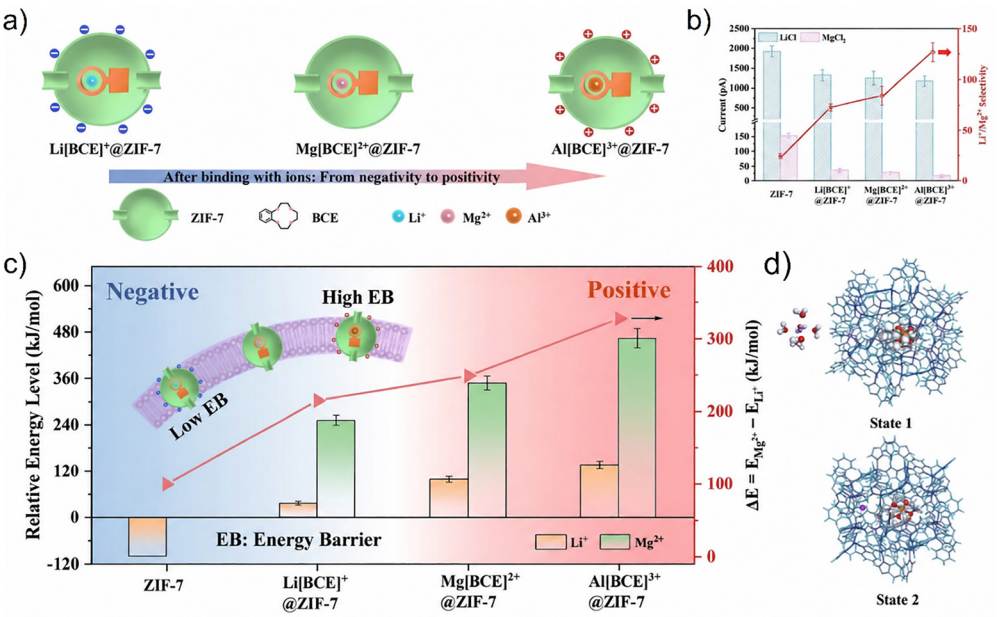


Fig. 34 Charge-regulated Li^+/Mg^{2+} separation in benzo-12-crown-4-ether@ZIF-7 sub-nanochannels. (a) Schematic of the surface charge inversion mechanism. (b) Ion transport currents for LiCl and $MgCl_2$ and the resulting Li^+/Mg^{2+} selectivity. (c) First-principles calculated energy barriers for Li^+ and Mg^{2+} transport through each membrane. (d) Molecular dynamics snapshots of BCE@ZIF-7 in two representative states. Reproduced with permission from ref. 21. Copyright 2023 Wiley-VCH GmbH.

 This journal is © The Royal Society of Chemistry 2026

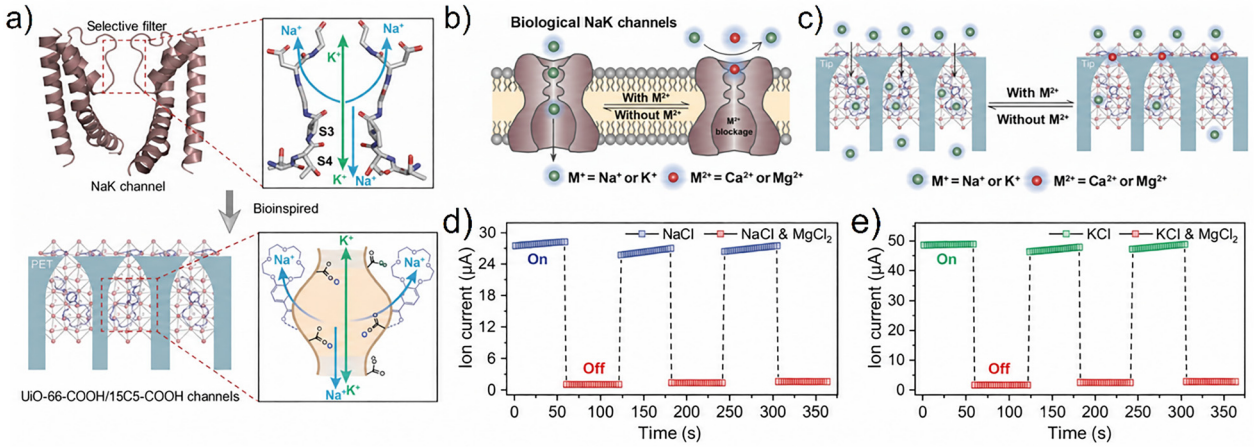


Fig. 35 Biomimetic NaK channel membrane based on crown ether-coordinated UiO-66. (a) Design analogy. (b) Biological NaK channel gating mechanism: monovalent ions (M^+) permeate freely, while divalent ions (M^{2+} = Ca^{2+} or Mg^{2+}) block the channel. (c) Artificial membrane counterpart: arrays of crown ether@UiO-66 channels on a PET support reproduce Mg^{2+}-triggered gating behaviour. (d) Dynamic Mg^{2+}-gated switching of Na^+ transport. (e) Analogous Mg^{2+}-gated switching of K^+ transport: KCl current is reversibly toggled by $MgCl_2$. Reproduced with permission from ref. 183. Copyright 2026 Wiley-VCH GmbH.

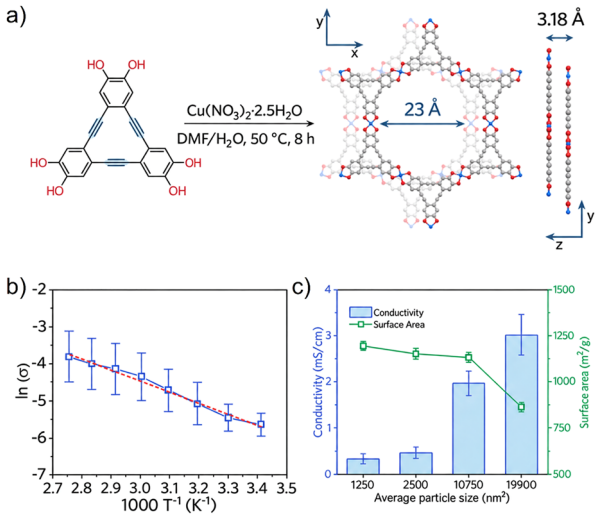


Fig. 36 2D conductive MOF Cu-HHTC constructed from a macrocyclic hexahydroxytribenzocyclyne linker. (a) Synthesis of Cu-HHTC. (b) Arrhenius plot of ln(σ) *versus* 1000/*T*, confirming thermally activated semiconducting charge transport. (c) Electrical conductivity (blue bars, left axis) and BET surface area (green squares, right axis) as a function of average particle size. Reproduced with permission from ref. 184. Copyright 2022 American Chemical Society.

Energy storage does not pick a favourite macrocycle, it assigns each to the sub-task its exchange kinetics fit. In most cases, however, the macrocycle remains an auxiliary (interlayer, buffer, additive) rather than the primary electrode, and the heterogeneous metrics (areal, gravimetric, capacitive) resist cross-comparison: the benchmarking gap of Section 5.1.3 in miniature.

4.4.4. Biocompatible cargo transport: cyclodextrin-based drug delivery. Cyclodextrin-based MOFs are the only framework class constructed entirely from food-grade, FDA-recognized-as-safe ingredients, γ-CD and alkali metal cations, offering intrinsic biocompatibility combined with permanent porosity (BET >1200 $m^2\ g^{-1}$, pore diameter ~1.7 nm). The foundational synthesis demonstrated room-temperature crystallization from γ-CD and KOH, reflecting the moderate binding constants of the CD–alkali–metal coordination. The same biocompatible scaffold has since served as a template for growing ultrafine silver nanoparticles, and GRGDS surface functionalization combines their antibacterial action with haemostasis in a single wound-healing platform.[190] Translating this intrinsic biocompatibility into deployable form factors, Zhang, Zhou, and co-workers grew γ-CD-MOF crystals directly onto cellulose fibres through *in situ* vapour-diffusion crystallization. The resulting free-standing CelluMOF composites retain the framework's permanent porosity while gaining the mechanical flexibility of the textile substrate (Fig. 41).[191] The resulting fabrics capture volatile organic compounds (styrene, aniline, and benzaldehyde) from ambient air and function as colorimetric CO_2 indicators. CD-MOF processability thus extends well beyond powder-based formulations into wearable and consumer-facing platforms. KMOF-1, a mesoporous crown ether-based MOF constructed from 18-crown-6 linkers and K^+ centres, achieves 1034 $m^2\ g^{-1}$ surface area and demonstrates acid-responsive release of VEGF aptamers with nuclease protection. KMOF-1 thus extends macrocyclic MOF drug delivery beyond the CD family into the crown ether domain (Fig. 42).[192]

What emerges from the transport applications is not a catalogue of functions but a single architectural insight: the macrocycle is a valve, and the MOF lattice is the manifold that wires those valves together. Protons hop along CD hydroxyl relays, electrons delocalize through conjugated tribenzocyclyne sheets, lithium ions shed their solvation shells at crown ether stations, and drug molecules exit through CD-MOF pores. Protons, electrons, ions, and cargo differ only in the species admitted: in each case a molecular-scale gating event, crystallographically replicated, becomes a material-scale transport property. The distinction between "conductor," "membrane," and "drug carrier" is

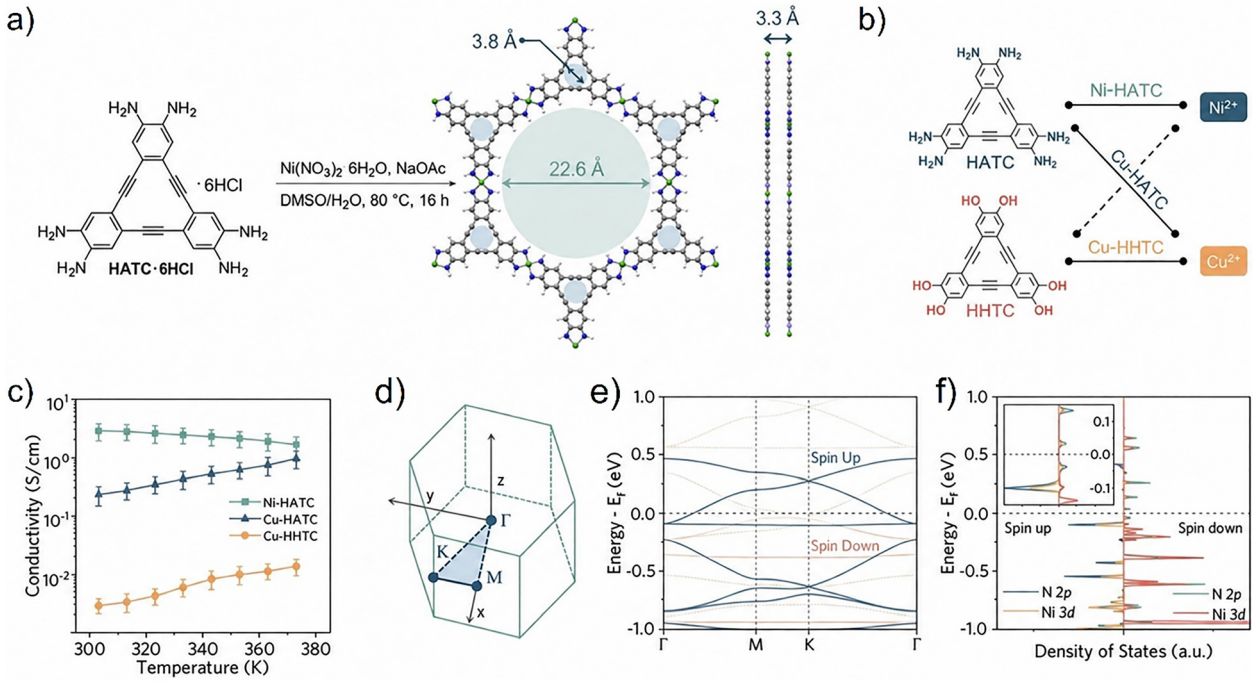


Fig. 37 Nanoporous synthetic metal Ni-HATC based on a hexaaminotribenzocyclyne macrocyclic linker. (a) Synthesis of Ni-HATC from the hexaamine macrocycle HATC·6HCl and $Ni(NO_3)_2$ in DMSO/H_2O. (b) Linker comparison: the electron-donating hexaamino ligand HATC yields Ni-HATC (metallic) and Cu-HATC. (c) Variable-temperature conductivity. (d) First Brillouin zone of the 2D hexagonal lattice with high-symmetry points Γ, M, and K. (e) DFT band structure of Ni-HATC, showing spin-split bands crossing the Fermi level. (f) Projected density of states for Ni 3d and N 2p orbitals near the Fermi level (inset, expanded view). Reproduced with permission from ref. 185. Copyright 2025 Elsevier Inc.

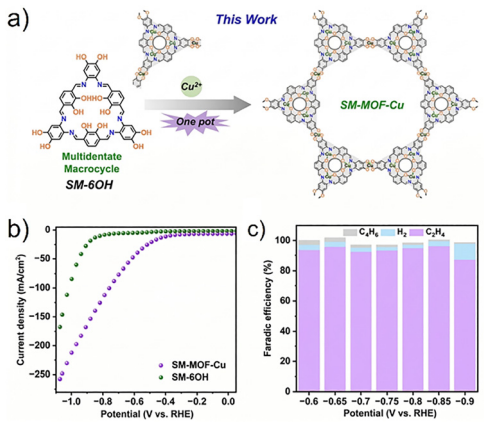


Fig. 38 Salphen macrocycle-based 2D conjugated MOF for electrocatalytic acetylene semi-hydrogenation. (a) One-pot synthesis of SM-MOF-Cu from the multidentate hexaaza-macrocyclic linker SM-6OH bearing N_2O_2 salphen binding pockets and Cu^{2+} ions, yielding a 2D c-MOF with enlarged macrocyclic pores. (b) Linear sweep voltammetry curves comparing SM-MOF-Cu and the free ligand SM-6OH, demonstrating substantially higher current densities for the framework. (c) Faradaic efficiencies for C_2H_4, H_2, and C_4H_6 at potentials from −0.6 to −0.9 V *vs.* RHE: SM-MOF-Cu achieves 96.6% Faradaic efficiency for ethylene at −0.85 V. Reproduced with permission from ref. 186. Copyright 2025 Wiley-VCH GmbH.

not intrinsic to the material, it is set by which species the valve admits and what driving force is applied. This universality has a practical consequence that the field has not yet exploited: a single macrocycle–MOF membrane could, in principle, conduct protons under a chemical potential gradient, transport electrons under a voltage bias, and release cargo under a pH switch, simultaneously. The barrier is no longer synthesis, it is the absence of a theoretical framework that predicts how multiple transport modes couple within the same periodic lattice. Building that theory, bridging molecular host–guest thermodynamics with solid-state transport physics, is the defining intellectual challenge for the next phase of macrocycle–MOF research.

4.5. Summary

What separates a macrocycle from a functional group is not size but time. A carboxylate binds a metal ion at a rate dictated by solvent exchange; a macrocycle binds the same ion at a rate set by its own preorganization, cavity fit, and donor-atom cooperativity. This self-determined kinetics connects every application in this section. Separation, gating, catalysis, and transport each place a different demand on this single variable, a residence time that must exceed those of competitors, respond to an external signal, permit both activation and release, or sit in the narrow window between trapping and indifference.

The framework lattice disciplines this kinetics. A macrocycle in solution samples every conformation and acts alone; in a lattice it is held to a few and acts in concert with its neighbours. The consequence is not merely amplification but emergence, cooperative ion selectivity, band-like electronic transport, coherent proton relay, that no discrete macrocycle can produce

 This journal is © The Royal Society of Chemistry 2026

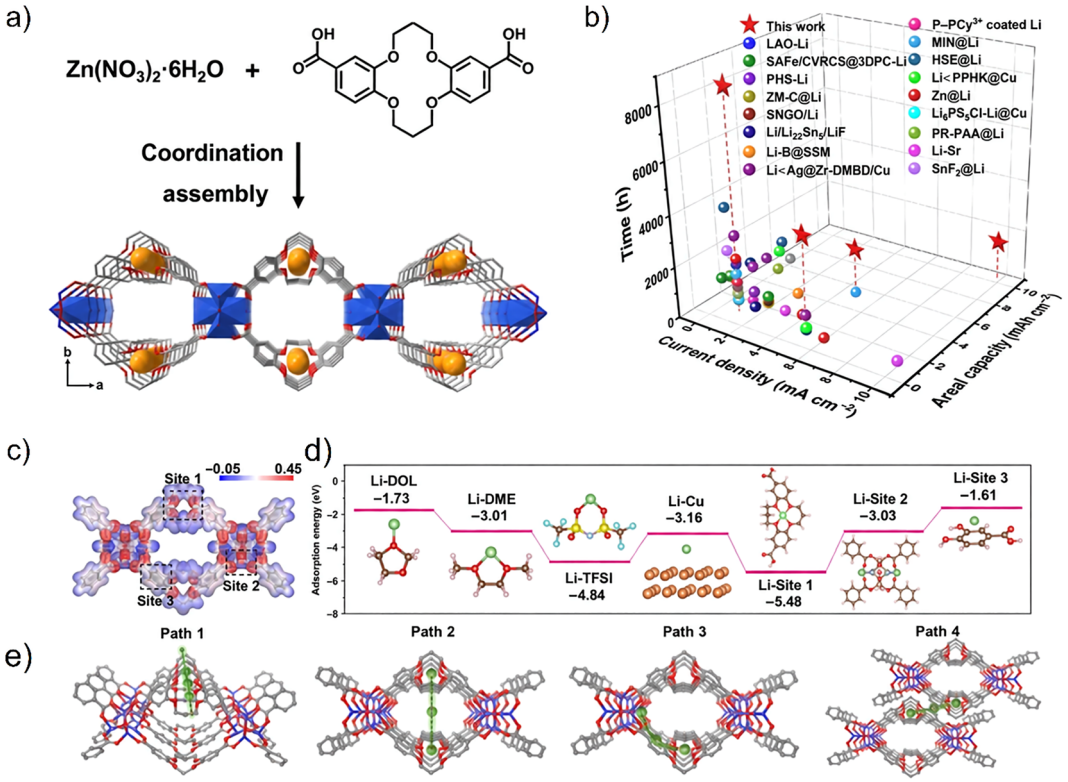


Fig. 39 2D crown ether coordination network NKU-2000 as a lithiophilic interfacial layer for dendrite-free lithium metal anodes. (a) Coordination assembly of NKU-2000 from $Zn(NO_3)_2$ and a benzo-14-crown-4 dicarboxylate linker. (b) 3D performance comparison of NKU-2000-modified Li anodes (red stars) with literature benchmarks across cycling time, current density, and areal capacity. (c) Electrostatic potential map of NKU-2000 revealing three distinct Li^+ adsorption sites. (d) DFT-calculated adsorption energies for Li^+ with electrolyte components (DOL, DME, $TFSI^-$, Cu) and the three framework sites. (e) Four possible Li^+ migration pathways across the NKU-2000 surface. Reproduced with permission from ref. 187. Copyright 2025 Chinese Chemical Society.

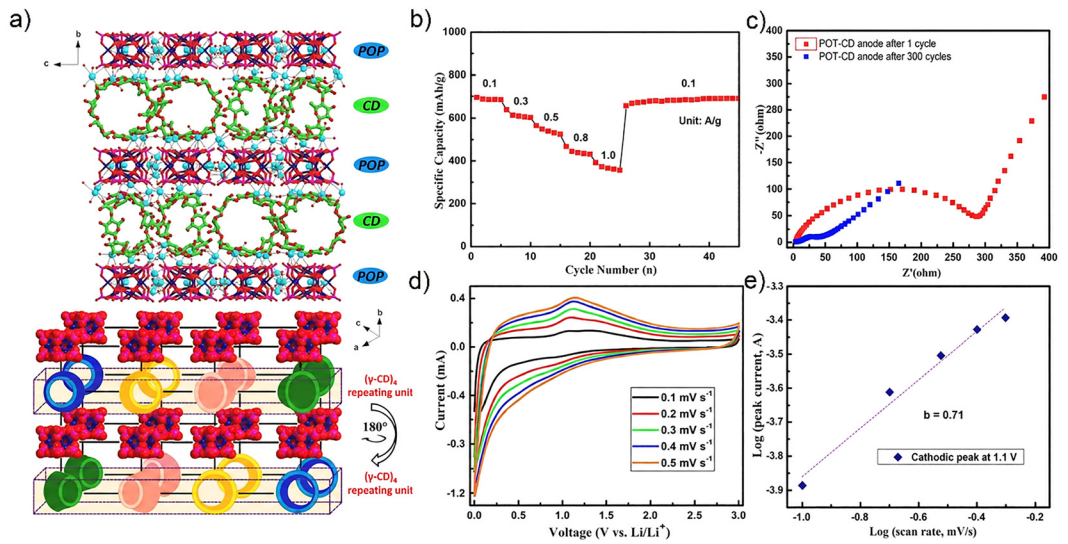


Fig. 40 Polyoxometalate–cyclodextrin MOF hybrid as a lithium-ion battery anode with anomalous capacity enhancement. (a) Crystal structure of POP-CD: alternating Keggin-type polyoxotungstate and γ-cyclodextrin layers linked by $K^+/Na^+\cdots O$ bonds (top); the staggered double layer, in which γ-CD toroids in neighbouring sublayers adopt opposite orientations, serves as the repeating unit (bottom). (b) Rate performance of the POT-CD anode at current densities of 0.1–1.0 A g^{-1}. (c) Electrochemical impedance spectroscopy (Nyquist plots) after 1 cycle and 300 cycles. (d) Cyclic voltammetry curves at scan rates of 0.1–0.5 mV s^{-1}. (e) Log(peak current) *versus* log(scan rate), giving b = 0.71 for the cathodic peak at 1.1 V. Reproduced with permission from ref. 189. Copyright 2019 American Chemical Society.

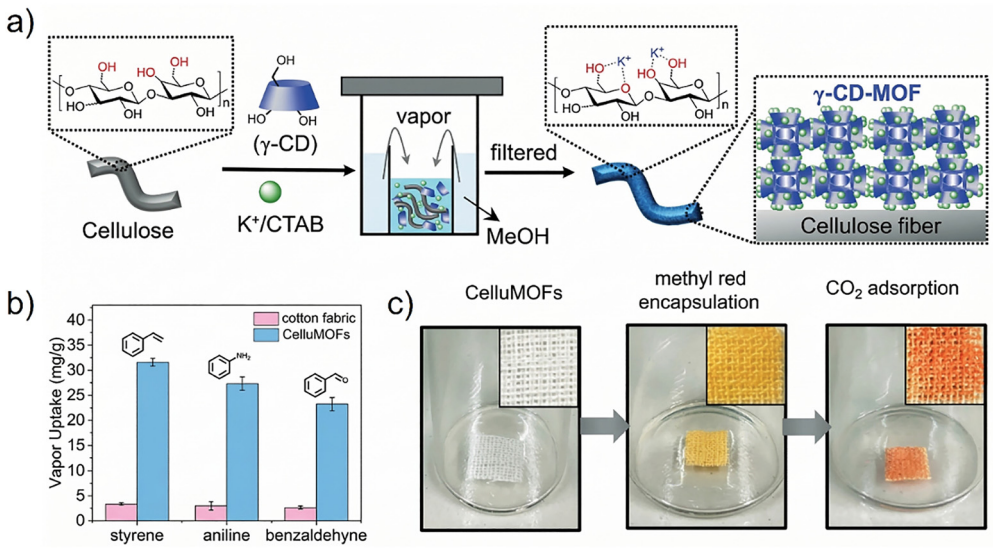


Fig. 41 Green, facile fabrication of CelluMOFs, cellulose fibre-supported γ-CD-MOF composites. (a) Synthesis scheme: cellulose fibres are immersed in a solution of γ-CD, K^+/CTAB, and methanol vapour diffusion drives *in situ* crystallization of γ-CD-MOF directly on the cellulose scaffold. (b) Volatile organic compound (VOC) vapour uptake for styrene, aniline, and benzaldehyde. (c) Colorimetric CO_2 sensing demonstration. Reproduced with permission from ref. 191. Copyright 2021 Wiley-VCH GmbH.

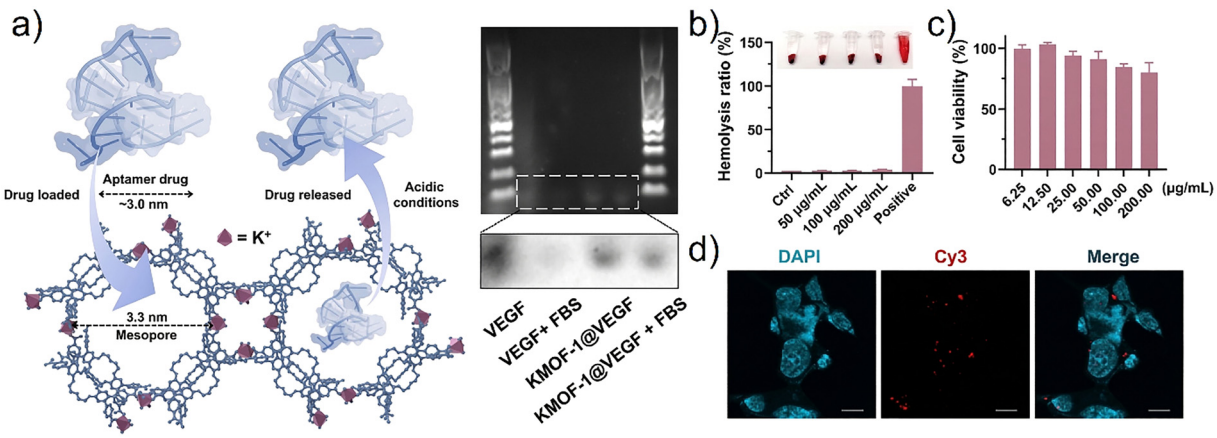


Fig. 42 Mesoporous crown ether-based MOF (KMOF-1) for aptamer drug delivery with nuclease protection. (a) Schematic of the loading and release mechanism. (b) Hemolysis assay at 50–200 μg mL^{-1}. (c) Cell viability at KMOF-1 concentrations of 6.25–200 μg mL^{-1}. (d) Confocal fluorescence images (DAPI, Cy3, and merged channels) of cells treated with Cy3-labeled aptamer-loaded KMOF-1. Reproduced with permission from ref. 192. Copyright 2025 American Chemical Society.

on its own. The lattice architecture decides which of the macrocycle's latent capabilities is silenced and which is voiced.

5. Challenges, emerging frontiers, and outlook

Supramolecular chemistry proposed that non-covalent interactions, if deliberately organized, could produce function rivalling biological systems.[8] Reticular chemistry proposed that periodic lattices could turn molecular properties into material properties.[5] Macrocycle–MOF systems inherit both propositions, and Section 4 confirms that the inheritance is real. But it also exposes a tension that neither parent field had to confront alone. The very preorganization that makes a macrocyclic cavity exquisitely selective at the molecular level also makes it expensive, synthetically demanding, and resistant to the compromises that engineering requires. The molecular design is often elegant, while the engineering follow-through is almost always absent. The challenges and frontiers outlined below ask what it would take to close this gap, not by abandoning molecular elegance, but by demanding that it survive contact with reality.

5.1. Current challenges

5.1.1. Scale-up, cost, and operational durability. The transition from laboratory to industry is the single greatest bottleneck. Whereas conventional MOFs have reached multi-hundred-tonne

 This journal is © The Royal Society of Chemistry 2026

annual production (BASF manufactures CALF-20 for Svante's CO_2 capture at this scale), macrocycle-integrated MOFs remain at the milligram-to-gram level, with no published continuous-flow protocol, and mechanochemical routes demonstrated in only a few cases.[193] Techno-economic analyses of conventional MOFs offer a useful reference point. Aqueous ambient-pressure synthesis brings the projected cost of MIL-100(Fe) to roughly $30 per kilogram at the kilotonne scale, and multikilogram pilot data place CAU-10-H at about $14 per kilogram. In both analyses the organic linker is the dominant cost driver.[194,195]

The cost barrier is compounded by the macrocyclic component itself, since functionalized crown ethers and calixarenes require multi-step syntheses that terephthalic acid does not. Seen against these linker-cost analyses, however, the cost problem is not intrinsic to macrocycles but to their functionalization. γ-Cyclodextrin is a food-grade commodity cheaper than many conventional linkers, and the aqueous ambient-pressure chemistry it supports is precisely the route class these analyses identify as the least expensive. Spray-drying has already produced CD-MOFs at the gram scale with high drug loadings.[196] The CD family is therefore a plausible candidate for the first macrocyclic framework manufactured at scale.

Beyond synthesis, long-term operational stability under industrially relevant conditions, continuous aqueous flow, high ionic strength, humidity cycling, sterilization, has been systematically evaluated in only a handful of cases. The 8500-hour cycling stability of the crown ether network NKU-2000 as a lithium-anode interfacial layer, and the polymer-encapsulated CD-MOFs retaining structural integrity beyond 30 days in aqueous media, provide rare but encouraging benchmarks. Comparable endurance testing across all macrocycle–MOF classes is essential before any translational claim can be taken seriously.[187,197]

In our view, translation will arrive earliest where the macrocycle serves as an auxiliary component such as an interfacial layer, membrane filler, or electrode additive, since per-device loadings are only milligrams and performance rather than production volume becomes limiting. Meaningful comparison of endurance claims will further require a minimal common protocol, covering continuous-flow operation beyond 100 hours, humidity cycling, and quantified metal and macrocycle leaching.

5.1.2. Structural verification and *operando* mechanistic insight. Proving that the macrocyclic cavity retains its pre-organized conformation and host–guest competence after framework integration is non-trivial. Single-crystal X-ray diffraction provides definitive proof for highly crystalline phases, but many macrocycle–MOF composites are polycrystalline or amorphous. Solid-state NMR, pair distribution function analysis, and three-dimensional electron diffraction (3D ED/microED) can provide complementary evidence, however their routine application remains rare. More fundamentally, the functional studies reviewed in Section 4 are dominated by static, pre-/post-reaction characterization. *Operando* techniques, time-resolved XRD, *in situ* IR/Raman, *operando* XAS, that capture the dynamic evolution of macrocycle–guest interactions during catalysis, transport, or gating are still exceedingly scarce. Without such data, the mechanistic role of the macrocyclic cavity, as opposed to framework-level effects, remains inferred rather than demonstrated.

5.1.3. Standardized benchmarking and limited macrocycle diversity. Catalytic, separation, and sensing studies frequently report performance under non-standardized conditions, varying temperatures, solvents, competing-ion matrices, and catalyst loadings, making cross-study comparison unreliable. Community-wide adoption of benchmarking protocols, analogous to those established for MOF gas storage, would accelerate the identification of genuinely superior macrocyclic designs.[198] Compounding this problem is the narrow macrocycle palette actually explored. Presently, γ-CD dominates the CD-MOF literature while 18-crown-6 and its benzo-fused variants dominate crown ether–MOFs. Only a handful of cyclam and cyclen derivatives have been tested as aza-macrocyclic linkers. Meanwhile, TACN-based frameworks, salphen macrocycles, and hybrid macrocycles with mixed N/O or N/S donor sets remain at the proof-of-concept stage.[174,186] Together, this reveals that the interaction-mode and rigidity axes central to this review have been experimentally validated over only a fraction of the accessible parameter space.

5.1.4. Multi-macrocycle integration. Current designs overwhelmingly employ a single macrocycle type per framework. The tandem recognition–transformation sequences that characterize biological multi-enzyme systems, a gating macrocycle controlling substrate access to a catalytic macrocycle, have yet to be realized. Co-incorporating two structurally distinct macrocycles into a single lattice with controlled spatial arrangement demands strategies (sequential linker installation, post-synthetic loading, core–shell growth) that have been individually demonstrated but not yet combined into a coherent multi-macrocycle design methodology.

5.1.5. Toxicity, degradation, and the cost of green credentials. Among the macrocyclic frameworks reported to date, biocompatibility has been established almost exclusively for the cyclodextrin family. CD-MOFs are assembled from food-grade γ-CD and alkali cations, and their drug-delivery performance is supported by hemolysis, cell-viability, and *in vivo* biosafety data.[199–201] No comparable toxicological profile has been reported for frameworks built on cucurbiturils, pillararenes, calixarenes, or aza-macrocycles, despite their advancement toward biomedical applications.

The gap is not merely one of missing datasets. Toxicity in MOF nanoparticles arises predominantly from degradation rather than from the intact framework: loss of structural integrity under physiological conditions releases metal ions and linker fragments whose accumulation, not the parent material, drives the observed cellular stress.[202] Macrocyclic frameworks are particularly vulnerable in this respect. Their metal nodes, Zr, Cu, Cd, and lanthanides, are selected for coordination chemistry, not for biological compatibility, and their linkers are synthetic hosts whose metabolic fate has never been established. Degradation products have rarely been a design consideration for either component. Three quantities would help close this gap, yet are seldom reported: metal and linker leaching under physiological and environmental conditions, the identity and clearance of degradation products, and the dose–response behaviour of the free macrocycle released as the lattice breaks down. The last deserves separate attention,

since the biological profile of a released host need not resemble that of the intact material, and cyclodextrins, the best characterized of these hosts, may not be representative of synthetic macrocycles in this regard. Standardized toxicological protocols are still emerging for MOFs generally, and macrocycle-specific assessment guidelines have yet to receive systematic attention.

A parallel asymmetry governs synthesis. Mechanochemical and aqueous room-temperature routes (Sections 3.4 and 4.4.4) demonstrate that macrocyclic frameworks can be assembled with minimal solvent waste: wash-free mechanochemical CD-MOF synthesis reaches full crystallinity in five minutes with a BET surface area comparable to the conventional vapour-diffusion material and no solvent effluent, and CD-MOFs crystallize from aqueous KOH at ambient temperature.[54,96,97] Yet these routes succeed precisely where the host is already benign and water-compatible. The macrocycles requiring the harshest solvothermal conditions are also those demanding the longest functionalization sequences, so their true environmental cost lies upstream, in linker synthesis, and is never accounted for in the framework step. Green credentials in this field are therefore inherited from the macrocycle rather than engineered into the process, a pattern that mirrors the durability argument of Section 5.2, and one that will hold until solvent-free and flow methods are extended to hosts that do not already tolerate water.

5.2. Emerging frontiers and outlook

Amid the above challenges, a handful of results reviewed in Section 4 have achieved performance metrics that approach or meet application thresholds, and they share a common design logic worth examining. Among these are CD-MOFs, which crystallize at room temperature from food-grade γ-CD and aqueous KOH, and NKU-2000, which is capable of sustaining 8500 hours of electrochemical cycling as a lithium-anode interfacial layer. A third, VPI-100, retains crystallinity across a wide pH range in both organic and aqueous media.[23,73,187] These are not isolated lucky strikes. In each case, the durability or scalability derives from a property intrinsic to the macrocycle itself rather than from post-synthetic engineering. Three examples make the point: the CD hydroxyl network provides self-assembly under mild aqueous conditions few conventional linkers can match; the crown ether oxygen array lowers the Li^+ desolvation barrier through a fast, reversible ion-exchange cycle that inherently resists fatigue; and the cyclam nitrogen donors supply kinetic inertness, stabilizing the metal centre through thousands of redox turnovers without auxiliary protection. The lesson here is that the most translatable macrocycle–MOF systems are those in which the macrocyclic property that delivers the function also delivers the stability, where recognition and resilience are not competing design objectives but two expressions of the same host–guest thermodynamics.

This principle immediately identifies where the next breakthroughs should come from, in particular, macrocycle families whose intrinsic chemistry simultaneously addresses a functional need and an engineering constraint. Bambus[*n*]urils, glycoluril-derived macrocycles achieving picomolar anion dissociation constants in water, are one such candidate. Among these, the same deep, hydrophobic cavity that binds perchlorate or iodide with extraordinary selectivity also confers hydrolytic stability, because the glycoluril backbone is chemically robust in aqueous media.[203] No bambusuril-based MOF has been reported, yet the functional gap they would fill, high-affinity anion capture from aqueous streams, is precisely the regime where cucurbiturils (cation-selective) and calixarenes (conformationally labile in water) fall short. Mixed-donor aza-crown ethers with N_2O_2 or N_2O_4 donor sets offer a different convergence. Their intermediate exchange kinetics, faster than cyclam, slower than 18-crown-6, provide a tuneable residence-time window for multivalent-ion transport that neither pure O-donor nor pure N-donor macrocycles can access. TACN-based frameworks, whose enforced facial N_3 geometry produced the OER pre-catalyst Co-TMBT-MOF, and salphen macrocycles, whose programmable N_2O_2 pockets enabled SM-MOF-Cu for acetylene semi-hydrogenation, represent the first incursions into this under-explored territory. Yet systematic metal-centre variation across first-row transition metals has barely begun.[174,186]

A complementary frontier lies in *in situ* reticular editing (ISRE), a strategy that harnesses reactive fragments generated during solvothermal crystallization to sculpt cooperative binding pockets within the growing framework. Ren, Ma, and co-workers demonstrated this concept by exploiting DMF-mediated *N*-formylation of cyclen secondary amines during assembly of Zr-macrocyclic frameworks (MMCFs), installing formamide and dimethylamino-propionic acid functionalities without additional synthetic steps (Fig. 43). The resulting MMCF-7-AA achieves an SO_2 uptake of 12.5 mmol g^{-1} at 1 bar and 1.43 mmol g^{-1} at 2500 ppm, among the highest reported for any MOF, alongside benchmark SO_2/CO_2 selectivities under realistic flue-gas conditions. The *in situ* approach shows how simple precursor scaffolds can be evolved into high-performance sorbents.[204]

Navigating this expanded design space will require computational guidance. Graph neural networks trained on MOF structure–property datasets already predict gas adsorption and electronic structure with useful accuracy, while large language models (LLMs) have been shown to extract synthesis parameters from the MOF literature at scale, recovering tens of thousands of reaction conditions from published texts with high fidelity.[205] On the supramolecular side, machine-learning and physics-based models now estimate host–guest binding free energies for cyclodextrins and cucurbiturils, in favourable cases approaching chemical accuracy across hundreds of complexes.[206,207] Macrocycle–MOF design sits at the intersection of these two efforts and would benefit from both: the solution-phase models supply the affinity term, the framework models the transport and stability terms.

Three obstacles stand between this prospect and practice. The first is data volume. Macrocyclic frameworks number in the hundreds, against the tens of thousands of structures on which the successful MOF models were trained, and the imbalance is severe: γ-CD and 18-crown-6 alone account for a large share of reported systems, so a model trained on this corpus would learn the field's synthetic habits rather than its chemistry. The second is descriptor mismatch. Cavity diameter

 This journal is © The Royal Society of Chemistry 2026

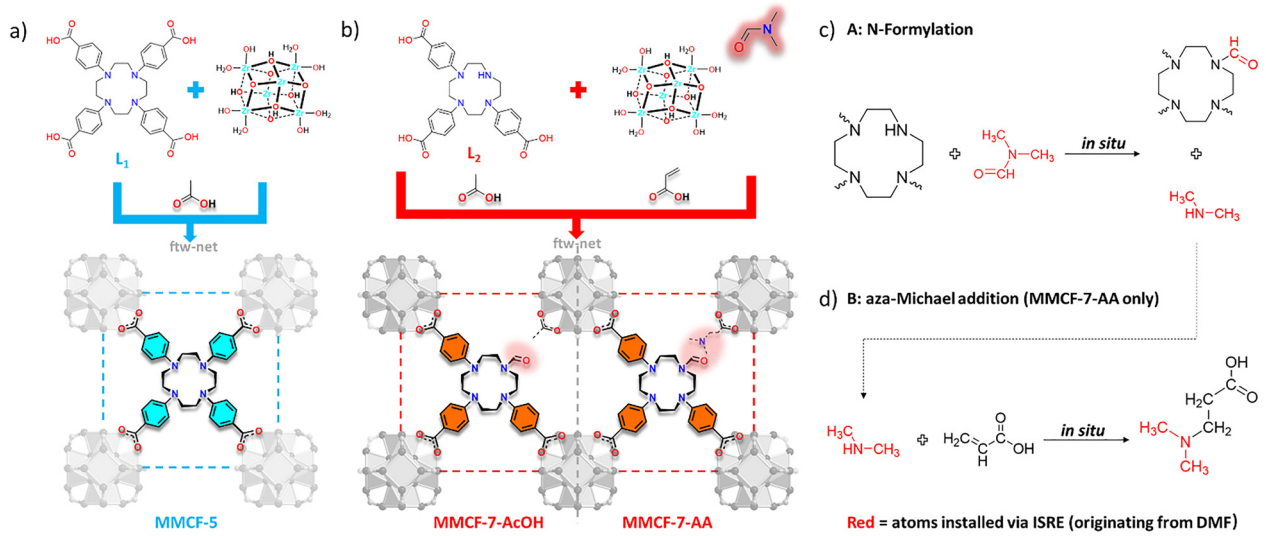


Fig. 43 *In situ* reticular editing (ISRE) of cyclen-based Zr-macrocyclic frameworks. (a) The tetratopic ligand L_1 reacts with $ZrCl_4$ to form MMCF-5 with ftw topology. (b) The tritopic ligand L_2, bearing a free secondary amine, reacts with $ZrCl_4$ in DMF to give MMCF-7-AcOH and MMCF-7-AA (acetic and acrylic acid modulators); two concurrent *in situ* reactions install DMF-derived groups (red). (c) N-Formylation of the secondary amine to a formamide, releasing dimethylamine. (d) Aza-Michael addition (MMCF-7-AA only): dimethylamine adds to the acrylic acid modulator, giving framework-incorporated 3-(dimethylamino)propionic acid. Reproduced with permission from ref. 204. Copyright 2026 American Chemical Society.

and donor-atom electronegativity are readily tabulated, but the coordinates this review identifies as decisive, conformational freedom and exchange kinetics, are dynamic quantities that crystallographic databases do not record, and computing them at scale would require molecular dynamics on every candidate rather than a static structural descriptor. The third is transferability. A binding constant measured in water need not survive confinement in a lattice, where desolvation, restricted approach geometry, and cooperative effects between neighbouring cavities all intervene; models trained on solution-phase host–guest data would therefore need recalibration against solid-state measurements that remain scarce.

None of these obstacles is insurmountable, and each suggests a concrete step. A curated, open-access macrocycle–MOF database, assembled from the literature reviewed herein and annotated with both structural and kinetic descriptors, is the prerequisite for all three; LLM-assisted extraction now makes its construction tractable in a way that manual curation did not. Beyond screening, the more ambitious prospect is inverse design, specifying a target function and asking a generative model which macrocycle–lattice pairing satisfies it, but this will remain out of reach until the forward problem is solved on data broad enough to span the design space rather than the fraction of it that has so far been explored.

The ultimate test of these principles is a framework in which multiple macrocycle types collaborate in a tandem sequence. A crown ether gate would admit a specific substrate to an aza-macrocyclic catalytic site, with the product delivered through a CD-based transport channel. Metal-free active sites, such as the solid frustrated Lewis pairs that already accomplish selective alkyne semihydrogenation, could be gated in the same way.[208] Core–shell growth, sequential post-synthetic exchange, and the pre-metalation/mechanochemical toolkit of Section 3 each provide synthetic routes to such spatially organized architectures. Realizing them would transform macrocyclic MOFs from single-function materials into integrated chemical processors, the synthetic analogue of multi-enzyme pathways, built from macrocycles arrayed in a crystalline manifold.

The macrocycle is not a problem to be optimized; instead, it is a question to be asked. Each cavity poses the same question to every guest it encounters: do you fit? The answer, thermodynamic, kinetic, geometric, electronic, is the origin of every function reviewed in this article. What the MOF lattice adds is not a better answer but a better audience with 10^{18} identical cavities listening simultaneously, and a periodic structure that converts each molecular yes-or-no into a collective material response. The distance between where the field stands and where it could arrive is not measured by the number of new macrocycles synthesized or new MOF topologies discovered. It is measured by how deeply we learn to listen to the answers these cavities are already giving, and how honestly we test whether those answers hold.

6. Conclusion

In the context of reticular chemistry, a linker is often characterized by how it connects, whereas a macrocycle is often characterized by what it encloses. This functional distinction, easily overlooked, motivates the perspective taken in this review. Conventional MOF chemistry optimizes the space between nodes (pore diameter, window aperture, surface area) and treats the organic strut as a structural element whose chemical identity is secondary to its geometry.[209,210] Macrocycle-integrated MOFs invert this hierarchy with the chemically active space inside the building block, and the lattice existing to organize, replicate, and

amplify what happens there. The shift is not incremental: it relocates the site of molecular function from the framework pore to the linker cavity. In the process, reticular chemistry inherits the full thermodynamic and kinetic vocabulary of host–guest interaction that supramolecular chemistry spent fifty years developing.[7,8]

What the lattice contributes is not merely repetition but context. A macrocycle in solution is a molecule with a binding constant. The same macrocycle in a framework is a molecule with a binding constant, a fixed conformation, and a defined orientation relative to its neighbours. The macrocycle also occupies a position within a periodic potential that dictates whether the bound guest is captured, relayed, gated, or transformed. The framework does not change the macrocycle's chemistry, rather it selects which facet of that chemistry is expressed. This is why the same crown ether appears in separation, sensing, transport, and energy storage across four sections of this review, performing differently each time, not because its molecular identity has changed, but because the lattice context has.

The two-axis classification introduced here, interaction mode and structural rigidity, is an attempt to make this context-dependence navigable. It is not a taxonomy for its own sake. It is the recognition that function is an emergent property of the molecule-in-lattice system, traceable to the cavity's position on two continuous variables. The oxygen–nitrogen complementarity that recurs in every application domain is one consequence of this framework while the identification of vast, unpopulated regions of design space is another.

Where the field goes from here depends as much on framing as on technique. The tools are largely in place: reticular synthesis can build the lattices, macrocyclic chemistry can supply the cavities, computation can screen the combinations, and *operando* spectroscopy can interrogate the mechanisms. The opportunity ahead is to make one particular question routine: for each new macrocycle–MOF system, asking not only what it does, but why the lattice makes it do that, and whether a different lattice would make it do something else. When that question is asked as a matter of course, macrocyclic MOFs will have matured from a collection of systems into a design language.

Conflicts of interest

There are no conflicts to declare.

Data availability

No primary research results, software, or code have been included, and no new data were generated or analyzed as part of this review.

Acknowledgements

This work was supported by the Robert A. Welch Foundation (B-0027).

References

1 B. F. Hoskins and R. Robson, *J. Am. Chem. Soc.*, 1989, **111**, 5962–5964.
2 M. Kondo, T. Yoshitomi, H. Matsuzaka, S. Kitagawa and K. Seki, *Angew. Chem., Int. Ed. Engl.*, 1997, **36**, 1725–1727.
3 H. Li, M. Eddaoudi, M. O'Keeffe and O. M. Yaghi, *Nature*, 1999, **402**, 276–279.
4 O. M. Yaghi, M. O'Keeffe, N. W. Ockwig, H. K. Chae, M. Eddaoudi and J. Kim, *Nature*, 2003, **423**, 705–714.
5 H. Furukawa, K. E. Cordova, M. O'Keeffe and O. M. Yaghi, *Science*, 2013, **341**, 1230444.
6 C. J. Pedersen, *J. Am. Chem. Soc.*, 1967, **89**, 2495–2496.
7 D. J. Cram, *Angew. Chem., Int. Ed. Engl.*, 1986, **25**, 1039–1057.
8 J. M. Lehn, *Angew. Chem., Int. Ed. Engl.*, 1988, **27**, 89–112.
9 M. Yoon, R. Srirambalaji and K. Kim, *Chem. Rev.*, 2012, **112**, 1196–1231.
10 H. Kim, S. Yang, S. R. Rao, S. Narayanan, E. A. Kapustin, H. Furukawa, A. S. Umans, O. M. Yaghi and E. N. Wang, *Science*, 2017, **356**, 430–434.
11 S. M. Cohen, *J. Am. Chem. Soc.*, 2017, **139**, 2855–2863.
12 H. C. Zhou and S. Kitagawa, *Chem. Soc. Rev.*, 2014, **43**, 5415–5418.
13 K. M. Jablonka, D. Ongari, S. M. Moosavi and B. Smit, *Chem. Rev.*, 2020, **120**, 8066–8129.
14 G. W. Gokel, W. M. Leevy and M. E. Weber, *Chem. Rev.*, 2004, **104**, 2723–2750.
15 K. P. Wainwright, *Coord. Chem. Rev.*, 1997, **166**, 35–90.
16 J. Szejtli, *Chem. Rev.*, 1998, **98**, 1743–1754.
17 K. I. Assaf and W. M. Nau, *Chem. Soc. Rev.*, 2015, **44**, 394–418.
18 H. Zhu, L. Chen and B. Sun, *Nat. Rev. Chem.*, 2023, **7**, 768–782.
19 K. J. Hartlieb, J. M. Holcroft, P. Z. Moghadam, N. A. Vermeulen, M. M. Algaradah, M. S. Nassar, Y. Y. Botros, R. Q. Snurr and J. F. Stoddart, *J. Am. Chem. Soc.*, 2016, **138**, 2292–2301.
20 D. Shen, G. Wang, Z. Liu, P. Li, K. Cai, C. Cheng, Y. Shi, J.-M. Han, C.-W. Kung, X. Gong, Q.-H. Guo, H. Chen, A. C. H. Sue, Y. Y. Botros, A. Facchetti, O. K. Farha, T. J. Marks and J. F. Stoddart, *J. Am. Chem. Soc.*, 2018, **140**, 11402–11407.
21 J. Li, Y. Shi, C. Qi, B. Zhang, X. Xing, Y. Li, T. Chen, X. Mao, Z. Zuo, X. Zhao, Z. Pan, L. Li, X. Yang and C. Li, *Angew. Chem., Int. Ed.*, 2023, **62**, e202309918.
22 K. Zhu, C. A. O'Keefe, V. N. Vukotic, R. W. Schurko and S. J. Loeb, *Nat. Chem.*, 2015, **7**, 514–519.
23 J. Zhu, P. M. Usov, W. Xu, P. J. Celis-Salazar, S. Lin, M. C. Kessinger, C. Landaverde-Alvarado, M. Cai, A. M. May, C. Slebodnick, D. Zhu, S. D. Senanayake and A. J. Morris, *J. Am. Chem. Soc.*, 2018, **140**, 993–1003.
24 C. Tan, K. Yang, J. Dong, Y. Liu, Y. Liu, J. Jiang and Y. Cui, *J. Am. Chem. Soc.*, 2019, **141**, 17685–17695.
25 T. Ogoshi, T.-a. Yamagishi and Y. Nakamoto, *Chem. Rev.*, 2016, **116**, 7937–8002.
26 M. J. Prakash and M. S. Lah, *Chem. Commun.*, 2009, 3326–3341.
27 L. F. Lindoy, K. M. Park and S. S. Lee, *Chem. Soc. Rev.*, 2013, **42**, 1713–1766.

 This journal is © The Royal Society of Chemistry 2026

28 H. Zhang, R. Zou and Y. Zhao, *Coord. Chem. Rev.*, 2015, **292**, 74–90.
29 C. A. Stackhouse and S. Ma, *Polyhedron*, 2018, **145**, 154–165.
30 J. H. Lee and H. R. Moon, *J. Incl. Phenom. Macrocycl. Chem.*, 2018, **92**, 237–249.
31 Y. Zhou, K. Jie, R. Zhao and F. Huang, *Adv. Mater.*, 2020, **32**, 1904824.
32 S. Tashiro and M. Shionoya, *Acc. Chem. Res.*, 2020, **53**, 632–643.
33 I. Roy and J. F. Stoddart, *Acc. Chem. Res.*, 2021, **54**, 1440–1453.
34 S. V. Dummert, H. Saini, M. Z. Hussain, K. Yadava, K. Jayaramulu, A. Casini and R. A. Fischer, *Chem. Soc. Rev.*, 2022, **51**, 5175–5213.
35 Y. Liang, E. Li, K. Wang, Z.-J. Guan, H.-H. He, L. Zhang, H.-C. Zhou, F. Huang and Y. Fang, *Chem. Soc. Rev.*, 2022, **51**, 8378–8405.
36 Y. Wu, M. Tang, M. L. Barsoum, Z. Chen and F. Huang, *Chem. Soc. Rev.*, 2025, **54**, 2906–2947.
37 H. Zhao, Y. Li, C. Li and D. Guo, *J. Mater. Chem. A*, 2025, **13**, 23354–23376.
38 S.-Q. Cheng, Y. Liu and Y. Sun, *Coord. Chem. Rev.*, 2025, **534**, 216559.
39 H. Sun, K. Z. Wang, M. R. Yao, C. X. Yu, Y. H. Song, J. Ding, Y. L. Zhou, D. Liu and L. L. Liu, *Inorg. Chem. Front.*, 2023, **10**, 6566–6577.
40 K. Jie, Y. Zhou, E. Li and F. Huang, *Acc. Chem. Res.*, 2018, **51**, 2064–2072.
41 D. J. Cram, *Science*, 1988, **240**, 760–767.
42 L. Bai, B. Tu, Y. Qi, Q. Gao, D. Liu, Z. Liu, L. Zhao, Q. Li and Y. Zhao, *Chem. Commun.*, 2016, **52**, 3003–3006.
43 H. J. Park and M. P. Suh, *Chem. Commun.*, 2012, **48**, 3400–3402.
44 Z. Shao, S. Han, Y. Song, L. Zhai, X. Feng and Y. Zhang, *ChemSusChem*, 2025, **18**, e202501076.
45 X. Song, F. Gao, X. Wang, W. Fan and D. Sun, *Coord. Chem. Rev.*, 2026, **550**, 217415.
46 T. Xu, B. Wu, W. Li, Y. Li and X. Li, *Sci. Adv.*, 2024, **10**, eadn0944.
47 G. Ortiz, S. Brandes, Y. Rousselin and R. Guilard, *Chem. – Eur. J.*, 2011, **17**, 6689–6695.
48 M. Almáši, V. Zeleňák, A. Zukal, J. Kuchár and J. Čejka, *Dalton Trans.*, 2016, **45**, 1233–1242.
49 M. P. Suh, H. R. Moon, E. Y. Lee and S. Y. Jang, *J. Am. Chem. Soc.*, 2006, **128**, 4710–4718.
50 W. Y. Gao, Y. Chen, Y. Niu, K. Williams, L. Cash, P. J. Perez, L. Wojtas, J. Cai, Y. S. Chen and S. Ma, *Angew. Chem., Int. Ed.*, 2014, **53**, 2615–2619.
51 J. Ren, Y. Ye, Y. Zhang, W. Zhang, Q. Liu, X. Huang, A. M. Al-Enizi, A. Nafady, J. Liu, X. Guo and S. Ma, *Chem*, 2024, **10**, 2776–2791.
52 J. Ren, Z. Niu, Y. Ye, C. Y. Tsai, S. Liu, Q. Liu, X. Huang, A. Nafady and S. Ma, *Angew. Chem., Int. Ed.*, 2021, **60**, 23705–23712.
53 J. Jia, J. Zhu, L. Guo, J. Yu, J. Li and F. Li, *Sep. Purif. Technol.*, 2024, **348**, 127664.
54 R. A. Smaldone, R. S. Forgan, H. Furukawa, J. J. Gassensmith, A. M. Z. Slawin, O. M. Yaghi and J. F. Stoddart, *Angew. Chem., Int. Ed.*, 2010, **49**, 8630–8634.
55 Y. He, X. Hou, Y. Liu and N. Feng, *J. Mater. Chem. B*, 2019, **7**, 5602–5619.
56 B. A. Blight, T. I. Ahmad, H. J. Shepherd, C. S. Jennings, L. I. Ferland, S. J. Teat and J. S. Rossman, *Cryst. Growth Des.*, 2020, **20**, 43–48.
57 S. P. Bew, A. D. Burrows, T. Düren, M. F. Mahon, P. Z. Moghadam, V. M. Sebestyén and S. Thurston, *Chem. Commun.*, 2012, **48**, 4824–4826.
58 Y. Wu, M. Tang, Z. Wang, L. Shi, Z. Xiong, Z. Chen, J. L. Sessler and F. Huang, *Nat. Commun.*, 2023, **14**, 4927.
59 T. Ogoshi, S. Kanai, S. Fujinami, T.-a. Yamagishi and Y. Nakamoto, *J. Am. Chem. Soc.*, 2008, **130**, 5022–5023.
60 V. Böhmer, *Angew. Chem., Int. Ed. Engl.*, 1995, **34**, 713–745.
61 N. L. Strutt, J. Iehl, M. B. Lalonde, R. Q. Snurr, O. K. Farha, J. T. Hupp and J. F. Stoddart, *J. Am. Chem. Soc.*, 2012, **134**, 17436–17439.
62 L. L. Tan, H. Li, Y. C. Qiu, D. X. Chen, X. Wang and R. Y. Pan, *Chem. Sci.*, 2015, **6**, 1640–1644.
63 M. Yang, Z. Wang, Z. Huang, H. Zhao, J. Sun, Z.-Z. Gao, B. Yang and G. Wei, *J. Mol. Struct.*, 2025, **1324**, 140895.
64 S. J. Barrow, S. Kasera, M. J. Rowland, J. del Barrio and O. A. Scherman, *Chem. Rev.*, 2015, **115**, 12320–12406.
65 F. F. Li, M. Huo, J. Kong and Y. Liu, *Adv. Opt. Mater.*, 2024, **12**, 2400453.
66 S.-S. Jia, W.-S. Xu, Y. Chen and Y. Liu, *Chin. Chem. Lett.*, 2021, **32**, 2773–2776.
67 J. X. Lin, J. Liang, J. F. Feng, B. Karadeniz, J. Lü and R. Cao, *Inorg. Chem. Front.*, 2016, **3**, 1393–1397.
68 H. Yonezawa, S. Tashiro, T. Shiraogawa, M. Ehara, R. Shimada, T. Ozawa and M. Shionoya, *J. Am. Chem. Soc.*, 2018, **140**, 16610–16614.
69 Y.-X. Ma, B. Gao, Y. Li, W. Wei, Y. Zhao and J.-F. Ma, *ACS Appl. Mater. Interfaces*, 2021, **13**, 27066–27073.
70 K. Krūkle-Bērziņa and A. Mishnev, *ACS Omega*, 2023, **8**, 48221–48232.
71 M. Ceballos, G. Zampini, O. Semyonov, S. Funes-Hernando, J. M. Vila-Fungueiriño, S. Martínez-Giménez, S. Tatay, C. Martí-Gastaldo, T. Devic, B. Pelaz and P. D. Pino, *Cell Rep. Phys. Sci.*, 2024, **5**, 102318.
72 C. Valente, E. Choi, M. E. Belowich, C. J. Doonan, Q. Li, T. B. Gasa, Y. Y. Botros, O. M. Yaghi and J. F. Stoddart, *Chem. Commun.*, 2010, **46**, 4911–4913.
73 Y. Furukawa, T. Ishiwata, K. Sugikawa, K. Kokado and K. Sada, *Angew. Chem., Int. Ed.*, 2012, **51**, 10566–10569.
74 H. A. Patel, T. Islamoglu, Z. Liu, S. K. M. Nalluri, A. Samanta, O. Anamimoghadam, C. D. Malliakas, O. K. Farha and J. F. Stoddart, *J. Am. Chem. Soc.*, 2017, **139**, 11020–11023.
75 X. Sun, Z. Fu, T. Jiang, F. Ning, Y. Cheng, T. Fu, M. Zhu, H. Zhang, M. Zhang and P. Hu, *J. Chromatogr. A*, 2022, **1663**, 462750.
76 K. Wilson, D. B. Cordes, A. P. McKay, A. B. Naden, O. V. Magdysyuk, D. N. Rainer, A. R. Armstrong, R. E. Morris, A. V. Desai and R. Ettlinger, *Front. Chem.*, 2025, **13**, 1682298.

77 J. Liang, V. Gvilava, C. Jansen, S. Öztürk, A. Spieß, J. Lin, S. Xing, Y. Sun, H. Wang and C. Janiak, *Angew. Chem., Int. Ed.*, 2021, **60**, 15365–15370.
78 V. N. Vukotic, K. J. Harris, K. Zhu, R. W. Schurko and S. J. Loeb, *Nat. Chem.*, 2012, **4**, 456–460.
79 K. J. Hartlieb, A. W. Peters, T. C. Wang, P. Deria, O. K. Farha, J. T. Hupp and J. F. Stoddart, *Chem. Commun.*, 2017, **53**, 7561–7564.
80 D. J. Hoffart and S. J. Loeb, *Angew. Chem., Int. Ed.*, 2005, **44**, 901–904.
81 Y.-L. Zhao, L. Liu, W. Zhang, C.-H. Sue, Q. Li, O. Š. Miljanić, O. M. Yaghi and J. F. Stoddart, *Chem. – Eur. J.*, 2009, **15**, 13356–13380.
82 P. Martínez-Bulit, C. A. O'Keefe, K. Zhu, R. W. Schurko and S. J. Loeb, *Cryst. Growth Des.*, 2019, **19**, 5679–5685.
83 N. Farahani, K. Zhu, C. A. O'Keefe, R. W. Schurko and S. J. Loeb, *ChemPlusChem*, 2016, **81**, 836–841.
84 B. H. Wilson, L. M. Abdulla, R. W. Schurko and S. J. Loeb, *Chem. Sci.*, 2021, **12**, 3944–3951.
85 K. Zhu, V. N. Vukotic, C. A. O'Keefe, R. W. Schurko and S. J. Loeb, *J. Am. Chem. Soc.*, 2014, **136**, 7403–7409.
86 B. H. Wilson, C. S. Vojvodin, G. Gholami, L. M. Abdulla, C. A. O'Keefe, R. W. Schurko and S. J. Loeb, *Chem*, 2021, **7**, 202–211.
87 A. Saura-Sanmartín, G. Cutillas-Font, A. Martínez-Cuezva, M. Alajarín, F. Esteban-Betegón, P. Peña-Sánchez, F. Gándara and J. Berná, *Chem. Commun.*, 2024, **60**, 6431–6434.
88 D. Ke, J. F. Feng, D. Wu, J. B. Hou, X. Q. Zhang, B. J. Li and S. Zhang, *RSC Adv.*, 2019, **9**, 18271–18276.
89 W. Meng, S. Kondo, T. Ito, K. Komatsu, J. Pirillo, Y. Hijikata, Y. Ikuhara, T. Aida and H. Sato, *Nature*, 2021, **598**, 298–303.
90 W. Wang, W. Tai, J. Lou, L. Li, Q. Wu, B. Hu, J. Wang, X. Yin and C. Xiao, *Nat. Commun.*, 2026, **17**, 4365.
91 M. Kim, J. F. Cahill, H. Fei, K. A. Prather and S. M. Cohen, *J. Am. Chem. Soc.*, 2012, **134**, 18082–18088.
92 Q. Chen, J. Sun, P. Li, I. Hod, P. Z. Moghadam, Z. S. Kean, R. Q. Snurr, J. T. Hupp, O. K. Farha and J. F. Stoddart, *J. Am. Chem. Soc.*, 2016, **138**, 14242–14245.
93 P. Deria, J. E. Mondloch, E. Tylianakis, P. Ghosh, W. Bury, R. Q. Snurr, J. T. Hupp and O. K. Farha, *J. Am. Chem. Soc.*, 2013, **135**, 16801–16804.
94 J. D. Evans, C. J. Sumby and C. J. Doonan, *Chem. Soc. Rev.*, 2014, **43**, 5933–5951.
95 U. Jeong, N. A. Dogan, M. Garai, T. S. Nguyen, J. F. Stoddart and C. T. Yavuz, *J. Am. Chem. Soc.*, 2019, **141**, 12182–12186.
96 S. Fujita, K. Kadota, A. Koike, H. Uchiyama, Y. Tozuka and S. Tanaka, *RSC Mechanochem.*, 2024, **1**, 153–157.
97 B. Liu, Y. He, L. Han, V. Singh, X. Xu, T. Guo, F. Meng, X. Xu, P. York, Z. Liu and J. Zhang, *Cryst. Growth Des.*, 2017, **17**, 1654–1660.
98 D. S. Sholl and R. P. Lively, *Nature*, 2016, **532**, 435–437.
99 E. Y. Lee and M. P. Suh, *Angew. Chem., Int. Ed.*, 2004, **43**, 2798–2801.
100 S. Zhang, R. Ou, H. Ma, J. Lu, M. M. Banaszak Holl and H. Wang, *Chem. Eng. J.*, 2021, **405**, 127037.
101 O. Mehmood, S. Farrukh, A. Hussain, A. Rehman, Y. Liu, S. Butt and E. Pervaiz, *Chem. Pap.*, 2020, **74**, 3527–3543.
102 X. Zhang, M. C. Wasson, M. Shayan, E. K. Berdichevsky, J. Ricardo-Noordberg, Z. Singh, E. K. Papazyan, A. J. Castro, P. Marino, Z. Ajoyan, Z. Chen, T. Islamoglu, A. J. Howarth, Y. Liu, M. B. Majewski, M. J. Katz, J. E. Mondloch and O. K. Farha, *Coord. Chem. Rev.*, 2021, **429**, 213615.
103 J.-R. Li, J. Sculley and H.-C. Zhou, *Chem. Rev.*, 2012, **112**, 869–932.
104 W. Gong, W. Zhang, F. A. Son, K. Yang, Z. Chen, X. Chen, J. Jiang, Y. Liu, O. K. Farha and Y. Cui, *Chem*, 2021, **7**, 190–201.
105 Y. Wu, L. Shi, L. Xu, J. L. Sessler and F. Huang, *Nature*, 2025, **640**, 676–682.
106 L. Li, K. Kang, T. S. Chee, Z. Tian, Q. Sun and C. Xiao, *Adv. Sci.*, 2024, **11**, 2308663.
107 J. J. Gassensmith, H. Furukawa, R. A. Smaldone, R. S. Forgan, Y. Y. Botros, O. M. Yaghi and J. F. Stoddart, *J. Am. Chem. Soc.*, 2011, **133**, 15312–15315.
108 Z. Wang, Y. Wu, Z. Zhang, X. Sheng, S. Fang, Y. Liu, Y. Gong, M. Wang, N. Song and F. Huang, *J. Am. Chem. Soc.*, 2024, **146**, 23330–23337.
109 J. Liang, A. Nuhnen, S. Millan, H. Breitzke, V. Gvilava, G. Buntkowsky and C. Janiak, *Angew. Chem., Int. Ed.*, 2020, **59**, 6068–6073.
110 Q. Li, W. Zhang, O. Š. Miljanić, C.-H. Sue, Y.-L. Zhao, L. Liu, C. B. Knobler, J. F. Stoddart and O. M. Yaghi, *Science*, 2009, **325**, 855–859.
111 R. S. Forgan, R. A. Smaldone, J. J. Gassensmith, H. Furukawa, D. B. Cordes, Q. Li, C. E. Wilmer, Y. Y. Botros, R. Q. Snurr, A. M. Z. Slawin and J. F. Stoddart, *J. Am. Chem. Soc.*, 2012, **134**, 406–417.
112 D. W. Lim, S. A. Chyun and M. P. Suh, *Angew. Chem., Int. Ed.*, 2014, **53**, 7819–7822.
113 J.-F. Lu, S. Zou, Z.-Y. Chen, S.-Q. Lu, Z.-H. Zhu, L. You and S.-J. Liu, *Eur. J. Inorg. Chem.*, 2026, **29**, e70228.
114 C.-X. Yu, W. Jiang, C.-W. Zhang, H. Fang, L.-Z. Wang, M.-J. Gao, Y.-L. Zhou, Y. Qian and L.-L. Liu, *Inorg. Chem.*, 2024, **63**, 15105–15114.
115 L. Huang, X. Ding, S. Xu, Y. Feng, G. Wang, Q. Guo, N. Liu, Q. Shi and J. Gao, *Chem. Eng. J.*, 2025, **519**, 164993.
116 C. Guo, M. Yuan, L. He, L. Cheng, X. Wang, N. Shen, F. Ma, G. Huang and S. Wang, *CrystEngComm*, 2021, **23**, 3349–3355.
117 W.-Y. Gao, Y. Niu, Y. Chen, L. Wojtas, J. Cai, Y.-S. Chen and S. Ma, *CrystEngComm*, 2012, **14**, 6115–6117.
118 X. Zhang, X. Xing, X. Zhao, J. Yang, M. Liu, B. Liu, X. Gao and H. Huang, *Chem. Eng. J.*, 2025, **503**, 158435.
119 X. Zhang, S. Wu, Y. Huang, W. Chen, Z. Li, X. Huangfu and S. Li, *J. Hazard. Mater.*, 2025, **489**, 137535.
120 L. Li, Z. Liu, X. Xu, L. Xu, X. Yang, H. Guan, Z. Li and C. Xiao, *Nat. Commun.*, 2025, **16**, 2606.
121 W. Wang, J. Lou, Q. Wu, B. Hu, J. Wang, X. Yin and C. Xiao, *J. Am. Chem. Soc.*, 2026, **148**, 15397–15403.
122 C. Liu, P. Wang, X. Liu, X. Yi, D. Liu and Z. Zhou, *Chem. – Asian J.*, 2019, **14**, 261–268.
123 D. Wu, J. J. Gassensmith, D. Gouvea, S. Ushakov, J. F. Stoddart and A. Navrotsky, *J. Am. Chem. Soc.*, 2013, **135**, 6790–6793.

 This journal is © The Royal Society of Chemistry 2026

124 M. E. Zick, S. M. Pugh, J. H. Lee, A. C. Forse and P. J. Milner, *Angew. Chem., Int. Ed.*, 2022, **61**, e202206718.
125 S. A. Lim, M. E. Zick, J. Kim, B. J. Rhodes, J. Randrianandraina, T. A. Pitt, R. T. Jerozal, J.-H. Lee, A. C. Forse and P. J. Milner, *J. Am. Chem. Soc.*, 2025, **147**, 25715–25726.
126 L. Xu, C.-Y. Xing, D. Ke, L. Chen, Z.-J. Qiu, S.-L. Zeng, B.-J. Li and S. Zhang, *ACS Appl. Mater. Interfaces*, 2020, **12**, 3032–3041.
127 L. Li, J. Wang, Z. Zhang, Q. Yang, Y. Yang, B. Su, Z. Bao and Q. Ren, *ACS Appl. Mater. Interfaces*, 2019, **11**, 2543–2550.
128 J. M. Holcroft, K. J. Hartlieb, P. Z. Moghadam, J. G. Bell, G. Barin, D. P. Ferris, E. D. Bloch, M. M. Algaradah, M. S. Nassar, Y. Y. Botros, K. M. Thomas, J. R. Long, R. Q. Snurr and J. F. Stoddart, *J. Am. Chem. Soc.*, 2015, **137**, 5706–5719.
129 L. Wang, X.-Y. Liang, Z.-Y. Chang, L.-S. Ding, S. Zhang and B.-J. Li, *ACS Appl. Mater. Interfaces*, 2018, **10**, 42–46.
130 Y. Zhang, L. Zhang, Y. Bian, J. Yu, Y. Xu, Z. Shu, S. Shan, Y. Jiao and J. Chen, *J. Environ. Chem. Eng.*, 2024, **12**, 113312.
131 Z. Chen, P. Fang, J. Li, X. Han, W. Huang, W. Cui, Z. Liu, M. R. Warren, D. Allan, P. Cheng, S. Yang and W. Shi, *Natl. Sci. Rev.*, 2024, **11**, nwae342.
132 L. Feng, X. Chen, M. Cao, S. Zhao, H. Wang, D. Chen, Y. Ma, T. Liu, N. Wang and Y. Yuan, *Angew. Chem., Int. Ed.*, 2023, **62**, e202312894.
133 L. Hu, K. Li, W. Shang, X. Zhu and M. Liu, *Angew. Chem., Int. Ed.*, 2020, **59**, 4953–4958.
134 W. Gong, Y. Xie, X. Wang, K. O. Kirlikovali, K. B. Idrees, F. Sha, H. Xie, Y. Liu, B. Chen, Y. Cui and O. K. Farha, *J. Am. Chem. Soc.*, 2023, **145**, 2679–2689.
135 C. X. Yu, W. Jiang, M. Lei, M. R. Yao, X. Q. Sun, Y. Wang, W. Liu and L. L. Liu, *Small*, 2024, **20**, e2308910.
136 C.-X. Yang, Y.-Z. Zheng and X.-P. Yan, *RSC Adv.*, 2017, **7**, 36297–36301.
137 Z. Han, K.-Y. Wang, Y. Guo, Z.-H. Wang, R.-R. Liang, Y. Yang, J. Huo, D.-S. Guo and H.-C. Zhou, *J. Am. Chem. Soc.*, 2025, **147**, 25162–25166.
138 Y. Inokuma, S. Yoshioka, J. Ariyoshi, T. Arai, Y. Hitora, K. Takada, S. Matsunaga, K. Rissanen and M. Fujita, *Nature*, 2013, **495**, 461–466.
139 S. Yoshioka, Y. Inokuma, V. Duplan, R. Dubey and M. Fujita, *J. Am. Chem. Soc.*, 2016, **138**, 10140–10142.
140 L.-M. Chang, Q.-H. Li, P. Weidler, Z.-G. Gu, C. Wöll and J. Zhang, *CCS Chem.*, 2022, **4**, 3472–3481.
141 H. Jiang, K. Yang, X. Zhao, W. Zhang, Y. Liu, J. Jiang and Y. Cui, *J. Am. Chem. Soc.*, 2021, **143**, 390–398.
142 X. X. Zhang, J. S. Bradshaw and R. M. Izatt, *Chem. Rev.*, 1997, **97**, 3313–3362.
143 J. Yu, Z. Li, M. Xia, L. Zhang, D. Zhao, B. Li, C. Chen, Y. Jiao, Y. Xu and H. Lin, *J. Membr. Sci.*, 2023, **679**, 121714.
144 H. Liu, S. M. Xie, P. Ai, J. H. Zhang, M. Zhang and L. M. Yuan, *ChemPlusChem*, 2014, **79**, 1103–1108.
145 Y. Lu, J. Y. Chan, H. Zhang, X. Li, Y. Nolvachai, P. J. Marriott, X. Zhang, G. P. Simon, M. M. Banaszak Holl and H. Wang, *J. Membr. Sci.*, 2021, **620**, 118956.
146 Z. Jiang, Z. Chen, X. Yu, S. Lu, W. Xu, B. Yu, C. L. Stern, S.-Y. Li, Y. Zhao, X. Liu, Y. Han, S. Chen, K. Cai, D. Shen, K. Ma, X. Li and A. X.-Y. Chen, *J. Am. Chem. Soc.*, 2025, **147**, 7325–7335.
147 N. L. Strutt, H. Zhang and J. F. Stoddart, *Chem. Commun.*, 2014, **50**, 7455–7458.
148 M. P. Suh and H. R. Moon, *Adv. Inorg. Chem.*, 2006, **59**, 39–79.
149 X. D. Zhang, Y. Zhao, K. Chen, P. Wang, Y. S. Kang, H. Wu and W. Y. Sun, *Dalton Trans.*, 2018, **47**, 3958–3964.
150 J.-Y. Gu, X.-R. Chen, F. Li, W.-Y. Ding, J. Cao, W.-W. Ge and K. Chen, *J. Mol. Struct.*, 2026, **1359**, 145517.
151 T. Zhou, L. Shi, A. Liu and M. Liu, *J. Mol. Struct.*, 2026, **1359**, 145568.
152 H. Zhang, W. Jiang, J. Yang, Y.-Y. Liu, S. Song and J.-F. Ma, *CrystEngComm*, 2014, **16**, 9939–9946.
153 B. H. Wilson and S. J. Loeb, *Chem*, 2020, **6**, 1604–1612.
154 V. N. Vukotic, C. A. O'Keefe, K. Zhu, K. J. Harris, C. To, R. W. Schurko and S. J. Loeb, *J. Am. Chem. Soc.*, 2015, **137**, 9643–9651.
155 L. Feng, Y. Qiu, Q. H. Guo, Z. Chen, J. S. W. Seale, K. He, H. Wu, Y. Feng, O. K. Farha, R. D. Astumian and J. F. Stoddart, *Science*, 2021, **374**, 1215–1221.
156 A. Saura-Sanmartin, A. Martinez-Cuezva, D. Bautista, M. R. B. Marzari, M. A. P. Martins, M. Alajarin and J. Berna, *J. Am. Chem. Soc.*, 2020, **142**, 13442–13449.
157 W. Xie, Y. Yin, R. Gu, J. Xu, X. Su, Y. Wang, R. Liu, X. Liu and J. Huang, *Chem. Eng. J.*, 2022, **443**, 136371.
158 F. Luan, Y. Wang, S. Zhang, X. Zhuang, C. Tian, X. Fu and L. Chen, *Analyst*, 2020, **145**, 1943–1949.
159 J. J. Gassensmith, J. Y. Kim, J. M. Holcroft, O. K. Farha, J. F. Stoddart, J. T. Hupp and N. C. Jeong, *J. Am. Chem. Soc.*, 2014, **136**, 8277–8282.
160 X. L. Yang, Z. Y. Yang, R. Shao, R. F. Guan, S. L. Dong and M. H. Xie, *Adv. Mater.*, 2023, **35**, e2304046.
161 S. Guo, H. Han, X. Gao, Y. Zhai, J. Wang, Z. Zhang, X. Liu, R. Yuan, L. Yang and X. Wang, *Microchem. J.*, 2025, **213**, 113845.
162 M. Schulz, A. Gehl, J. Schlenkrich, H. A. Schulze, S. Zimmermann and A. Schaate, *Angew. Chem., Int. Ed.*, 2018, **57**, 12961–12965.
163 Y. Y. Liu, X. Zhang, K. Li, Q. C. Peng, Y. J. Qin, H. W. Hou, S. Q. Zang and B. Z. Tang, *Angew. Chem., Int. Ed.*, 2021, **60**, 22417–22423.
164 J. Liu, J. Lu, W. Ji, G. Lu, J. Wang, T. Ye, Y. Jiang, J. Zheng, P. Yu, N. Liu, Y. Jiang and L. Mao, *Anal. Chem.*, 2024, **96**, 2651–2657.
165 M. X. Wu, J. Gao, F. Wang, J. Yang, N. Song, X. Jin, P. Mi, J. Tian, J. Luo, F. Liang and Y. W. Yang, *Small*, 2018, **14**, 1704440.
166 X. Luan, Z. Xiang, J. Dong, C. Wang, X. Li, Q. Shi and X. Du, *ACS Appl. Mater. Interfaces*, 2023, **15**, 27264–27276.
167 R. Breslow and S. D. Dong, *Chem. Rev.*, 1998, **98**, 1997–2012.
168 X.-Y. Chen, H. Chen, L. Đorđević, Q.-H. Guo, H. Wu, Y. Wang, L. Zhang, Y. Jiao, K. Cai, H. Chen, C. L. Stern, S. I. Stupp, R. Q. Snurr, D. Shen and J. F. Stoddart, *J. Am. Chem. Soc.*, 2021, **143**, 9129–9139.
169 A. Núñez-López, M. Galbiati, N. M. Padial, C. R. Ganivet, S. Tatay, E. Pardo, D. Armentano and C. Martí-Gastaldo, *Angew. Chem., Int. Ed.*, 2019, **58**, 9179–9183.

170 C. Rao, L. Zhou, Y. Pan, C. Lu, X. Qin, H. Sakiyama, M. Muddassir and J. Liu, *J. Alloys Compd.*, 2022, **897**, 163178.
171 J. Zhu, J. Liu, Y. Machain, B. Bonnett, S. Lin, M. Cai, M. C. Kessinger, P. M. Usov, W. Xu, S. D. Senanayake, D. Troya, A. R. Esker and A. J. Morris, *J. Mater. Chem. A*, 2018, **6**, 22195–22203.
172 N. Y. Huang, X. W. Zhang, Y. Z. Xu, P. Q. Liao and X. M. Chen, *Chem. Commun.*, 2019, **55**, 14781–14784.
173 J. Martín-Caballero, A. San José Wery, S. Reinoso, B. Artetxe, L. San Felices, B. El Bakkali, G. Trautwein, J. Alcañiz-Monge, J. L. Vilas and J. M. Gutiérrez-Zorrilla, *Inorg. Chem.*, 2016, **55**, 4970–4979.
174 J. N. S. Ang, M. Chatti, K. N. Dinh, S. R. Batten, A. N. Simonov and D. R. Turner, *Mol. Syst. Des. Eng.*, 2023, **8**, 1004–1012.
175 Z. Zhang, Q. Xu, W. Li, Y. Zhu, J. S. Qin, Y. Yang, H. Rao and L. Chen, *J. Am. Chem. Soc.*, 2025, **147**, 33330–33336.
176 D.-W. Lim and H. Kitagawa, *Chem. Rev.*, 2020, **120**, 8416–8467.
177 N. Keller and T. Bein, *Chem. Soc. Rev.*, 2021, **50**, 1813–1845.
178 B. Zhang, H. Chen, L. Jiang, Y. Shen, D. Zhao and Z. Zhou, *Chin. J. Chem. Eng.*, 2022, **52**, 95–102.
179 H. Ding, L. Wu, T. Guo, Z. Zhang, B. M. Garba, G. Gao, S. He, W. Zhang, Y. Chen, Y. Lin, H. Liu, J. Anwar and J. Zhang, *Cryst. Growth Des.*, 2019, **19**, 3888–3894.
180 K. Lu, A. Liebman Pelaez, L. C. Wu, Y. Cao, C. H. Zhu and H. Fu, *Inorg. Chem.*, 2019, **58**, 1794–1805.
181 Y.-Q. Gu, Y. Tian, N.-H. Wang, Y.-M. Cui, X.-S. Wu, M. Ma, X. Han and Z.-M. Su, *Cryst. Growth Des.*, 2025, **25**, 2874–2881.
182 S. Liu, Y. Xiong and F. Dong, *RSC Adv.*, 2024, **14**, 31868–31876.
183 C. Zhao, N. Li, S. Shi, J. Hou, L. Gao, B. D. Freeman, H. Wang and H. Zhang, *Angew. Chem., Int. Ed.*, 2026, **65**, e202521527.
184 H. T. B. Pham, J. Y. Choi and S. Huang, *J. Am. Chem. Soc.*, 2022, **144**, 10615–10621.
185 H. T. B. Pham, X. Fang, J. Y. Choi, S. Huang and J. Park, *Chem*, 2025, **11**, 102487.
186 P. Chen, M. Liu, R. Li, X. Su, G. Xing, X. R. Ren, D. Wang, J. Zhang and L. Chen, *Angew. Chem., Int. Ed.*, 2025, **64**, e202511048.
187 R. Zhang, Z. Chen, J. Jiang, X. Liao, J. Guo, W. Huang, J. Liu, S. Dang, J. Xu, H. Wang, Z. Zhou, K. Zhang, P. Cheng and W. Shi, *CCS Chem.*, 2025, **7**, 3160–3171.
188 J.-Q. Sha, X.-H. Zhong, L.-H. Wu, G.-D. Liu and N. Sheng, *RSC Adv.*, 2016, **6**, 82977–82983.
189 P. Yang, W. Zhao, A. Shkurenko, Y. Belmabkhout, M. Eddaoudi, X. Dong, H. N. Alshareef and N. M. Khashab, *J. Am. Chem. Soc.*, 2019, **141**, 1847–1851.
190 S. Shakya, Y. He, X. Ren, T. Guo, A. Maharjan, T. Luo, T. Wang, R. Dhakhwa, B. Regmi, H. Li, R. Gref and J. Zhang, *Small*, 2019, **15**, e1901065.
191 B. Zhang, H. Chen, Q. Hu, L. Jiang, Y. Shen, D. Zhao and Z. Zhou, *Adv. Funct. Mater.*, 2021, **31**, 2105395.
192 B. Fang, T. Shan, S. Chen, F. Pan, X. Yang, D. Xiao, F. Huang and Z. Mao, *ACS Cent. Sci.*, 2025, **11**, 1651–1658.
193 M. Nazari, F. Zadehahmadi, M. M. Sadiq, A. L. Sutton, H. Mahdavi and M. R. Hill, *Commun. Mater.*, 2024, **5**, 170.
194 M. I. Severino, C. Freitas, V. Pimenta, F. Nouar, M. L. Pinto and C. Serre, *Ind. Eng. Chem. Res.*, 2025, **64**, 2708–2718.
195 K. S. Mertin, A. Mohtar, M. Bordonhos, M. L. Pinto, T. May, R. Herrmann and N. Stock, *Ind. Eng. Chem. Res.*, 2026, **65**, 7045–7055.
196 J. Y. Tse, K. Kadota, T. Nakajima, H. Uchiyama, S. Tanaka and Y. Tozuka, *Cryst. Growth Des.*, 2022, **22**, 1143–1154.
197 Y. Zhou, S. Luo, B. Niu, B. Wu, J. Fu, Y. Zhao, V. Singh, C. Lu, G. Quan, X. Pan, J. Zhang and C. Wu, *ACS Biomater. Sci. Eng.*, 2019, **5**, 5180–5188.
198 *Nat. Mater.*, 2025, **24**, 157.
199 K. J. Hartlieb, D. P. Ferris, J. M. Holcroft, I. Kandela, C. L. Stern, M. S. Nassar, Y. Y. Botros and J. F. Stoddart, *Mol. Pharmaceutics*, 2017, **14**, 1831–1839.
200 H. Li, N. Lv, X. Li, B. Liu, J. Feng, X. Ren, T. Guo, D. Chen, J. F. Stoddart, R. Gref and J. Zhang, *Nanoscale*, 2017, **9**, 7454–7463.
201 T. Simon-Yarza, A. Mielcarek, P. Couvreur and C. Serre, *Adv. Mater.*, 2018, **30**, 1707365.
202 R. Ettlinger, U. Lächelt, R. Gref, P. Horcajada, T. Lammers, C. Serre, P. Couvreur, R. E. Morris and S. Wuttke, *Chem. Soc. Rev.*, 2022, **51**, 464–484.
203 S. Grewal, P. Slávik and V. Šindelář, *Angew. Chem., Int. Ed.*, 2025, **64**, e202510912.
204 J. Ren, Y. Song, Y. Ye, P. VanNatta, Y. Zhang, A. M. Al-Enizi, A. Nafady, K. Tan and S. Ma, *J. Am. Chem. Soc.*, 2026, **148**, 17218–17227.
205 Z. Zheng, O. Zhang, C. Borgs, J. T. Chayes and O. M. Yaghi, *J. Am. Chem. Soc.*, 2023, **145**, 18048–18062.
206 A. Ozcan, F. X. Coudert, S. M. J. Rogge, G. Heydenrych, D. Fan, A. P. Sarikas, S. Keskin, G. Maurin, G. E. Froudakis, S. Wuttke and I. Erucar, *J. Am. Chem. Soc.*, 2025, **147**, 23367–23380.
207 X. Wang, L. Qiu, H. Wang, W. Tang, J. Leng, J. Z. H. Zhang, P. Procacci and Z. Sun, *Adv. Sci.*, 2026, **13**, e19782.
208 S. Ma, J. Wang, L. Su, C. Yang, X. Li, Z. Yan and Z. Tang, *CCS Chem.*, 2026, **8**, 772–780.
209 L. Gong, S. C. Pal, Y. Ye and S. Ma, *Acc. Mater. Res.*, 2025, **6**, 499–511.
210 X. Zheng, L. Cai, S. C. Pal, L. Hu, C. Lin, Z. Li, L. Gong and Y. Ye, *Sep. Purif. Technol.*, 2026, **380**, 135384.

This journal is © The Royal Society of Chemistry 2026